MEDICAL ULTRASONICS:

ADAPTIVE TIME GAIN COMPENSATION

IN DIAGNOSTIC IMAGING

Stephen D. Pye B.Sc.

Thesis presented for the Degree of Doctor of Philosophy
of the University of Edinburgh, 1987 .

To my Mother and Father

Dorothy and William Pye.

God bless all our gains...

E M Browning

ACKNOWLEDGEMENTS

I wish to thank Professor J R Greening for his support and for making the facilities of the department available to me. I am very grateful to my supervisor Norman McDicken for his excellent guidance.

I acknowledge the financial support of the Medical Research Council and the Scottish Home and Health Department.

Dr Roger Wild and his registrars have shown a keen interest throughout the project and I am grateful to them for giving so much of their time to the clinical trials. I am indebted to the radiographers, Vicki, Sheila, Dorothy, Irene and Anita for their patience and invaluable help.

I thank Tom Anderson and Doug Morrison for their help in designing the electronics, and Harry Ferguson for his help in constructing it. My thanks to Betty Anderson for her expert typing of the script.

I thank Martin Connell for his assistance with the computing.

I would like to thank Mrs Liddle of the Erskine Medical Library for her diligence in acquiring a number of obscure articles, and I thank the medical photographers of the Western General Hospital for their excellent reproduction of the images.

I thank my fellow students Thanasis Loupas and Nicholas Nicolson for their help and encouragement.

I would like to thank my friend Jeremy Nicoll for a touch of sanity and the chance to practice my art-work on his thesis.

I thank my many flatmates, who have been good companions throughout my life in Edinburgh, especially Christine MacKay, Christine and Neil, Fergus, Donald, Marion, Marissa, Lyndsay, Val, Mark, Dave Taylor, Dave Hossack, Craig, Greg, Ian, John, Debbie, Janie, Tony and Sue.

Most of all, I thank my parents and my brothers and their families, without whom I would never have got as far as page one.

I declare that the work contained in this thesis is my own and the thesis has been composed by myself

Stephen D. Pye

July 1987

CONTENTS

ABSTRACT

Large errors can occur with time gain compensation (TGC) which is set up manually since one gain function is unlikely to be appropriate for all scan lines and the operator may not have sufficient time or experience to optimise it. Adaptive TGC offers the benefit of improved images which are less operator dependent.

The clinical application of simple adaptive TGC in abdominal and obstetric ultrasound is described.

Recent developments in digital electronics allow powerful methods of gain control to be implemented. A microcomputer controlled system has been built to investigate various methods of adaptive TGC. The microcoputer is interfaced to a real-time scanner from which it can collect echo data. The echo data is processed by programs written in a combination of assembly language and Fortran IV, and the microcomputer can then set up a unique TGC function for each scan line in the image. The design and construction of the microcomputer system are described.

Several algorithms for adaptive TGC have been developed. These range from the derivation of a single gain function applied across the whole image to more sophisticated algorithms which apply a unique TGC function to each scan line and are capable of detecting regions of low attenuation.

The algorithms were tested using tissue equivalent phantoms, and clinically in routine abdominal and obstetric scanning. The results were compared with those of a skilled operator setting up the TGC by hand. The performance of the algorithms was also investigated using computer simulations. The clinical results show that adaptive TGC is capable of producing consistently better images than a skilled operator setting the TGC manually.

Further developments of adaptive TGC are considered - in particular, the implementation of a hard-wired system which would operate in real-time and the development of an interactive gain control system.

Chapter 1

INTRODUCTION

An image is a likeness of the real world. Sound is a powerful way of forming images. In the natural world, bats and dolphins are able to form acoustic images and use them as an aid to navigation. Man has found many applications for imaging with sound: in geological exploration, sonar, acoustic microscopy, non-destructive evaluation, and clinically to visualise the structure and motion of the internal organs of the body.

1.1 DIAGNOSTIC ULTRASOUND

The diagnostic information obtained using high frequency sound - ultrasound - is acquired quite safely, non-invasively and is often information that cannot be obtained using other types of medical imaging.

The clinical applications of ultrasound are described in an excellent series of texts "Clinics in Diagnostic Ultrasound" published by Churchill Livingstone. McDicken (1981) outlines the physical principles of ultrasound and describes the uses of modern instrumentation. The physical and technical aspects of medical ultrasound are dealt with thoroughly in texts by Wells (1977) and Hill (1986).

1.2 THE ULTRASOUND IMAGE

Diagnostic ultrasound is a pulse-echo technique. Sound pulses transmitted into the body from a hand held probe are scattered and reflected by tissue and two dimensional images are formed using the echoes returning to the probe.

Ultrasound frequencies between 1MHz and 15MHz are used for imaging. In this frequency range, the wavelength of sound in soft tissue is between 1.5mm and 0.1mm.

Most modern ultrasound scanners are real-time machines, in that they form and display many images each second. This is a very useful feature since it allows the movement of internal structures to be studied and large volumes of tissue can be scanned in a short time. The use of grey scale displays allows low level signals from parenchyma to be seen as well as large signals from strongly reflecting surfaces. However, the images produced are not quantitative in the sense that the display brightness at each point does not correspond to a single tissue property. The display brightness is affected by many things: the acoustic scattering and attenuation properties of tissue, the focussing of the transducer in the probe and the characteristics of the receiving electronics and display system. Numerous artifacts may appear in an image. These have been well documented in a paper by Kremkau and Taylor (1986).

Ideally, the brightness of each part of an image would represent, say, backscattering power or the local attenuation coefficient. Attempts have been made to produce such images. Estimates can be made of tissue properties in each part of the scan plane by combining information gathered from many transducer positions (Duck and Hill, 1979; Farrell, 1982). The accurate reconstruction of a quantitative image requires complex mathematical techniques which have still to be fully developed. The results obtained so far are not clinically useful. They have poor resolution and often contain gross artifacts due to the effects of diffraction and refraction.

Much work is being done to estimate tissue attenuation coefficients using pulse-echo data obtained from one transducer

position. Again, there are many sources of error. The attentuation of sound in tissue is often due more to absorbtion than scattering and so assumptions must be made about the nature of sound propagation. Also, the scattering of sound by many closely spaced objects introduces acoustic noise into the echo signal. The signal must then be averaged over a large region - typically several square centimetres. A number of techniques have been employed for estimating attentuation coefficients in vivo, but none are suitable for measuring the attentuation in small regions. Excellent review papers have been published by Leeman et al (1984) and Ophir et al (1984).

Ultrasound images are normally displayed on a TV monitor. The dynamic range of the brightness display of a good monitor is about 20dB. The echo signals returning to the transducer have a dynamic range of over 100dB. This is due to several effects. The variations in scattering and reflectivity at any given depth contribute 30 to 50dB. The range of echo amplitudes produced by the focussing of the transducer might be 10 to 15dB. The dynamic range due to the attentuation of ultrasound by tissue varies considerably but can be as much as 90dB.

A well designed ultrasound scanner should be capable of compressing the signal range of 100dB or more received at its front-end into the 20dB range of a TV monitor. Without the aid of rigorous methods for calculating attenuation or scattering, the instrumentation must still retain clear information about areas of subtle parenchymal change and about the structure of major boundaries. This is a challenging task. Other acoustic imaging methods do not face the same problem. In diagnostic ultrasound, the medium through which sound propagates is also the object to be imaged. Other acoustic imaging methods do not often examine extended objects. They seek to identify either point objects against a noisy background, as in non-destructive evaluation, or to

examine objects lying on a plane surface, as in microscopy and sea-bed sonar, or to map the positions of discrete interfaces, as in geological exploration.

Ultrasound images have in fact improved dramatically during the last 20 years, benefiting from the technical advances made in electronics and computing. A comparison between a scanner of the 1970s and a modern scanner would show that most of the instrumentation has altered considerably. Bi-stable displays have been replaced by grey scale, static scanning by real-time, digital scan converters have been introduced and the ultrasound beam can be manipulated to achieve beam steering and variable aperture imaging. One aspect of the instrumentation which has changed little is the signal processing carried out by the rf amplifier in the receiver.

1.3 THE ECHO SIGNAL PATH

The path of echo signals through an ultrasound scanner is illustrated in figure 1.1 . Variations in pressure produced by scattered sound waves arriving at the piezo-electric transducer are converted into variations in voltage. This voltage signal may then be buffered by a pre-amplifier mounted in the probe before going to the receiver. The most important function of the receiver is signal processing performed to compensate for the attentuation of ultrasound by tissue and to reduce the dynamic range of the signal so that it can be digitised and stored by the scan converter. Most of the reduction in dynamic range is achieved by varying the voltage gain of the receiver so that echoes from deep structures are amplified more than echoes from superficial ones. This process is known as "time gain compensation" (TGC) or by other names such as "depth gain control" or "swept gain".

The influence of the processing carried out by the receiver on

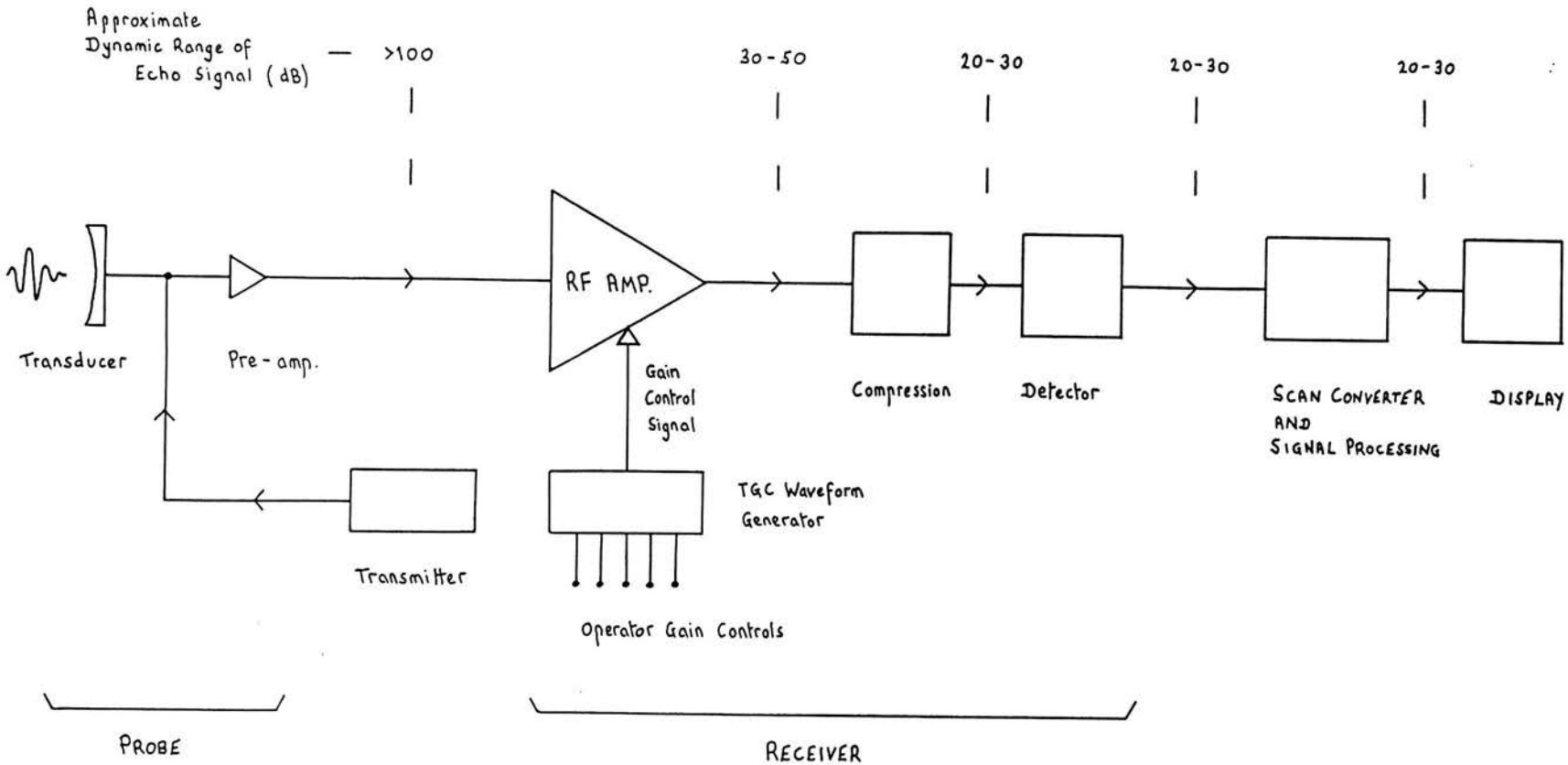

Figure 1.1 Echo Signal Path through a Scanner

subsequent processing and on the final image is discussed by Schafer and Lewin (1984) and Brown (1981). Several implementations of TGC are described by Maginness (1979). TGC is usually applied to the first stages of the rf amplifier in the receiver. This is done because the front end of the rf amplifier is designed to operate with small signals and distortion may occur if large signals are applied (Wells, 1977).

At the output of the rf amplifier, the echo signal has a dynamic range of about 40dB. Most scanners employ some further form of signal compression, often logarithmic, which gives more weight to the low level echoes and reduces the signal range to between 20 and 30 dB. Additional compression may also be applied to isolated large signals so as to prevent them overloading the display. Since only echo amplitudes are used for clinical imaging, the envel ope of the rf waveform is then extracted from the original signal. This process is known as "detection". The detected echo signal is then digitised and temporarily stored in the scan converter, which holds information for a complete image. The purpose of the scan converter is to allow the ultrasound image to be displayed on a standard TV monitor. Echo information goes from the output of the scan converter to the display in TV raster format. The operation of digital scan converters is described by Ophir and Maklad (1979) and Robinson and Knight (1982).

Other forms of signal processing such as dynamic focussing, thresholding, edge enhancement and averaging may also be carried out. Operations done before scan conversion are usually referred to as "pre-processing" and those done after scan conversion are referred to as "post-processing". The signal path described here is similar to that of many scanners, although there are a lot of variations. For example, some machines digitise the rf signal and detection is then carried out digitally.

1.4 MANUAL TGC

One of the skills that an operator has to learn in order to obtain well-balanced images is the ability to set up the TGC controls. Most ultrasound scanners are fitted with several TGC controls. These might adjust the initial gain of the receiver, the rate at which the gain increases with time (the TGC slope) and the delay between the transmission of a pulse and the time at which the gain begins to rise. These features are illustrated in figure 1.2 . One or two other controls are often provided to adjust either the overall receiver gain or the output power of the transmitter. Several of the controls are interactive so that changing one setting may necessitate changing another.

This approach to gain compensation was originally borrowed from ultrasound devices used in non-destructive evaluation. When applied to diagnostic imaging, manual TGC is a crude and often inaccurate method. Its shortcomings are all the more obvious when it is used in the same signal path as the elegant and effective techniques of dynamic focussing and digital scan conversion. Manual TGC can only provide crude gain compensation since the flexibility of the gain control function is restricted; often only a single control adjusts the TGC slope. The same gain function is also applied to all scan lines in the image, despite the non-uniformity of the tissues that may be present. For example, in an obstetric scan, the ultrasound beam may pass in one direction through foetal head and placenta, and in another direction through a deep pool of liquor.

The limited flexibility of manual TGC often leads to poor images. The signal in some parts of the image may be too low, while in other regions the signal saturates, giving a uniform bright white area which

Figure 1.2 Manual TGC : the initial gain, delay and gain slope can be adjusted by the operator.

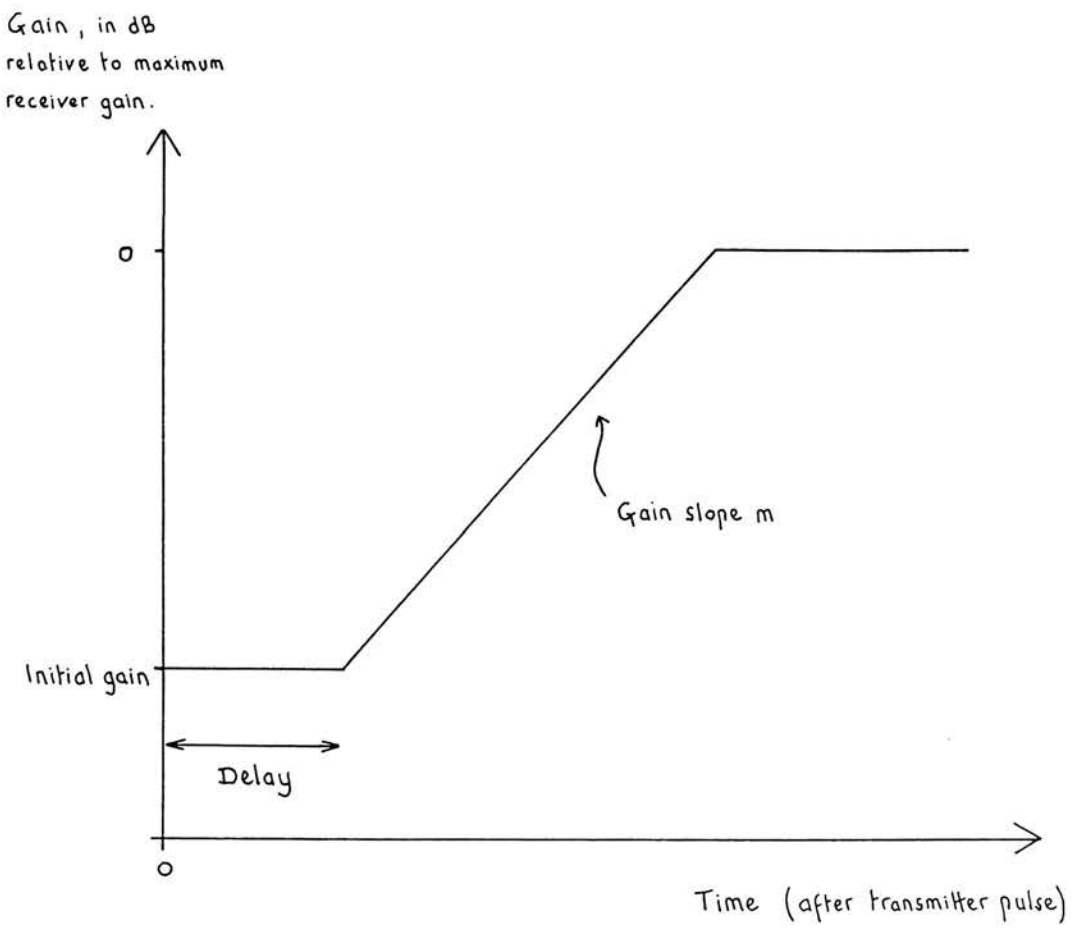

conceals tissue structure. Details of tissue structure which are lost when the echo signal saturates in the rf amplifier cannot be recovered by applying signal compression at a later stage.

Movement of the probe introduces errors into the TGC settings which would involve the operator in an unacceptable amount of control manipulation if he were continually to try to correct them. The higher frequencies of ultrasound now being employed to obtain better resolution are attenuated more strongly in tissue and this leads to larger errors in the TGC. Using 5MHz ultrasound, for example, the compensation for a 1cm depth of liquor should be about 10dB less than for a 1cm depth of soft tissue. In heart work, tissue movement creates an additional problem.

More flexible methods of gain control have been developed, in which the operator can alter the gain in a number of depth ranges independently (Barnes et al, 1975). This approach was first used in cardiology and is now found in many abdominal and obstetric scanners. Better gain settings can be achieved in this way although the gain function is still constant across the image and still requires adjusting when the scan plane changes.

Accurate calculations of TGC values are not yet possible. TGC set manually is both inflexible and time consuming for the operator. It is therefore desirable to look for other ways of obtaining good TGC settings.

1.5 ADAPTIVE SIGNAL PROCESSING

"Adaptive processing" is a term used to describe a wide range of different techniques. Adaptive techniques are concerned with identifying certain features in the observed data. The signal processing

is then adjusted to achieve the desired output. Adaptive techniques can often be fruitful in situations where rigorous calculations are either complex or impossible (Bowen and Brown, 1981; Venetsanopoulos and Cappellini, 1986).

In areas of acoustic imaging other than medical ultrasound, sophisticated adaptive methods are used for a number of applications but not for gain compensation; only simple forms of gain compensation are used. The TGC is either adjusted manually, or automatically using gain control circuits similar to those found in radio receivers. Robinson (1984) describes the use of adaptive processing in seismic migration.

1.6 ADAPTIVE TGC

In the field of medical ultrasound, adaptive TGC is a process in which the scanner uses echo information to set up the gain compensation. The potential benefits of allowing the scanner to control the TGC have been recognised for some time. (McDicken, 1974; DeClercq and Maginness, 1975; Robinson et al, 1979; Melton and Skorton, 1983; Blackwell, 1983). The TGC would become much more versatile, changing for each scan line so as to cope with different tissue types. The TGC would also adapt as the scan plane changed. This should result in improved images.

From the operator's point of view, he or she would be able to make more effective use of their time, spending less time on making control adjustments and more on making a diagnosis. Reducing the number of front panel controls also makes training easier, which is particularly important in hospital departments where there is a high staff turnover.

Very few commercial scanners have been fitted with any form of adaptive TGC, possibly because of a lack of confirmation of its clinical usefulness.

1.7 REVIEW OF ADAPTIVE TGC

The literature concerned with adaptive gain compensation is quite sparse. The first published account of adaptive TGC is given by McDicken (1974) who describes the application of an automatic gain control like those used in radio receivers. The output of the detector in the receiver is integrated, inverted and fed back to control the gain of the rf amplifier. This method was tested in an A scan unit and in a static B scanner with a bi-stable display. The results achieved were quite acceptable in many situations. The main disadvantage was that very large echoes supressed small ones close by.

DeClercq and Maginness (1975) describe an adaptive gain control that generates a single TGC function for the whole image. The range is subdivided into 8 segments and the peak echo signal from each segment is stored on a capacitor. The TGC function is formed by sequentially reading out and smoothing together the stored values. The operator can control the overall gain setting. The gain control was fitted into a real-time cardiac scanner.

Melton and Skorton (1983) describe an adaptive TGC system designed for cardiac scanning. The TGC adapts to the echo pattern along each scan line. The returning echo signal is integrated with a 2μS time constant and then a threshold is applied. Signals above the threshold are identified as coming from myocardium and signals below the threshold are identified as coming from blood. Appropriate TGC slopes are then applied. The system takes account of the focussing properties of the transducer and of frequency dependent atten uation. Tests on fixed hearts showed this technique to be sensitive to the values of the atten uation coefficients used. If the chosen values differed by more than 10% from the actual values, significant artifacts were produced in

the image.

A further paper by Melton et al (1983) reports the use of their system as an aid to the measurement of cardiac ventricle size.

Pincu et al (1986) have used the same thresholding method as Melton and Skorton, but implemented off-line on a computer. Images were digitised prior to application of TGC. Gain compensation and image formation were then carried out in software. This system was also used in cardiac work.

O'Donnell (1983) describes a method of adaptive gain compensation similar in concept to that of Melton and Skorton, but using the first order statistics of the image to set two threshold levels. An image is digitised and an amplitude histogram of the data is constructed. It is assumed that the histogram will contain a dominant peak corresponding to the signals from the predominant tissue type in the image. Signals lying above and below the peak are considered to come from regions of high attenuation and low atten uation, respectively. Each pixel in the image is then assigned one of three attenuation coefficients according to its position in the histogram. A new image is generated using these coefficients. This process of histogram formation and thresholding is repeated until the image is stable. The technique was tested on a tissue phantom and was found to reduce bright-up artifacts distal to regions of low attenuation.

Korba and Cousin (1979) and Greenleaf et al (1983) report using automatic gain control, but only as a means of collecting ultrasound data and not in a way suitable for imaging.

Uchiumi et al (1979) describe ultrasound breast scanning in a water bath using a form of adaptive TGC. The TGC slope is set manually, but the gain rise is triggered by the first echo received from the skin surface and so the start point of the gain function adapts to the shape

of the body.

Other references to adaptive TGC occur in the Japanese literature, but the texts have so far been unobtainable (Uchida et al, 1974; Kobayashi and Sekeba, 1978; Itoh et al, 1979).

1.8 AN OUTLINE OF THIS PROJECT AND THESIS

Given the potential benefits of adaptive TGC and its limited availability in commercial scanners, the first task of this project was to assess the value of a commercial adaptive TGC system in clinical practice. Two clinical trials were carried out in obstetric and abdominal ultrasound. These trials and their results are presented in Chapter 2.

The main task of this project was to develop a versatile gain control system and use it to explore various approaches to adaptive TGC. The need for flexibility immediately suggested using a computer based system - probably a microprocessor development system or small microcomputer. Microprocessors have the disadvantage of being slow. This was not considered to be a serious difficulty, since if a technique suitable for general clinical application was found it could be incorporated later into a hard-wired system that would operate in real-time. The design and construction of the versatile system are described in Chapter 3.

Once built, the versatile system was linked to a real-time scanner and several methods of adaptive TGC were developed and tested using tissue phantoms and by performing computer simulations. The simulations are described in Chapter 4. The most promising adaptive methods were evaluated clinically.

The various methods of adaptive TGC that were developed take the form of computer algorithms. Chapter 5 presents six of these

algorithms. The chapter is divided into several sections. The first section provides an introduction and each of the other sections describes one of the algorithms, its application, computer simulation and clinical trial.

The results of all the algorithms are summarised and discussed in Chapter 6.

The final chapter briefly discusses further developments of adaptive TGC - the implementation of a hard-wired system and the design of an interactive TGC system using a touch-sensitive screen.

Chapter 2

CLINICAL TRIALS OF A COMMERCIAL ADAPTIVE TGC SYSTEM

2.1 INTRODUCTION

A number of ultrasound scanners have been built in recent years which incorporate some form of adaptive gain control either as an alternative to the manual gain controls or as a replacement for them. As a first step towards determining the value of adaptive TGC in general clinical practice it was decided to perform clinical trials of a commercial system in routine obstetric and abdominal scanning (Pye et al, 1983; Pye et al, 1985). The scanner used was a MARTI real-time mechanical sector scanner manufactured by Fischer Ultrasound Ltd., and fitted with both adaptive and manual gain controls. The adaptive gain control operates by measuring the mean signal level within each of twelve 2cm depth ranges (see figure 2.1). A single TGC function is then automatically set up and applied to all the scan lines in the image. The TGC adjusts so that the average signal level from each depth range is approximately the same, given the restriction that the gain must change smoothly with depth. The system has a response time of about half a second. The only variable that can be adjusted by the operator is the overall gain.

This technique is similar to that of DeClercq and Maginness, described in section 1.7, except that it uses the mean rather than the peak echo signal within each depth range.

In addition to the adaptive TGC, the scanner possesses five manual TGC controls. Two of these are used to set the transmitter output power in 2dB and 10dB steps. The other three determine the initial gain of the receiver, the TGC slope and the delay between the transmission of a pulse and the time at which the gain begins to rise.

Figure 2.1 The commercial adaptive TGC measures the echo signal level in twelve 2 cm depth ranges :

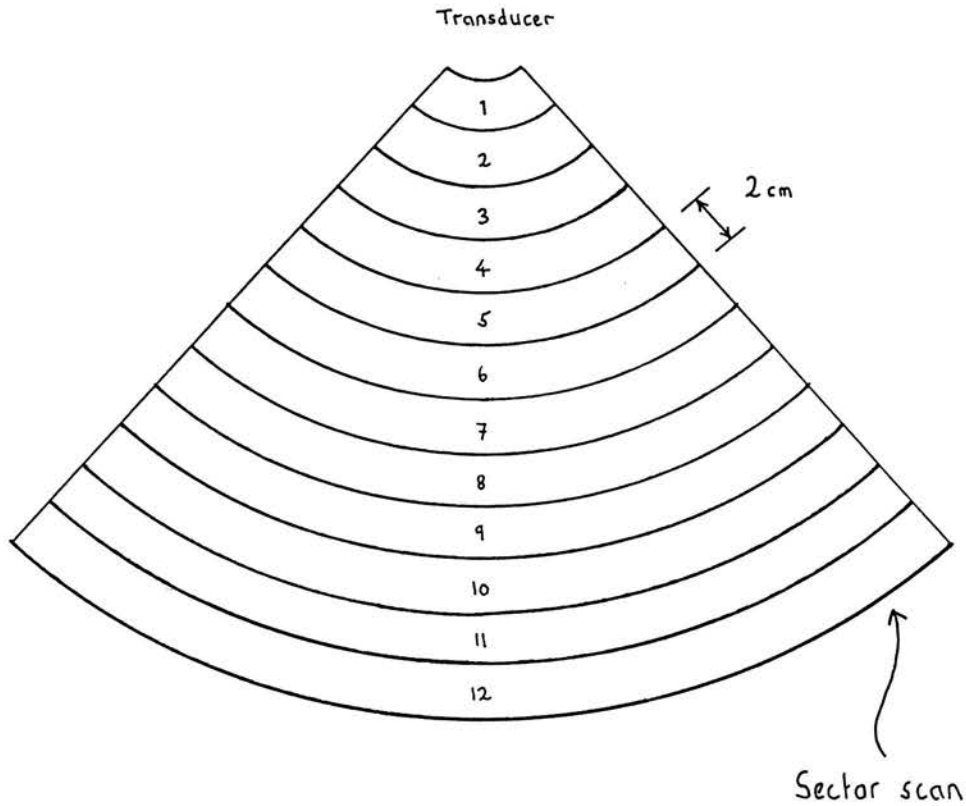

The clinical trials assessed the adaptive system in two ways:

(1) by a comparison of the images produced using the manual and adaptive gain controls;

(2) by estimating the different amounts of control manipulation needed to use the manual and adaptive controls.

A number of individuals are identified in this text by their initials. Their full names are contained in the acknowledgements section at the front of the thesis.

2.2 OBSTETRIC TRIAL

2.2.1 METHOD

Photographs of 100 pregnancies were obtained with gestations ranging from 8 weeks to 40 weeks. Both 3.5MHz and 5.0MHz probes were used. The obstetric images were recorded on grey tone film using a multi-format camera by four experienced radiographers over a period of eight weeks. The photographs were taken in pairs, by first setting up the manual controls and recording the image, and then, without moving the probe, switching on the adaptive system and recording the new image. So as to minimise any changes in the structures within the scan plane the time between the photographs was kept as short as possible - typically 30 seconds. Various sections through the uterus were used and the manual and adaptive control settings were noted for each pair of photographs.

As a measure of the amount of control manipulation involved, the number of control adjustments that had to be made in order to produce each image was counted.

2.2.2 RESULTS

A total of 119 pairs of photographs were obtained, of which 13 were not comparable due to large fetal movements. The remaining pairs of comparable photographs were judged by a consultant radiologist (SRW) and a hospital physicist (DCM) both experienced in ultrasonic imaging. The images were judged by the radiologist on the diagnostic information they contained, and by the physicist on the presentation of echo signals in the whole image. There was no communication between the judges. Each judge viewed all the photographs at one sitting. One pair of photographs at a time was presented on a viewing box and the area surrounding them was masked off to prevent glare. The manual and adaptive images were randomly positioned to left or right. The judges were asked to say which image they preferred, or whether they thought there was no significant difference in overall image quality. The results are presented in table 2.1 .

If the manual and adaptive methods produced no significant differences, we would expect there to be roughly equal numbers of manual and adaptive images preferred. Using a two tailed χ^2 test due to McNemar (Everitt,1977) , we find that $P<0.001$ for both the radiologist's and physicist's results. Both judges thus preferred significantly more adaptive than manual images.

Examples of the images obtained are contained in Appendix 1 .

A common defect in the images produced using the manual gain controls was regions of saturation within which structural details were obscured. This frequently occurred at the anterior and posterior uterine walls, which are composed of groups of strong reflectors and are often normal to the ultrasonic beam. Since the two walls are separated by several centimetres it is not always possible to compensate

Table 2.1 Obstetric trial of commercial adaptive TGC

Number of patients	= 100
Total number of pairs of images	= 119
Number of comparable pairs of images	= 106

CATEGORY	PHYSICIST	RADIOLOGIST
Adaptive image preferred	48	48
No overall difference	53	48
Manual image preferred	5	10
	$\chi^2 = 33.3$	$\chi^2 = 23.6$
	$P < 0.001$	$P < 0.001$

accurately by using the manual controls.

Saturation also occurred often at structures lying within or below regions of liquor. Since the attenuation of the ultrasound beam in liquor is negligible, manual TGC geared to attenuation in tissue will overcompensate.

The improvements produced by the adaptive system were mainly due to a reduction in the amount of saturation in these situations. Since the gain of this system is constant across the scan plane, there was no evidence of compensation for shadowing due to limbs or bones.

The photographs in which there were no marked differences between the manual and adaptive images usually contained no strongly reflecting surfaces normal to the ultrasonic beam, nor any regions of fluid for which the manual TGC could not compensate adequately.

In 10% of the photographs the adaptive images were inferior to the manual ones. In all cases this was due to an increase in the noise level in large volumes of liquor. Where liquor extended across the width of the image the adaptive TGC measured a very low average signal level at that depth and compensated by applying a large gain, making noise and multiple reverberation artifacts clearly visible.

The images in which the adaptive TGC improved upon or matched the manual TGC were obtained using both 3.5MHz and 5.0MHz probes with pregnancies between 8 and 40 weeks (the range of pregnancies included in the study).

The inferior adaptive images occurred in pregnancies later than 23 weeks, when there are pools of liquor large enough to fill the width of the image.

2.2.3 CONTROL MANIPULATION

Of the total number of control adjustments used to produce the

paired photographs, 80% were used for the manual images and 20% for the adaptive images. In general, two or three adjustments of the manual controls were made per scan, increasing to about 10 in the cases where it was difficult to produce a well balanced image. No more than two adjustments of the adaptive TGC were ever necessary in one scan and for a series of pregnancies at the same stage the adaptive TGC could be set initially and then left without adjustment.

The adaptive system clearly involves the operator in less control manipulation. This result is not surprising since, like many scanners, the MARTI has five manual controls, several of which are interactive so that changing one setting may necessitate changing another. Manipulating five controls also diverts the operator's attention from the screen, whereas a single control can be adjusted without looking at the instrument panel. This is an advantage, since delicate adjustments of the probe are necessary to image small structures within the uterus and anything that distracts the operator's attention makes this task more difficult.

Many modern scanners are fitted with manual TGC which allows the gain or slope to be set independently in a number of depth ranges. This is usually done with a set of slider pots. Such an arrangement has at least as many gain controls as the MARTI, and requires as much adjustment.

2.3 ABDOMINAL TRIAL

2.3.1 METHOD

The abdominal trial followed the same protocol as the obstetric trial. The clinical examinations were performed by two experienced radiologists (SRW and HM) over a period of six months. A 3.5MHz probe

was used and pairs of images were recorded using manual TGC and adaptive TGC. The images were of the normal anatomy and pathology of the liver, kidney, gallbladder, bladder, pancreas and spleen.

2.3.2 RESULTS

A total of 115 pairs of photographs were obtained from 100 patients, of which 7 pairs were not comparable due to movement of the probe or patient. There were 50 of the comparable pairs which showed pathology and 58 were of normal anatomy. The comparable pairs of photographs were judged by a consultant radiologist (SRW) and a hospital physicist (NMcD). The results are presented in table 2.2 . For the physicist's results, $P<0.001$ which is highly significant. For the radiologist's results, $P>0.25$ which is not significant. The comments of the judges showed that this variation was due to the different criteria they were using. There were many pairs for which the physicist thought the adaptive image had a better overall balance, but the radiologist judged the images to be similar because he did not see any improvement in the clinically important structures.

The adaptive TGC control usually produced a well-balanced image with good grey scale and no large areas of saturation. It tended not to produce acoustic enhancement behind regions of fluid. This was sometimes regarded as a useful feature by the radiologist; for example, when imaging structures deep to ascites, renal obstruction or behind the gallbladder or bladder; and sometimes as a poor feature, such as when trying to confirm the identity of a cyst. The adaptive TGC did not affect the acoustic shadows cast by gallstones and kidney stones and never altered the appearance of liver metastases. Examples of the pairs of images obtained are contained in Appendix 1 .

Table 2.2 Abdominal trial of commercial adaptive TGC

Number of patients	= 100
Total number of pairs of images	= 115
Number of comparable pairs of images	= 108

CATEGORY	PHYSICIST	RADIOLOGIST
Adaptive image preferred	66	17
No overall difference	30	79
Manual image preferred	12	12
	$\chi^2 = 36.0$	$\chi^2 = 0.55$
	$P < 0.001$	$P > 0.25$

2.3.3 CONTROL MANIPULATIONS

I was not present when all the abdominal images were recorded and so an accurate tally of the number of control adjustments was not kept. It was noted that the adaptive system required fewer adjustments than the manual TGC. Both radiologists found this an advantage, since having to pause to adjust controls makes it more difficult to perform a thorough search through the abdomen where the different tissues present may require the gain settings to be changed several times.

2.4 CONCLUSIONS

The trial of an adaptive TGC system in routine obstetric and abdominal work demonstrated that for 90% of patients it was capable of producing images as good as, or better than, the manual TGC. Using the adaptive system in obstetric imaging, only about one quarter the number of control manipulations per scan were required.

After the scanner had been in use for three months, all four radiographers and both radiologists preferred to use the adaptive rather than the manual gain controls. However, the manual controls were employed in particular circumstances where it was necessary to emphasise a specific region rather than to try to obtain a well balanced image. For example, to confirm the nature of a cystic structure, to measure BPD in an obese patient or to image a retroverted uterus. For this reason it is desirable to have adaptive TGC as well as, rather than instead of, manual TGC.

It is concluded that the potential benefits of adaptive TGC described in Chapter 1 can be achieved in routine clinical practice. The next stage of this project was to develop a versatile TGC system that could be used to investigate many approaches to adaptive TGC and obtain further improvements in image quality.

Chapter 3

DESIGN AND CONSTRUCTION OF THE VERSATILE TGC SYSTEM

3.1 INTRODUCTION

This chapter describes the design and construction of a versatile TGC system for use with real-time ultrasound scanners. The versatile system has since been used with a Z series machine manufactured by GL Ultrasound Ltd. Only the novel aspects of the system are thoroughly covered here; the design and operation of ultrasound scanners are described in other texts (Wells, 1977; McDicken, 1981; Hunt et al, 1983).

It was decided to base the versatile TGC system around a commercially available microcomputer and to design and build the interface electronics required to link the microcomputer to a real-time scanner. This approach has several advantages. A microcomputer can be used to test many gain control algorithms and it is more powerful than a simple microprocessor development system. If necessary, the microcomputer system could be extended by purchasing extra hardware. High and low level language packages are available for most microcomputers. An introduction to microcomputers is contained in the excellent text "The Art of Electronics" by Horowitz and Hill (1982).

A microcomputer offers great flexibility, but at the cost of reduced speed. The control centre of a microcomputer is a microprocessor, and microprocessors carry out tasks more slowly than dedicated hardware. The interface electronics was thus designed to relieve the microcomputer of as much work as possible.

The format of this chapter is as follows: an overview of the versatile system (section 3.2), a detailed account of the hardware (sections 3.3. to 3.5), and a general description of the software

(section 3.6).

3.2 OVERVIEW OF THE VERSATILE SYSTEM

The versatile system performs three principal tasks: collecting echo data, using the echo data to generate TGC functions and applying the TGC functions to control receiver gain. Figure 3.1 is a block diagram of the system.

The microcomputer can read the number of scan lines per frame via a digital input-output port (IO port). It then selects up to 32 of these lines to be digitised and stored. The selection is made by writing to a special area of memory called the "line map". Once this has been done the chosen lines are digitised from the next complete scan frame and are stored in an area of memory called the "echo map". The signal to be digitised is taken from the input of the receiver in the scanner and amplified by a second receiver external to the scanner. The gains of both receivers are individually controlled by the microcomputer. The use of two receivers increases the flexibility of the system; different TGC functions can be used for echo data collection and for image display.

The digitisation and storage of echo data take place independently of the microcomputer which can continue with other tasks.

Once the echo data has been collected it is processed by programs written in a combination of Z80 assembly language and Fortran IV, and TGC functions are generated to control both receivers. The TGC functions are stored in areas of memory called the "gain maps". There are two gain maps, one for each receiver. Each gain map contains TGC information for a complete scan frame. Just before the TGC function for a particular line is required, it is read at 4MHz out of its gain map into a buffer memory. Then, while echoes are arriving at the transducer,

Figure 3.1 Versatile TGC System

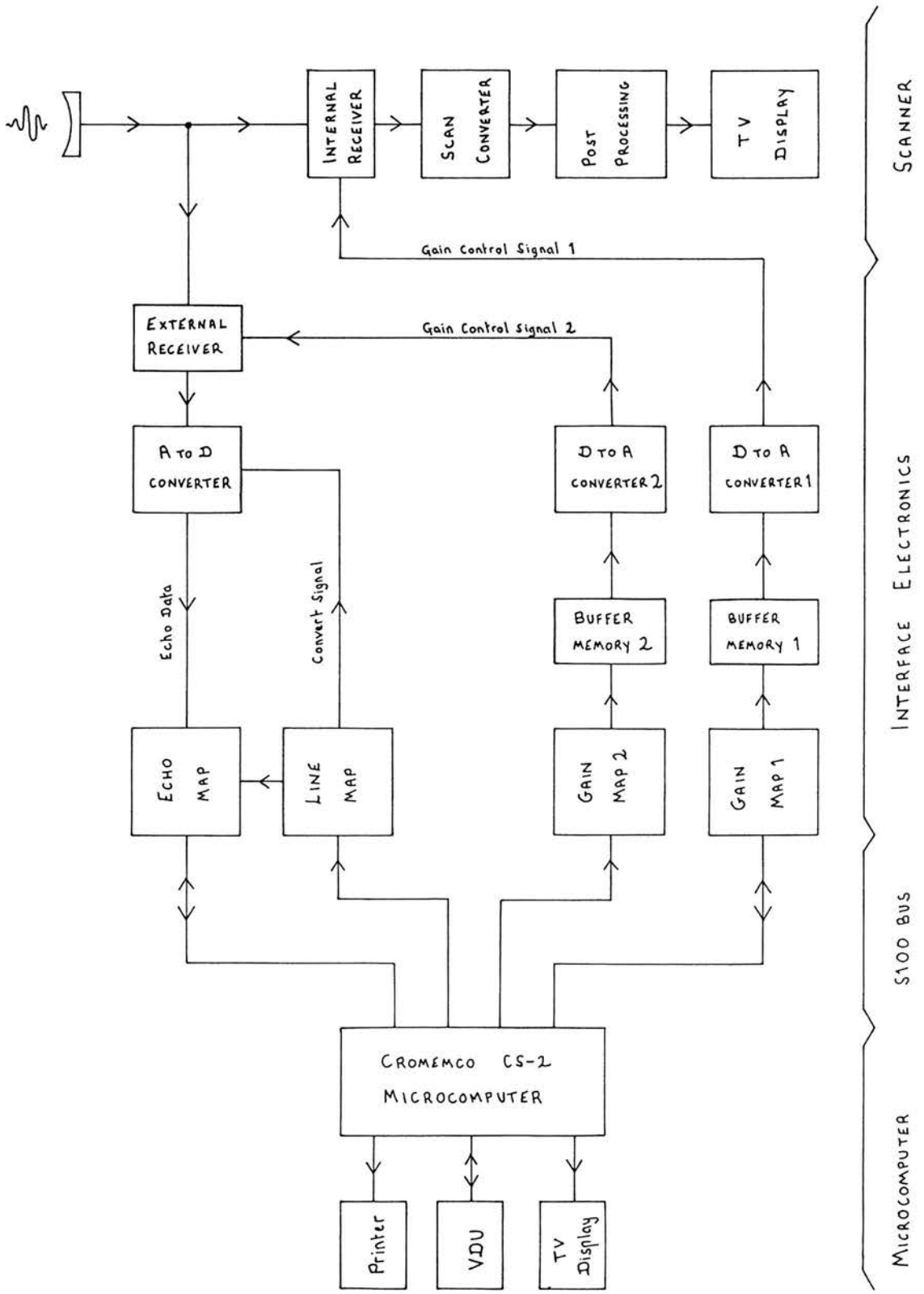

the data is read out of the buffer memory at 250kHz. The digital values are transformed into analogue voltage signals by a D to A converter and they are then smoothed and applied to the gain control line of the appropriate receiver. The use of buffer memories maximises the time for which the microcomputer can have access to the gain maps.

The hardware used in this project can be divided into three parts:

(1) Microcomputer.

(2) Real-time scanner.

(3) Interface electronics specially built for the versatile TGC system.

These are described in sections 3.3 to 3.5.

3.3 MICROCOMPUTER

3.3.1 Cromemco CS-2

The microcomputer chosen for this project was a Cromemco CS-2. This was one of the most powerful machines available at the time which could be purchased with the equipment grant. It has the advantages of an S100 bus and a CP/M based operating system, both of which are widely used and well documented. The CS-2 also has 21 bus slots, 14 of which are available for mounting the interface electronics. Disk storage is provided by dual 5.25 inch floppy disk drives. S100 microcomputers and interfacing techniques are thoroughly covered by Libes and Garetz (1981) and the CP/M operating system is described in detail by Hogan (1982).

Seven S100 computer cards were purchased:

(1) Z80/68000 dual processor card. Although this card carries

two microprocessors, the CP/M based operating system is designed for the Z80 and leaves very little scope for using the 68000. The 68000 can only be used by programs handwritten in machine code.

(2) Floppy disk controller card.

(3) RAM memory card with 256K bytes of memory.

(4) UART digital interface carrying two serial and two parallel ports. This was used for sending data to a dot matrix printer.

(5) Parallel IO card carrying eight 8 bit parallel ports. These were used for obtaining status information from the interface.

(6) Graphics display card with 512 x 512 x 4 bit resolution. This was used for displaying echo data and TGC functions.

(7) Fast arithmetic card carrying eight AM9511A dedicated arithmetic chips. This was purchased to increase the computing speed of the CS-2. The eight arithmetic chips can run in parallel.

Two language packages were purchased: Fortran IV and Z80 Macro Assembler.

3.3.2 Organisation of the microcomputer memory

The Z80 is an 8 bit microprocessor and so can address a maximum of 64k bytes of continuous memory. The 256k byte memory card is arranged in four 64k pages. Each page is divided into two 32k blocks, which can be switched on and off independently. Individual pages are selected by the microprocessor sending a command byte to an IO control port. The memory selection on the 256k memory card is controlled by a PROM. The

PROM supplied by the manufacturers was replaced with a modified PROM so that the echo map, line map and gain maps could be incorporated as separate pages of memory. The organisation of the microcomputer memory is shown in figure 3.2 and is summarised below. (Numbers followed by H are written in hexadecimal.)

Page 0: the top 15k and the first 100H of page 0 contain the CP/M compatible operating system called CDOS. The remainder of the low 32k of page 0 is available for user programs.

Pages 1, 2 and 3 are available for data storage, though they are not in fact used by any of the gain control algorithms.

The echo map page contains the 32k of the echo map and the low 32k of page 0.

The line map page contains the 256 locations of the line map and the low 32k of page 0.

The gain map page contains the 16k of gain map 1, the 16k of gain map 2 and the low 32k of page 0.

3.4 REAL-TIME SCANNER

The Z series scanner required some modification before it could be used with the versatile TGC system. In order to obtain the echo signal, an extra turn of wire was put around the input transformer of the receiver in the scanner and connected via a short coaxial cable to the input of the external receiver. The signal coming from the probe thus goes to both receivers. Noise picked up by the short coaxial cable raised the noise level at the input of the internal receiver by $< 0{\cdot}5$ dB . This increase is not visible on the image display.

The only other signal that the microcomputer requires from the scanner is the PRF. (Pulse Repetition Frequency - this signal is active while echoes are being collected by the scanner.) The PRF is available

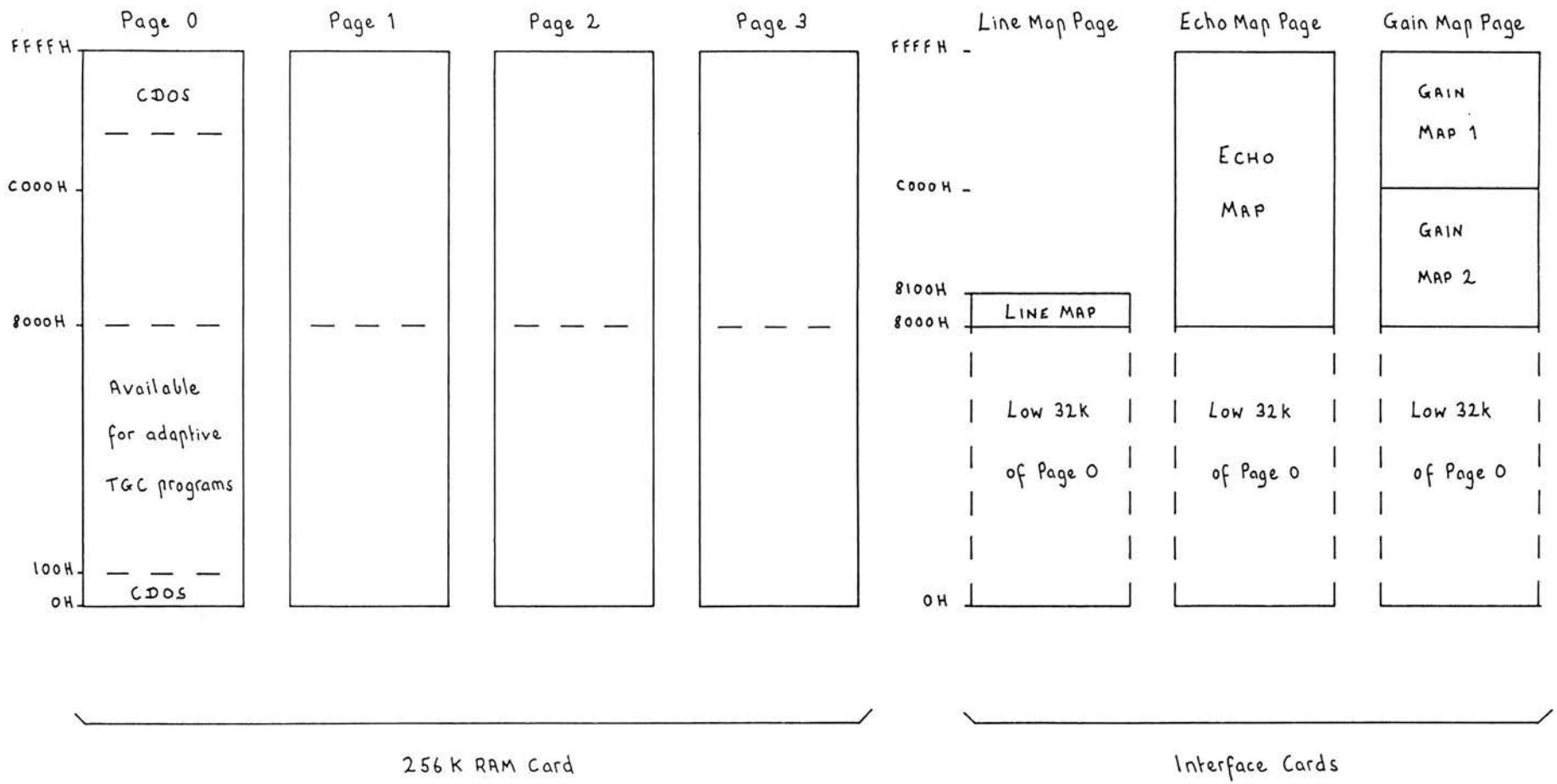

Figure 3.2 Organisation of the microcomputer memory.

at an external socket on the Z machine.

A switch was inserted into the gain control line of the Z machine so that the operator can select either the scanner's own manual TGC or the versatile TGC.

The Z machine can operate with three types of ultrasound probe: a mechanical sector scan probe with rotating transducer head, a mechanical sector scan probe with a single oscillating transducer, and a linear array. Of these, the only one that presents a problem to the versatile TGC is the oscillating probe. The problem arises because the oscillating probe produces two frames of scan lines during one complete oscillation. The versatile TGC system can set a different TGC function for each scan line. The digital control logic may be simplified if the transducer always starts its sweep from the same side of the image. The rotating probe and linear array always start scanning from the same side of the image, but the oscillating probe scans from alternate sides. It was decided to implement the simpler logic design and not to use the oscillating probe with the versatile TGC.

3.5 INTERFACE ELECTRONICS

The interface electronics was built on five S100 computer cards which are mounted on the microcomputer bus. Four of these cards carry the echo map, line map, gain maps and their control circuits and the fifth carries the analogue to digital (A to D) converter. Figure 3.3 shows a photograph of one of the cards: the others are constructed in the same way. So as to minimise noise the external receiver is mounted in a separate box beside the internal receiver.

The design and construction of the electronics is described in the

Figure 3.3 : One of the five S100 cards carrying the interface electronics.

(a) Top view

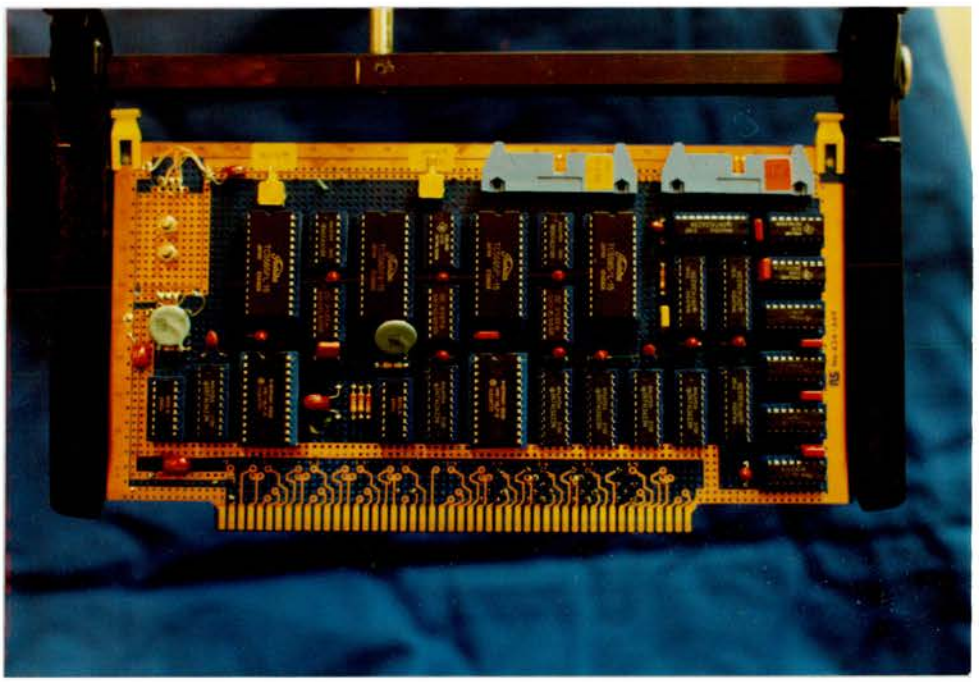

(b) Underside

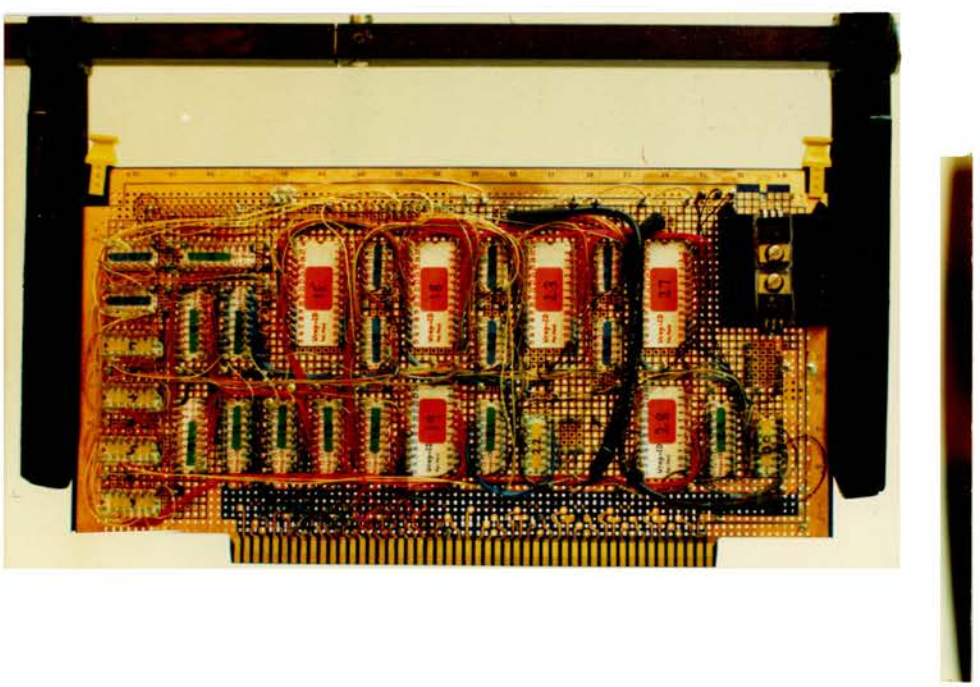

next eight sections under the following headings:

(1) External receiver.

(2) Analogue to Digital Converter.

(3) Echo Map and Line Map.

(4) Simulated PRF signal.

(5) Gain Maps - Design.

(6) Gain Maps - Operation.

(7) Digital to Analogue Converters.

(8) System Response Time.

3.5.1 External Receiver

The external receiver was taken from a MARTI scanner, which uses a receiver identical to those in the Z machines. The receiver consists of a three stage synchronously tuned rf amplifier followed by a fixed logarithmic compression stage and then detection. The logarithmic compression was removed from the external receiver (see section 3.5.2).

The input of the rf amplifier is protected from high transmitter voltages by a pair of diodes. A small transformer is included in the signal path to help match the impedances of the transducer and amplifier. The voltage gain of the amplifier can be varied through 60dB. A signal applied to the gain control line of the receiver and changing linearly from 0 to 7 volts results in the overall gain of the receiver changing from 20 to 80dB (see figure 3.4). A diode network transforms the linear control signal into a roughly exponential signal which is applied to the first and second stages of the amplifier. This signal actually deviates from a true exponential curve by up to 6 dB. So that the microcomputer can control the gain of the receivers accurately, the internal and external receivers were calibrated and

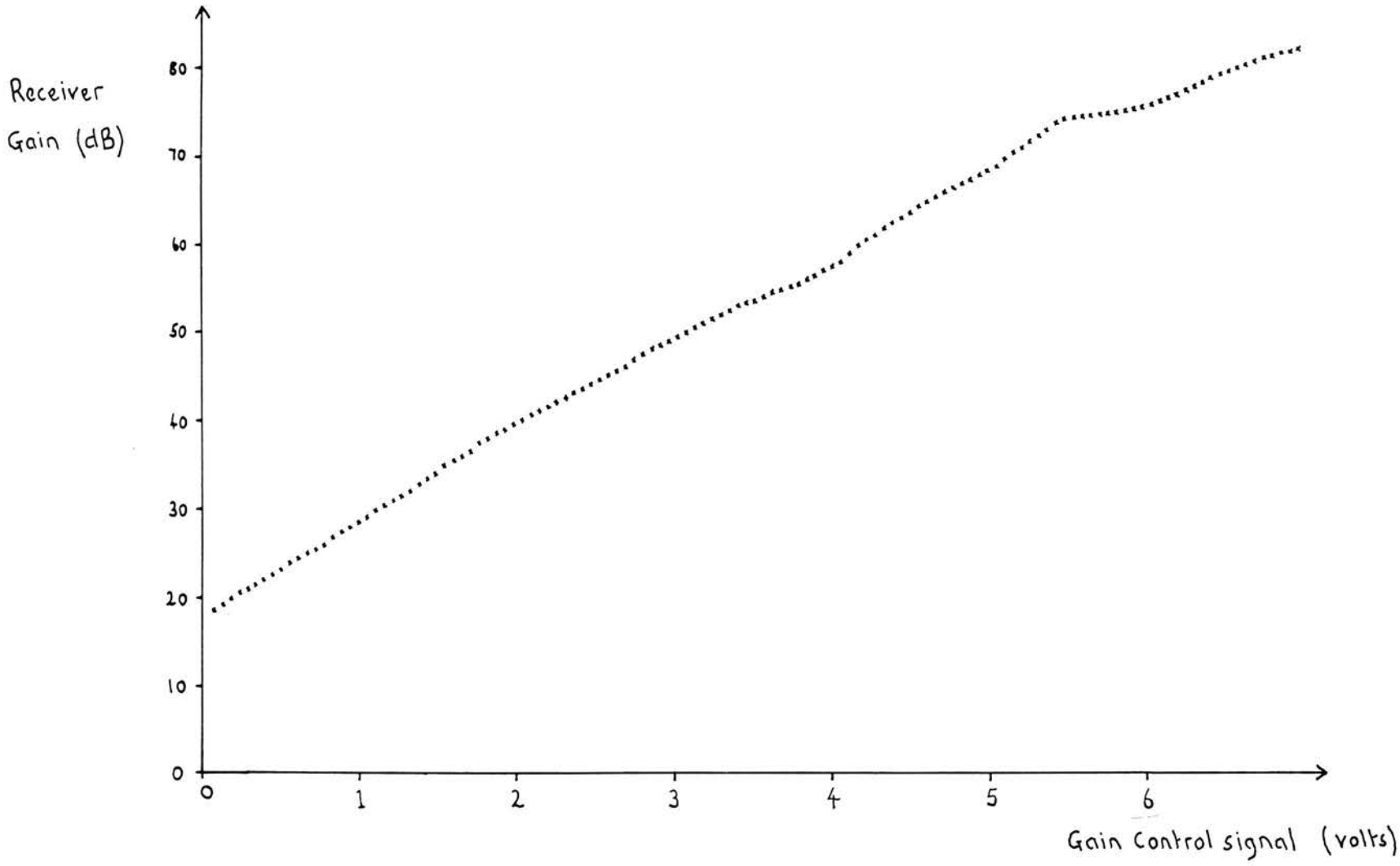

Figure 3.4 Receiver Gain Control

look-up tables were written to allow the microcomputer to convert from control voltage to gain and vice versa. The look-up tables are incorporated into the gain control programs and allow the gain to be set to within 0.5dB.

3.5.2 Analogue to Digital Converter

The most widely used method of acquiring ultrasound data for subsequent processing is to convert the analogue voltage signal directly into digital form using a fast A to D converter, and then store the data in digital memory. This method is well suited to the present application since once the data is in digital memory it can readily be accessed by the microcomputer.

How often does an A to D converter need to sample the echo signal? The sampling theorem states that the minimum sampling rate necessary to completely recover a bandwidth limited signal is at least twice the maximum frequency component of the signal. The presence of wideband noise and the fact that few real signals have a well defined upper frequency limit mean that it is usually necessary to sample at three or four times the maximum significant frequency. For the same reasons, aliasing cannot be entirely excluded.

Since the microcomputer controls the presentation of echo amplitudes without explicitly attempting to measure attenuation, there is no need to retain the phase information in the echo signal and it is only necessary to sample the detected signal.

The upper frequency limit of detected pulses from a 3.5MHz transducer was measured using a Marconi model TF2370 spectrum analyser. The transducer formed part of the mechanical sector scan probe of a MARTI scanner. It was positioned so as to transmit pulses into a water bath and pick up the echoes returning from a plane reflecting surface

10cm from the probe face. The signal to the spectrum analyser was taken immediately after the detector in the receiver. The maximum frequency component detectable above the noise level was 1.2MHz. Sampling at three times this frequency would give a sampling rate of 3.6MHz.

The dynamic range of the echo signal at the input of the receiver can be greater than 100dB - no A to D converter able to work at megahertz sampling rates can match this range. The receiver can reduce the dynamic range of the echo signal using TGC and fixed compression. However, the effects of both TGC and any fixed compression have to be included in the calculations made by the microcomputer. Fixed compression by itself cannot reduce the dynamic range of the echo signal to that of the A to D converter. It would be a waste of computing time to include both TGC and fixed compression if TGC alone is sufficient. Clearly this depends on the range of the TGC and the A to D converter. The gain of the external receiver is variable through 60dB. This was considered sufficient to reduce a 100dB dynamic range echo signal to the 48dB range of an 8 bit A to D converter. The logarithmic compression stage was removed from the external receiver.

The specifications of the A to D converter are thus a minimum sampling rate of 3.6MHz and 8 bit accuracy. There were few A to D converters available at the time of construction which met these requirements. It was decided to purchase an 8 bit parallel (flash) converter, type TDC10075, manufactured by TRW. This is capable of sampling at 20MHz. It was supplied already mounted on a small evaluation board so that little effort was needed to interface it to the receiver and microcomputer. The microcomputer has a 4MHz system clock, and it was convenient to use this as the sampling signal for the A to D converter.

The output of the detector in the receiver starts to saturate at

2.7V and clips at 3.3V. The A to D converter is set up to give maximum output (255) when the detector output is 2.55v.

3.5.3 Echo Map and Line Map

The limit of penetration for ultrasound in soft tissue averages 400 to 500 wavelengths or 180 to 220mm at 3.5MHz assuming the velocity of ultrasound in soft tissue to be 1540 ms^{-1}. Abdominal and obstetric scans rarely provide useful information beyond about 200mm.

Each scan line is sampled at 4MHz. This corresponds to sampling at range intervals of 0.193mm. It was decided to take 1024 samples per scan line - from the skin surface to a depth of 197mm. 1024 samples is a convenient number for two reasons; it allows all the clinically important information to be gathered, and since $1024 = 2^{10}$ the design of the digital circuitry is made easier.

It would have been useful to store every scan line in an image. The number of lines that can be held at one time was actually determined by the architecture of the microcomputer. The low 32k of the microcomputer's address space is available for user programs. Given that each scan line of data occupies 1k bytes, it was convenient to design a data store capable of holding 32 lines. This store is the echo map. The echo map occupies 32k and can be accessed by user programs in the low 32k of memory without any special arrangements being necessary for positioning the user program code.

The Z machine operating in 80° mechanical sector mode uses a minimum of 100 scan lines per frame, increasing to 255 at low frame rates. Since only 32 lines can be stored, the microcomputer has to have some means of selecting which lines it requires. A special area of memory called the line map was included in the interface, and by writing into it the microcomputer can select which scan lines are to be

digitised. Figure 3.5 is a block diagram of the echo and line maps and their control logic.

The interface electronics counts the number of lines per frame using the PRF signal and latches this number into one of the microcomputer IO ports. The microcomputer reads this port and decides which lines it requires. For example, the first 32 lines of the frame, 32 lines evenly spaced across the frame or perhaps just 8 lines from part way through the frame. The line map is a 256 x 1 bit memory, each bit corresponding to a scan line. The bit with the lowest address corresponds to the first line in the scan. The microcomputer selects the line map page of memory and writes a "1" into the locations in the line map corresponding to lines it requires stored and a "0" into the locations corresponding to lines it does not want.

When the line map has been filled and the microcomputer selects another page of memory, a BUSY flag is raised in the interface and echo data is digitised and stored from the next complete scan. The "1"s and "0"s stored in the line map are clocked out, one bit before each transmitter pulse. If the bit is a "1" the 256 μs of echo data following the transmitter pulse are digitised.

The digitisation and storage of echo data continue independently of the microcomputer which can check the BUSY flag periodically to see if data collection is complete.

The echo map comprises four 8k x 8 static RAM memory chips. During data storage the memory chips are addressed by the echo map line and sample counters. When the microcomputer selects the echo map page, the echo map occupies address space 8000H to FFFFH. The first scan line occupies 8400H to 87FFH and so on.

If the microcomputer tries to access either the line map or echo map while data acquisition is in progress, it is held in a wait-state by

Figure 3.5 Echo Map and Line Map

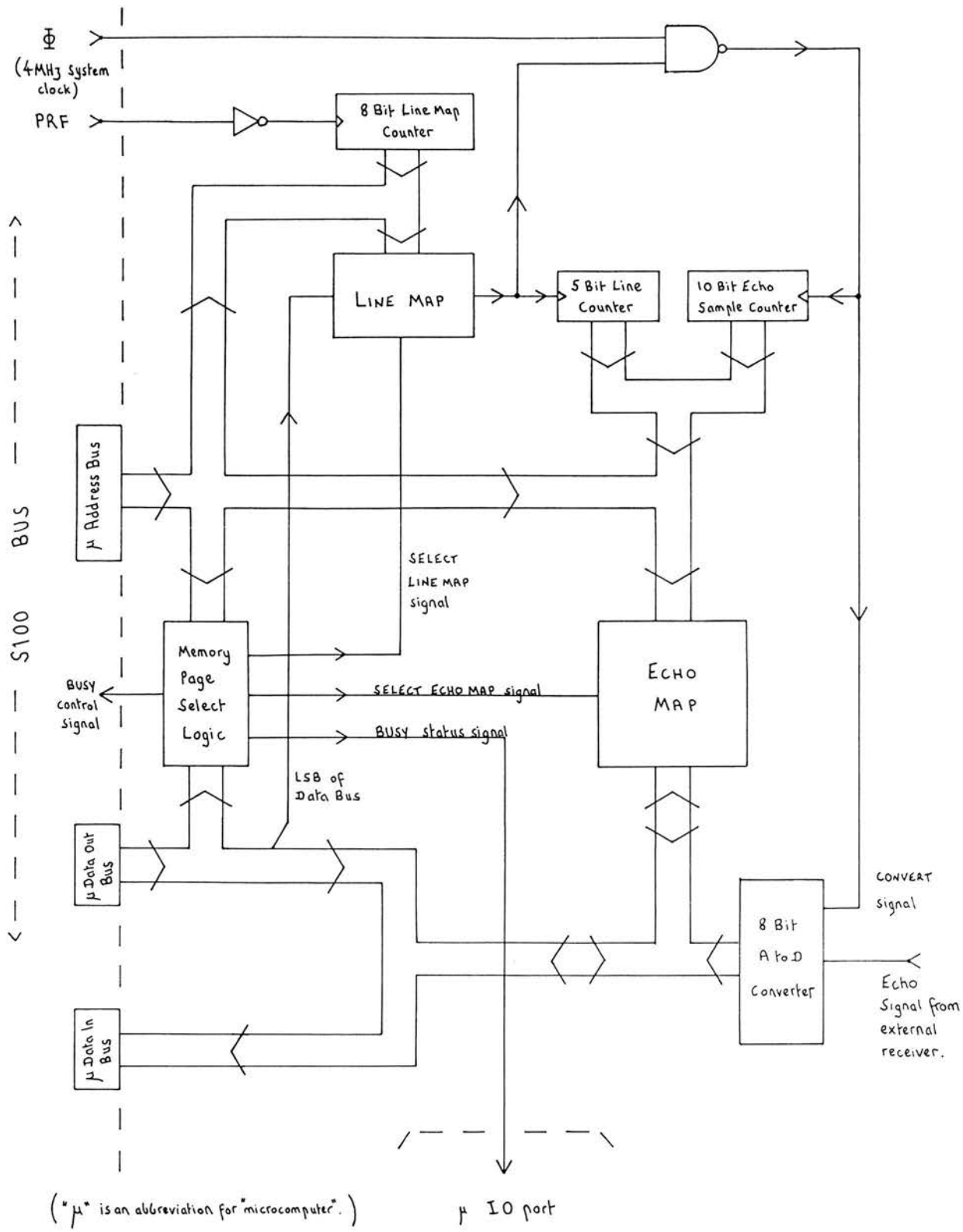

the interface until the end of the frame from which data is being collected. This prevents the microprocessor address lines and the echo map counters from clashing on the address bus.

3.5.4 Simulated PRF signal

The interface contains circuitry to simulate the PRF signal of the scanner. This simulated PRF signal can be switched on when the scanner is disconnected from the system and it allows the versatile TGC to be tested without using a scanner. Echo signals are simulated by connecting the attenuated output of an rf signal generator to the external receiver input.

The simulated PRF signal was particularly useful when the interface was being constructed. It provides a stable signal with predictable timing and a known number of lines per frame. This made the task of checking timing, signal levels and detecting glitches much easier.

3.5.5 Gain Maps - Design

Even if the desired form of a TGC function is known exactly, the TGC generated digitally by the microcomputer can only approximate to it due to two limitations:

(1) The TGC function can only change at discrete intervals in range, denoted here by Δx. The size of Δx is determined by the number of gain values allocated to each scan line in the gain maps.

(2) The precision of the TGC is limited. In other words, the value of the gain can only change by discrete amounts. The smallest amount (denoted here by Δg) is determined by the number of bits allocated to each gain value in the gain maps.

The next two sections discuss how small Δx and Δg must be so that their finite sizes are not apparent in the image.

3.5.5.1 Range Interval

Consider the simple situation shown in figure 3.6a where a transducer insonates two regions separated by a distinct boundary. Region B, furthest from the transducer, backscatters ultrasound much more strongly than region A. In vivo, region A might be the placenta and region B the posterior uterine wall. The desired TGC function is shown in figure 3.6b . Slopes of m_A and m_B dB cm^{-1} compensate for attenuation in regions A and B respectively. The decrease in gain at the boundary reduces the difference in signal level between the regions so as prevent overloading the A to D converter or the display.

If the boundary between regions A and B falls midway through a range interval in the TGC function, then the actual TGC will depart considerably from the ideal TGC for $\frac{\Delta x}{2}$ on either side of the boundary (see figure 3.6c). How small must Δx be so that this departure will not be visible on the display? Intuitively, we might say that $\frac{\Delta x}{2}$ should be less than the axial resolution of the scanner. The axial resolution of a scanner operating at 3.5MHz is about 1mm. An estimate of the necessary size of Δx would thus be $\frac{\Delta x}{2} \simeq 1mm$ or $\Delta x \simeq 2mm$.

The restriction on the size of Δx can probably be relaxed somewhat if the TGC function is smoothed slightly. The eye is a sensitive edge detector and so the departure of the echo amplitudes from their correct presentation will be less noticeable if there are no sharp edges in the TGC function.

It was decided to use a range interval of about 3mm. This corresponds to a go-return time interval of 4 μs, obtained by dividing the 4MHz system clock by 16. There are thus 64 independent TGC values

Figure 3.6 TGC range interval Δx (see text for details).

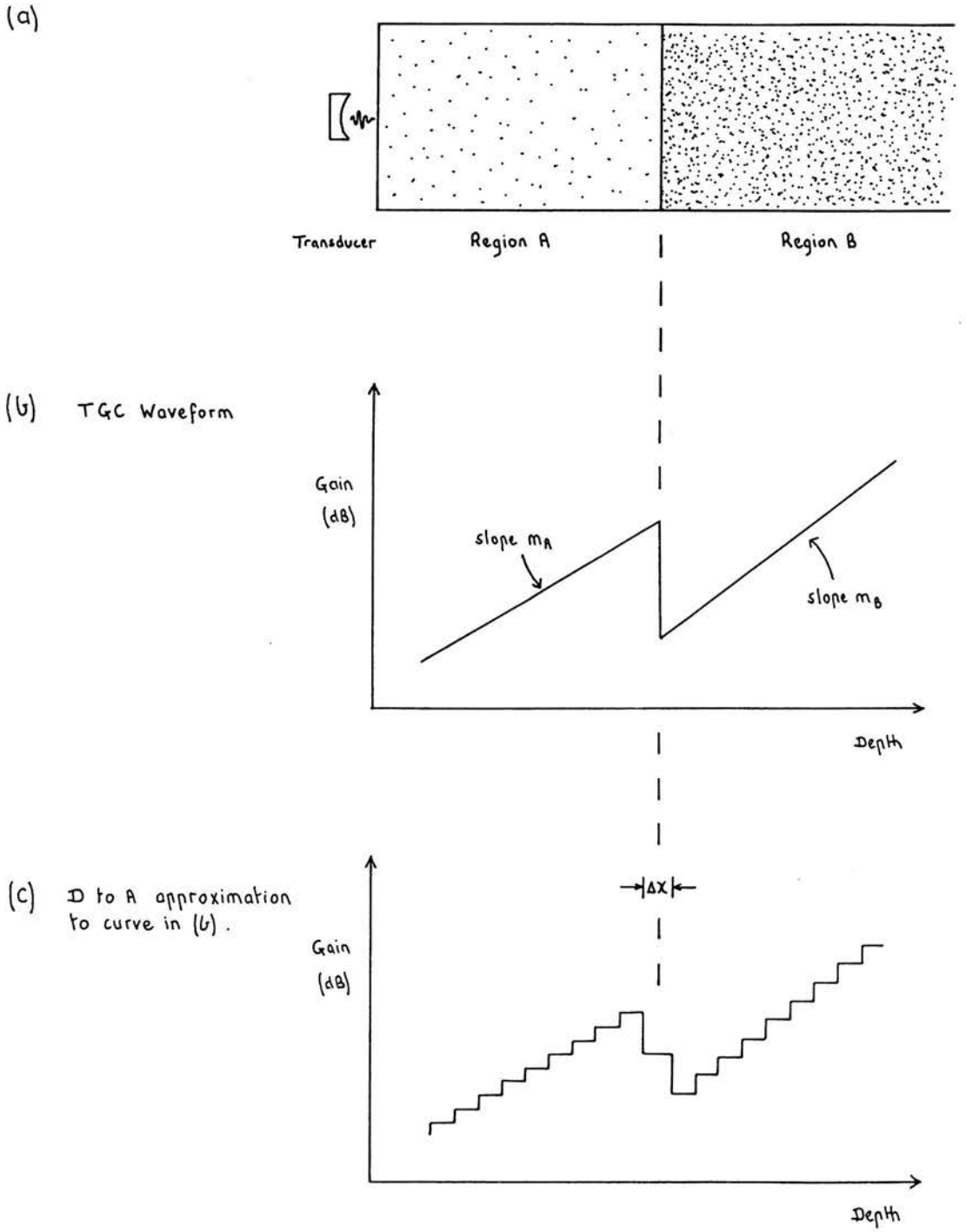

in a 256 μs scan line.

3.5.5.2 Precision

How small does Δg need to be? In their paper on contrast-detail analysis of ultrasound images, Smith et al (1983) report their measurements of threshold contrast for various sizes of disk shaped objects set in a uniform background. Objects with a diameter greater than 20mm required an object-background contrast of at least 1dB before they could be detected visually on the scanner display. Δg should thus be less than 1dB to avoid any possibility of the discrete size of Δg being noticeable.

The receiver gain can be varied through 60dB. 6 bits for each gain value allow 64 different gain values, making the gain variable in approximately 1dB steps. This is probably acceptable. Using 8 bits would allow 256 different gain values, making the gain variable in 0.3dB steps, which is certainly acceptable. Since the microcomputer is an 8 bit machine it can easily cope with 8 bit gain values.

In summary, an important factor in determining the necessary range interval for a TGC function is the spatial resolution of the scanner and an important factor in determining the necessary precision of a TGC function is the contrast resolution of the scanner. Contrast resolution is difficult to evaluate even for the simple case of a disk shaped object in a uniform background. The coherent nature of ultrasound gives rise to random fluctuations in the echo signal - visible as speckle - which tend to degrade the resolving power of the scanner. It remained to be seen whether the values of Δx and Δg chosen were suitable.

3.5.6 Gain Maps - Operation

The microcomputer uses different TGC functions to acquire echo

data and to set up the image. Two gain maps are thus required, one for the internal receiver and one for the external receiver.

A scan line of 256 μs duration has a TGC function composed of 64 x 8 bit gain values. The maximum number of scan lines per frame is 256 for the Z machine. Storing separate maps of gain information for the internal and external receivers with 256 lines per map requires 2 x 64 x 256 bytes = 32k bytes of memory. Both gain maps can thus be accomodated in one 32k block of memory (see section 3.3.2).

Figure 3.7 is a block diagram of the gain maps and their control circuits. Gain map 1 controls the internal receiver and gain map 2 controls the external receiver. During each scan frame the contents of the gain maps are read out line by line to the receivers by control logic in the interface.

Both gain maps have to be accessed frequently by the microcomputer so that it can update the TGC information. TGC data also has to be supplied to the receivers for 256 μs following each transmitter pulse. While data is being read from the gain maps by the on-board counters, the address and data buses of the interface are in use and so the microcomputer cannot access the gain maps. If the microcomputer was denied access to the gain maps for the 256 μs of each scan line the rate at which it could write data into the maps would be severely restricted. So as to maximise the amount of time that the microcomputer has access to the gain maps a buffer memory is positioned between each gain map and its D to A converter. During the short inactive period between scan lines the TGC data for the next line is transferred at 4MHz from each gain map into its buffer memory. This takes 16 μs. The gain maps are then available to the microcomputer. At the start of the next scan line the data in each buffer memory is clocked out at 250kHz to the D to A converters. The microcomputer is thus only barred from the gain maps

Figure 3.7 Gain Maps

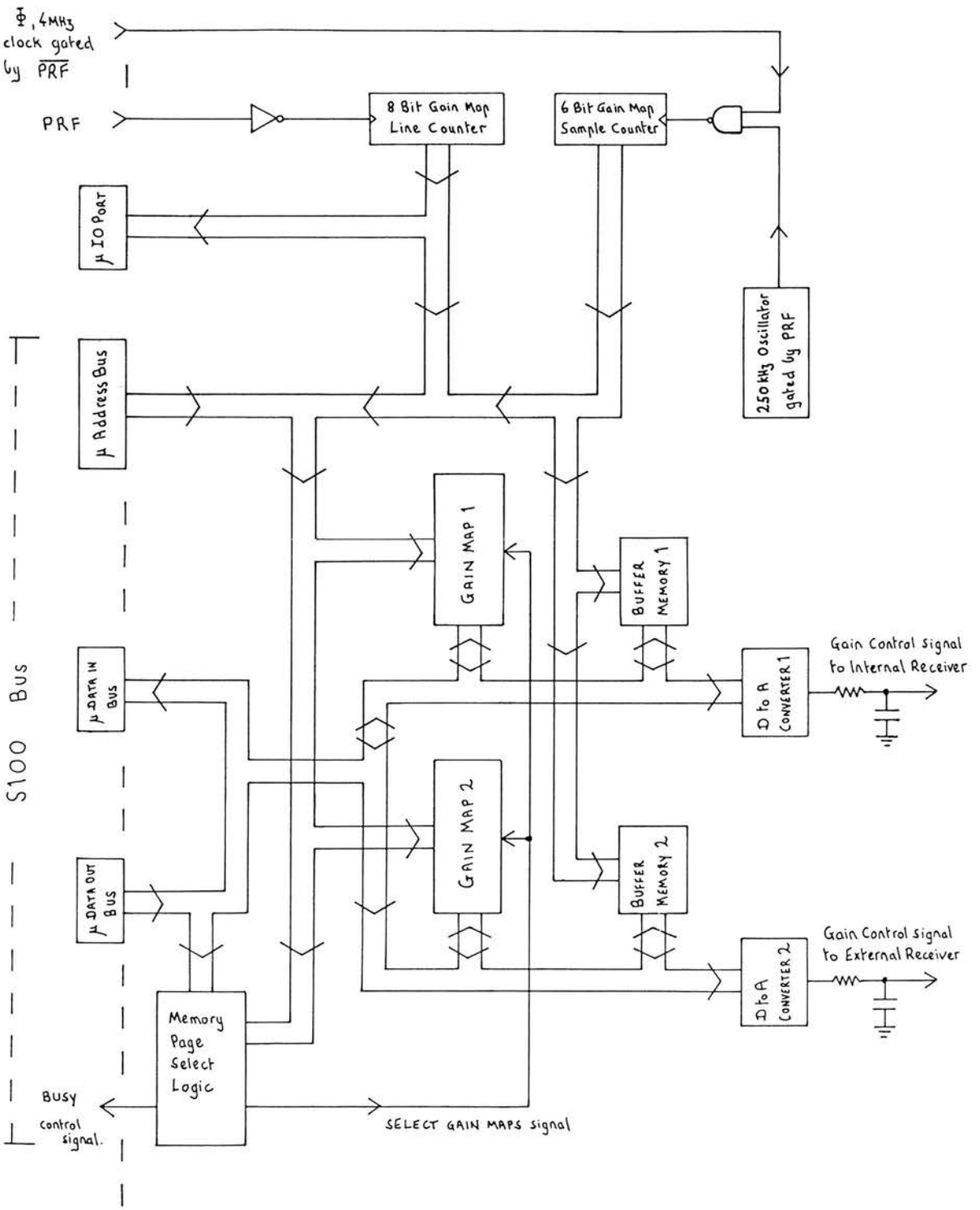

for 16 μs of each scan line. If the microcomputer tries to access the gain maps while the buffer memories are being loaded or if it is accessing the gain maps when the time comes to start loading the buffer memories, the interface holds the microcomputer in a wait state until loading is complete.

The two gain maps are identical in construction and operation except that they occupy different positions in the microcomputer memory, and the microcomputer can read and write to gain map 1 but only write to gain map 2. This latter difference occurred because there was not sufficient space on the S100 cards to fit the necessary circuits. It did not affect the operation of any of the gain control algorithms.

3.5.7 Digital to Analogue Converters

The specifications of the D to A converters are a sample rate of 250kHz and 8 bit accuracy. There were several inexpensive D to A converters available at the time of construction that met these requirements. The device chosen was an AD558 manufactured by Analog Devices.

In general, the output of a D to A converter consists of a series of steps with some noise glitches produced when the D to A converter latches a new input. The closest approximation that a D to A converter can make to a linear slope is a staircase waveform (see figure 3.8a and b). If the waveform in figure 3.8a corresponds to a TGC slope of 6dB cm^{-1} , then each step in the staircase of figure 3.8b will be about 2dB high. The D to A output thus departs from the desired slope by 1dB each time the D to A output changes. This error is all the more likely to be noticeable on an image display because it introduces a series of edges into the echo signal.

The most straightforward way of smoothing the D to A output so that

Figure 3.8 D to A converter output waveform

(a) TGC Waveform

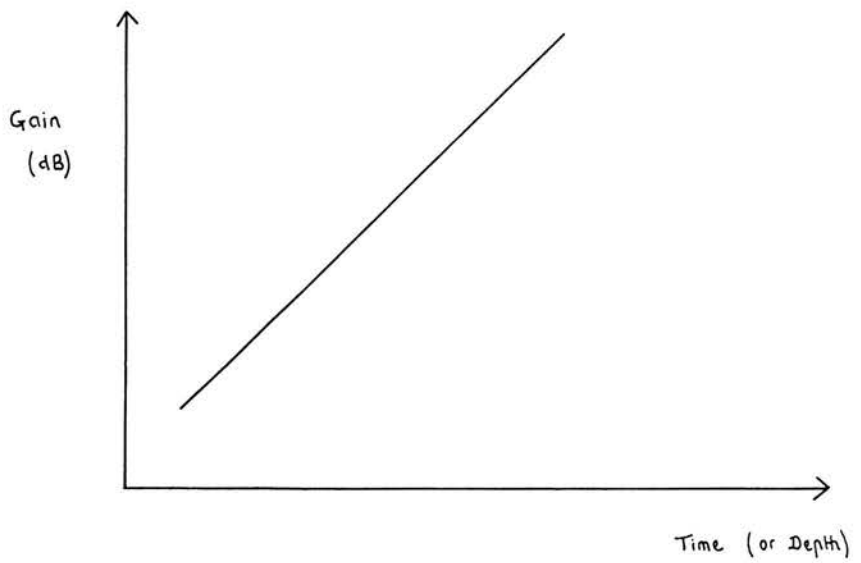

(b) D to A approximation to waveform in (a)

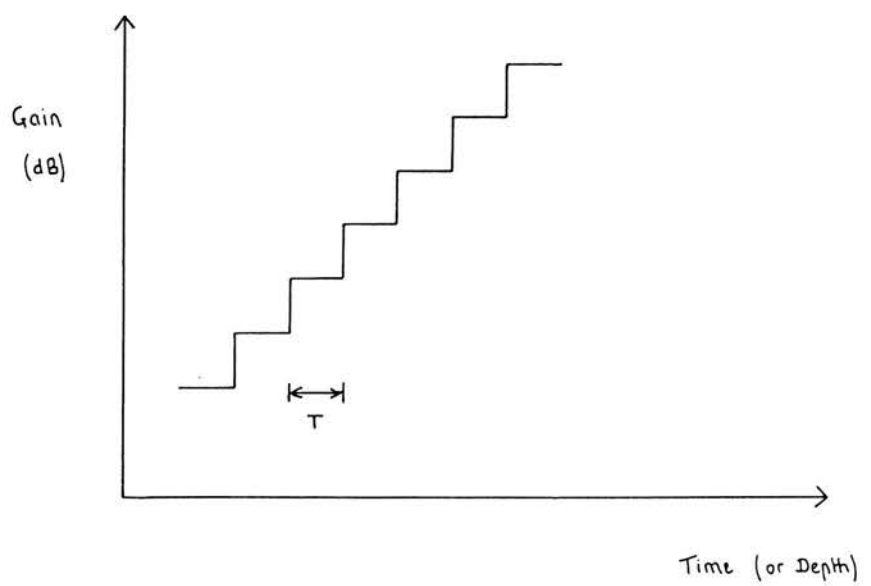

it more closely resembles a continuous function is to use a first order low pass filter (an RC filter). This method proved to be quite adequate, provided that the time constant τ of the RC filter is optimised. The optimum value of τ for smoothing a staircase waveform, such as that in figure 3.8b , with steps spaced T apart is given by

$$\tau = \frac{T}{2} \qquad \text{- Equation 3.1}$$

The output of a D to A converter is not a perfect staircase: each step has a rise time denoted here by τ_D . Under these circumstances, the optimum value of τ is given by

$$\tau + \tau_D = \frac{T}{2} \qquad \text{- Equation 3.2}$$

A computer program was written to calculate how much the optimally smoothed waveform departs from the desired straight line. If each step in the staircase is U high, the maximum deviation of the optimally smoothed waveform from the desired straight line is 0.14U and the mean deviation is 0.06U . The D to A output would have to ramp at over 20dB cm^{-1} before any part of the smoothed waveform departed from the desired straight line by more than 1dB. No soft tissues attenuate 3.5MHz by as much as 20dB cm^{-1} . 4 to 8 dB cm^{-1} is a typical range for the two-way attenuation of 3.5MHz ultrasound in soft tissue (Bamber, 1986).

In order to cope with the dynamic range of the echo signals, the versatile TGC uses both positive and negative slopes. It is as well to consider how the smoothed waveform departs from the ideal when a TGC function has several different slopes.

The optimum value of τ for the long positive slope shown in figure

3.8a applies equally well to a long negative slope. In this context, "long" can be applied to a section of the waveform with more than three or four consecutive steps of the same size. After a change in the slope, the error between the smoothed and ideal curves decreases and then increases gradually to a maximum value. It was computed that the error reaches over 99% of its maximum value three steps after a change in the slope. The value of τ optimal for a long linear slope should thus be optimal for a large variety of TGC functions.

The maximum rate of gain increase is limited by the settling time of the D to A converter, which becomes longer for large changes in D to A output. (That is, changes greater than about 120 out of 256 .) The maximum rate of gain increase is about 120dB cm^{-1}.

The maximum rate of decrease in gain is limited by the fact that sudden negative changes in the gain control signal couple directly into the echo signal path in the receiver and introduce spikes into the echo signal. The maximum rate of decrease in gain is about 60dB cm^{-1}.

3.5.8 System Response Time

During real-time scanning the field of view is constantly changing. Ideally, the versatile TGC system would adapt to these changes as soon as they occur. Several features in the hardware of the versatile TGC improve its response time. These are:

(1) The echo, line and gain map memories are part of the microcomputer memory and can be read and written to directly. An alternative would have been to access them via the microcomputer IO ports, thereby reducing the complexity of the hardware. However, this approach would have made data transfer three

or four times slower than using directly addressed memory. There were in fact several IO ports available on one of the cards if direct addressing had proved too difficult to implement.

(2) The digitisation and storage of echo data are independent of the microcomputer once the scan lines to be digitised have been chosen.

(3) The gain maps apply the stored TGC waveforms to the receivers independently of the microcomputer.

(4) The buffer memories between the gain maps and the receivers allow the microcomputer maximum access to the gain maps.

(5) The AM9511A fast arithmetic chips are used to perform calculations, such as logarithms, which are very time consuming when carried out by software.

As a consequence of the time saving features described above, the factor now limiting the operating speed of the versatile TGC system is the computing time required by the microcomputer. A simple gain control algorithm can completely update the gain maps several times per second whereas a more sophisticated algorithm can take several seconds to update the gain maps once. The software used by the adaptive TGC algorithms also contains features that improve the response time of the system. These are described in the next section.

3.6 SOFTWARE

Algorithms for the versatile TGC system have been written in a combination of Fortran IV and Z80 Macro Assembler. A high level language like Fortran is well suited to writing mathematical algorithms

because the tasks to be performed can be expressed as a series of algebraic Fortran statements. Each statement performs a recognisable function and corresponds to many machine language instructions. A program called a compiler translates the Fortran source code into machine language instructions. However, simple compilers produce inefficient programs and are unable to take advantage of the special features of a computer system. Assembly language programs, on the other hand, are highly efficient since each assembly language instruction corresponds to a single machine language instruction. Assembly language has disadvantages. It takes several times longer to write a program in assembly language than in a high level language. Once written, assembly language programs are difficult to understand, de-bug and modify. An introduction to assembly language programming is contained in the text "Z80 Assembly Language Subroutines" by Leventhal and Saville (1983).

3.6.1 Routines used by adaptive TGC algorithms

The main programs and mathematical parts of the adaptive TGC algorithms are written in Fortran IV. The execution times of the programs are significantly reduced by writing relatively simple but repetitive tasks in Z80 Macro Assembler. For example, multiplying all the values in an array by an integer; finding the median value of a set of numbers. The assembly language programs are called as subroutines from Fortran programs.

Assembly language routines were also written to control the interface electronics since this detailed level of control is not possible from Fortran. These routines include the commands to select different pages of memory and to read and interpret status information from the interface. Other assembly language routines perform data transfer between the echo, line and gain maps and the user program area.

3.6.2 Diagnostic Programs

A range of diagnostic programs were written in both Fortran and Macro Assembler. These were essential in testing the operation of the interface during and after construction. They include routines to test the echo and line maps to ensure that the correct scan lines are being digitised, that the wait-state generators are operating correctly and that there is no corruption of the echo data.

Gain map diagnostics test that both gain maps are being properly updated and that data can be read from gain map 1.

The memory paging system is tested by successively selecting different pages of memory, reading and writing to them, and then checking that data in other pages has not been corrupted.

Chapter 4

A COMPUTER SIMULATION OF TGC

4.1 INTRODUCTION

The ultimate test of a medical signal processing technique is its clinical usefulness. This is the reason for carrying out clinical trials of adaptive TGC. However, even if we assess the effectiveness of a particular algorithm we may be left pondering over why it succeeds or fails. The interaction of an adaptive TGC algorithm with two-dimensional image data is complex. It is not just the presence of certain types of scattering and attenuating tissue that is important, but their size, shape, orientation and their positions relative to the transducer and relative to each other. Our control over the production of echoes is limited and we have limited knowledge about the scattering and attenuation properties of tissue. Test objects allow us to examine situations about which we have some accurate information, but the range of test objects available is limited.

The advantage of computer simulation is that it allows us to create simple situations which can be easily analysed and easily changed. Although such simple situations might not occur clinically, they may nevertheless help our understanding.

4.2 CONTRAST RESOLUTION AND SPATIAL RESOLUTION

Two of the fundamental attributes of an imaging system are its contrast resolution and spatial resolution. Contrast resolution is a measure of the ability of an observer to distinguish regions of an image which have different mean signal levels. If the difference between the mean levels is small, the presence of noise will make it more difficult for the observer to recognise separate regions. Spacial

resolution is a measure of the ability of an observer to distinguish point objects lying close together in an image. In general, both contrast and spatial resolution will vary over the scan plane of an ultrasound image.

Computer simulations were carried out on five of the adaptive TGC algorithms presented in Chapter 5. The purpose of the simulations was to assess the effect of each algorithm on image contrast and spatial resolution.

4.3 IMAGE CONTRAST

A single situation has been simulated: that of a single object in a uniform background. The field of view is defined as 64 x 64 pixels, each pixel representing 3mm in size - the same as the versatile TGC range interval. The size of the field of view is fixed. The object is square and positioned centrally in the field of view, which is assumed to be insonated by a linear array lying along one side of the field of view as shown in figure 4.1a . The size of the object can be varied. The simulation involves several assumptions:

(1) Perfect focussing. That is, in the absence of attenuation and with a uniform scattering medium the echo signal from the transducer will be the same for all depths.

(2) Single scattering. That is, a signal returning to the transducer is the result of only one scattering event.

(3) No effects due to finite transducer aperture: a beamwidth of one pixel is assumed.

(4) No speckle.

Figure 4.1 Contrast Simulation : Object and Background.

(a)

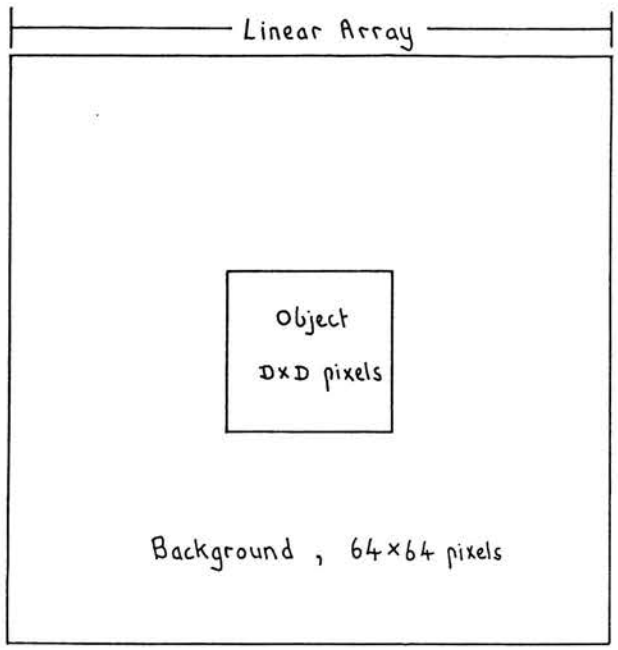

(b)

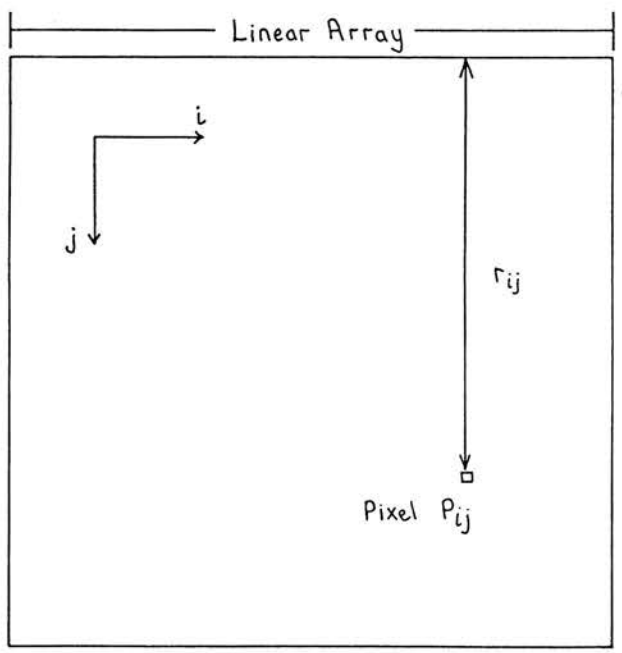

(5) No effects due to refraction.

(6) No effects due to dispersive attenuation.

(7) No effects due to non-linear propagation.

(8) No effects due to saturation in the receiver, or due to limited receiver gain.

(9) No effects due to the limited dynamic range of the A to D converter or display.

The amplitude S_{ij} of pixel P_{ij} in the simulated image is given by

$$S_{ij} = G_{ij} E a_{ij} e^{-r_{ij} \sum_{k=1}^{j-1} \alpha_{ik}} \qquad \text{- Equation 4.1}$$

where G_{ij} is the gain applied by the receiver to the signal from P_{ij} .

E is proportional to the amplitude of the transmitted pulse.

a_{ij} is proportional to the amplitude of the signal backscattered by P_{ij}

r_{ij} is the depth of P_{ij} below the transducer face (see figure 4.1b).

α_{ik} is the two-way attenuation coefficient of pixel P_{ik}.

For the background, the product Ea was set at 100 arbitrary units and α was set at 5dB cm^{-1}. For the object, Ea could be varied between 10 and 1000 arbitrary units and α could be varied from 1 to 10dB cm^{-1}. These values correspond roughly to a range of signal levels and attenuation observed in tissue. The actual combinations of backscattered amplitude and attenuation used have not been chosen to

match particular tissue types. The size of the object can be varied from 2 x 2 pixels to 32 x 32 pixels.

4.3.1 Figures of Merit

How are we to judge the quality of the simulated images? In order to make a quantitative comparison between the images produced by different algorithms it was decided to calculate simple figures of merit using the signal contrast in each image. This approach has the advantage of allowing easy comparison, but it runs the risk of failing to bring out important features in the images. The figures of merit used were as follows:

(1) The mean contrast C maintained between the object and the background in the simulated image. C is calculated by

$$C = \left| 20.\log_{10}\left[\frac{\bar{S}_o}{\bar{S}_B}\right] \right| \qquad \text{- Equation 4.2}$$

Where $\bar{S}_o$ is the mean pixel amplitude of the object and

$\bar{S}_B$ is the mean pixel amplitude of the background.

(2) The mean variation V_o of pixel amplitudes over the object. V_o is defined by

$$V_o = 20.\log_{10}\left[\frac{\sum_{K=1}^{N}\left(|S_o(K) - \bar{S}_o|\right)}{N\bar{S}_o} + 1\right] \qquad \text{- Equation 4.3}$$

Where $S_o(k)$ is the amplitude of the kth pixel in the object, which is composed of N pixels. The two dimensional ij notation has been dropped here for the sake of clarity.

(3) The mean variation V_B of pixel amplitudes over the background. V_B is defined in a similar way to V_o :

$$V_B = 20.\log_{10}\left[\frac{\sum_{k=1}^{L} \left(| S_B(k) - \bar{S}_B | \right)}{L\,\bar{S}_B} + 1 \right] \qquad \text{- Equation 4.4}$$

Where $S_B(k)$ is the amplitude of the kth pixel in the background, which is composed of L pixels.

In order to present the results of the simulations, a single figure of merit V is formed from V_o and V_B , such that

$$V = \frac{V_o + V_B}{2} \qquad \text{- Equation 4.5}$$

This is reasonable because V_o and V_B are usually of similar size.

4.3.2. Simulation Results

The simulation results for each algorithm are presented in the following way: for particular values of the backscatter amplitude and attenuation of the object, the values of C and V are plotted against object size. An example is shown in figure 4.2.

The values of C and V do not give any indication of important

Figure 4.2 Contrast Simulation : Example plots of C and V (see text for details).

(a)

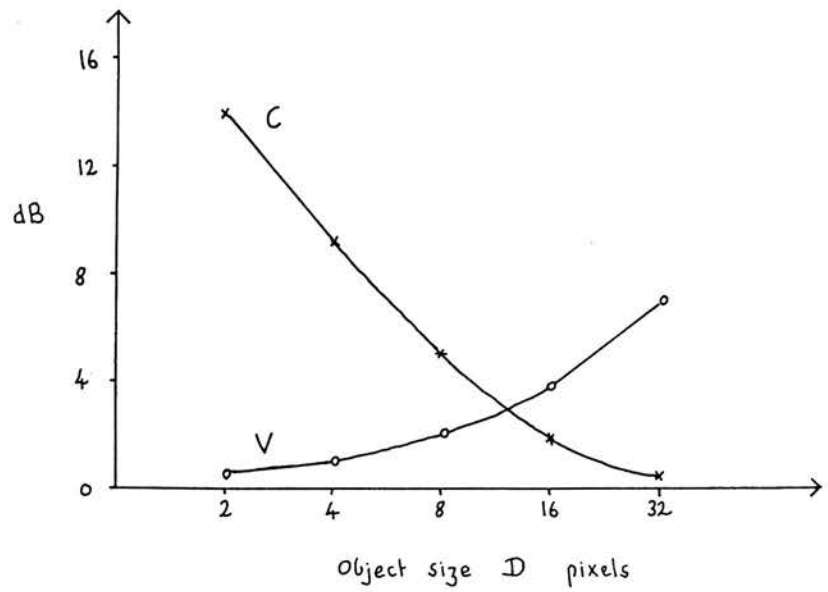

(b)

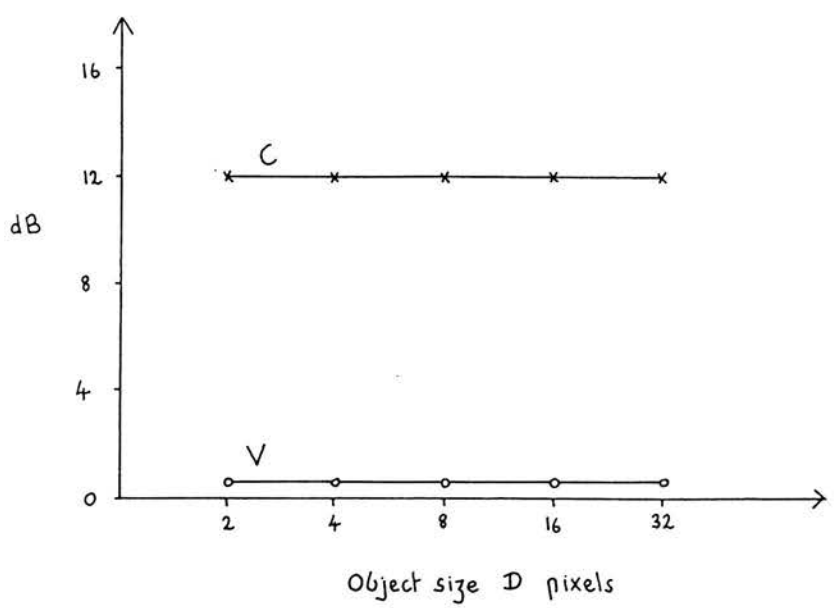

two-dimensional information in the image, such as the distribution of pixel amplitudes or the presentation of edges. They can give some useful information. Consider figure 4.2a : C drops steeply and V rises steeply as the object size increases. The object is thus probably less clearly presented at large object sizes than is the case shown in figure 4.2b where C remains a constant level above V. However, this is not necessarily so; even if C and V are close together the object/background boundary may be well-defined and the variation in amplitudes may be due to recognisable artifacts such as shadowing. The rough and ready usefulness of the plots of C and V has to be judged in conjunction with the results of the clinical trials of each algorithm. For this reason, the simulation results for each algorithm are presented in the section of Chapter 5 dealing with that algorithm. Included with the results for each algorithm are plots of C and V for simulated manual TGC settings. The manual TGC settings were calculated as follows: knowing the attenuation coefficients of the background and the object, the TGC slope m was set such that

$$m = \frac{A_o}{A}\alpha_o + \frac{A_B}{A}\alpha_B \qquad \text{- Equation 4.6}$$

Where A_o is the number of pixels in the object,

α_o is the attenuation coefficient of the object,

A_B is the number of pixels in the background.

α_B is the attenuation coefficient of the background, and

A is the total number of pixels in the field of view.

This is a reasonable way of optimising a single TGC slope for the whole image. In a clinical situation the settings could be different

because the operator might wish to optimise a particular part of the image.

A wide range of combinations of object backscatter amplitude and attenuation were simulated. Four combinations have been selected for presentation in this thesis because they are representative of the behaviour of the algorithms for a large number of combinations of backscatter amplitude and attenuation. The combinations used are given in table 4.1 .

4.4 SPATIAL RESOLUTION

A one-dimensional simulation has been used to assess the effect of each adaptive TGC algorithm on the presentation of strongly reflecting structures. The situation chosen was that of a group of strong reflectors situated in a uniform background. The effect of each algorithm is determined by applying the algorithm to the simulated pulse-echo data and then plotting the resulting A-scan. The physical assumptions made in the contrast simulation all apply here, except that the limited dynamic range of the A to D converter is taken into account. This is important in determining whether the structure of the group of reflectors is resolved.

Further details of this simulation and the results obtained are contained in the section of Chapter 5 dealing with algorithm 4. This is because algorithm 4 is the first algorithm which specifically tackles the problem of resolving groups of strong reflectors. Also, the result for each algorithm consists of a single A- scan line and there is a progression from one algorithm to the next which is difficult to appreciate unless all the results are presented together.

Table 4.1 Contrast Simulation :

Backscatter Amplitude and Attenuation.

	Backscatter Amplitude in dB relative to the background medium.	Two-way attenuation coefficient in dB cm^{-1}
Background	0	5
Object (a)	+20	6
(b)	+5	5
(c)	-5	4
(d)	-20	1

Chapter 5

ADAPTIVE TGC ALGORITHMS

The first part of this chapter consists of three introductory sections. These are:

(1) An outline of the strategy and development of the adaptive TGC algorithms.

(2) An explanation of the notation used to describe the TGC functions.

(3) The protocol for the clinical trials.

Each of the six sections following the introduction deals with a specific algorithm, its operation, simulation and imaging results.

5.1 TGC ALGORITHMS FOR REAL-TIME IMAGING

The motivation for developing adaptive TGC algorithms stems from the inability of manual TGC to consistently produce well-balanced images, even when set-up by a skilled operator. In addition, adaptive TGC can greatly reduce the number of control adjustments that the operator has to make. Even the most advanced modern scanners often produce poor images because of their inflexible gain controls.

Venetsanopoulos and Cappellini (1986) review the hardware and software currently used for real-time image processing. They comment that,

> "The design of image processing algorithms is accomplished to a large extent on an ad hoc basis, with little or no theoretical foundation. This is due to the lack of appropriate theoretical framework for describing images and image components and their perceptual effects on human observers."

So, before we can formulate TGC algorithms for ultrasound imaging we must be aware of the desirable features of an adaptive TGC system

from an observer's point of view. These are as follows:

(1) All echo signals should be brought within the dynamic range of the A to D converter and display, otherwise some of the information contained in the low and high amplitude signals will be lost.

(2) Uniform tissue regions should be presented at a uniform grey level (apart from fluctuations due to speckle). This requirement is difficult to meet completely, but image interpretation becomes a problem if it is not reasonably well satisfied.

(3) An adequate contrast should be maintained between regions of different tissue types. The word "adequate" begs the question "how much?" In this context, we might say that regions which are distinguishable using manually set TGC should still be distinguishable when adaptive TGC is applied. Adaptive TGC should not introduce noise into anechoic regions.

(4) The TGC algorithm should be stable. This requirement has two aspects:

(i) For any given image there will be many slightly different TGC settings which would provide adequate gain settings. A TGC algorithm should only be capable of selecting one set of waveforms. If the algorithm were to continually produce different TGC settings using the same raw echo data, the changing image may give the impression that physical changes, such as movement, are occurring. This would be misleading.

(ii) It is undesirable for a TGC algorithm to make drastic changes in its TGC settings if the scan plane only alters slightly. As with (i), the image may give the impression of physical change whereas most of the alteration is due to the signal processing.

(5) The TGC system should operate in real-time. This does not necessarily mean processing data at the same rate that the transducer

scans the body (10 to 30 frames per second). More realistically, the TGC should be updated every 0.5s or less, so that when the operator settles on the optimum scan plane there is an unobtrusive delay before the TGC catches up. From clinical experience of the versatile TGC system, response times of greater than 1s are not acceptable, times of about 0.5s are reasonable and times of less than 0.5s are quite acceptable.

(6) The TGC system should remove the need for the operator continually to make control adjustments.

(1) to (6) above can be summarised by saying that a TGC algorithm should be able to reduce automatically the large dynamic range of raw echo data to that of a TV display and still produce well-balanced images. The problem of displaying a large dynamic range signal on the limited range of a display occurs in other areas of imaging. These include aerial photographs degraded by clouds between the camera and the ground (Peli and Lim, 1981), thermal imaging systems (Dehne, 1978) and television images in which part of the scene is in shadow. In these circumstances, the balance of the image can usually be improved if the gain at each location in the image takes account of both the signal at that location and the average signal level over the surrounding area. The contrast in each part of the image can then be adapted to suit both the signal and the display. Peli and Lim describe an algorithm suitable for enhancing images degraded by cloud cover and Dehne describes a technique for removing DC restoration artifacts from infra-red images.

In the field of diagnostic ultrasound, there are many possible ways of combining the local and overall signal levels. We might look at various weightings for signals proximal, distal and on either side of each location. The statistics of each region could be used to

distinguish areas of speckle from voids and areas of acoustic shadow. The positions of edges could be plotted, and on a more sophisticated level, two-dimensional pattern recognition techniques might be used to trace boundaries so that individual weightings could be given to signals from different bounded regions. However, sophisticated algorithms demand sophisticated hardware. It would be a major task for a computer to process all the data in a real-time scan.

The algorithms developed in this chapter are geared to a real-time application using the minimum of hardware and so they all use simple techniques for adaptive processing. The most successful algorithms use a form of adaptive compression. The idea behind this technique is worth stating with some precision: the gain applied to each location in the image is formed from two components. One component is derived using echo information from close to that location, the other component is derived using echo information averaged over a large part of the image. The combination of the two is expressed by the relationship

$$H'_N(y) = \beta H_N(y) + (1-\beta) H_o(y) \qquad \text{- Equation 5.1}$$

Where y is depth, measured from the transducer along a scan line,

$H'_N(y)$ is the gain applied at depth y of the Nth scan line,

$H_N(y)$ is a gain value calculated using echo data from close to y on the Nth scan line,

$H_o(y)$ is a gain value formed using echo data averaged over a large part of the image, and

β is a parameter that can take values in the range 0 to 1 .

The success or failure of an algorithm depends largely on the rules

chosen for setting the values of β .

Algorithms 1 to 4 can be seen as developing the relationship expressed in equation 5.1 . Algorithms 5 and 6 are based on equation 5.1 but contain other features which cannot be easily included in the equation. In particular, algorithms 5 and 6 attempt to recognise large regions of low attenuation so that the TGC slope can be set accordingly.

Sections 5.4 to 5.9 each deal with a specific algorithm. Each section is organised more or less as follows:

(1) An outline of the algorithm.

(2) A detailed description and flow diagram of the algorithm.

(3) Simulation results.

(4) Imaging results.

5.2 NOTATION

The notation used to describe the manipulation of gain and echo data is defined below:

SYMBOL	MEANING
y	is radial distance from the transducer, measured from the transducer along a scan line.
G	is a gain function (TGC function) with 64 discrete values (or elements) each corresponding to a 4 μs interval.
G(k)	is the kth element of G. k increases as y increases.
G_N	is a gain function derived using echo data from the Nth scan line.

G_o is a gain function derived using echo data from the whole image.

G'_N is a gain function applied to the Nth scan line forming the image.

SG is a gain function derived from G by applying a local smoothing operator to each element of G.

E is a function with 64 elements, each element being the mean modulus of a 4 μs interval of echo data. E is referred to as an echo function.

E(k) is the kth element of E.

E_N is the echo function containing data from the Nth scan line.

E_o is an echo function obtained by combining echo data from the whole image.

$\bar{e}$ is a value in the range 1 to 255 defining the average grey level of the image.

NLIN is the number of scan lines in the image.

5.3 PROTOCOL FOR THE CLINICAL TRIALS

The clinical trials of the adaptive TGC followed a protocol similar to that of the trials of the commercial system described in Chapter 2. Because of the greater number of algorithms to be tested, fewer patients could be included in the study of each one than was the case for the commercial system. Each algorithm was tested on between 16 and 50 patients. Different groups of patients were used for each algorithm. All the algorithms were tested in both abdominal and obstetric work. Paired images were obtained as described in Chapter 2, and these were subsequently judged by a consultant radiologist (SRW) and a hospital physicist (NMcD). The images were obtained over a period of six months.

The obstetric images were recorded by four radiographers and the abdominal images by six radiologists.

When all the pairs of images had been collected, I and another physicist (TL) examined the images and excluded pairs which were not comparable due to gross movement. This made the judges' task easier because they did not have to decide whether the tissue sections were comparable to start with, before deciding which image they preferred.

Four of the six algorithms presented in this chapter were evaluated clinically. A total of 340 pairs of images were obtained from 114 patients and 119 of these pairs were excluded because they did not have comparable sections. The remaining 221 pairs of images were judged separately by the radiologist and physicist, both of whom took two periods of about two hours to go through all the results. The images were presented on grey-tone X ray film, one pair at a time. The judges were told that they would be seeing the results of many different processing techniques. The abdominal and obstetric images were presented separately, but within these groups the pairs were presented in random order so that the results of the different algorithms were mixed together. The left/right positions of the manual/adaptive images were also random. The first and last few millimetres of each image were covered up to prevent any near or far field artifacts from giving the judges a clue as to which image was manual and which was adaptive. (Many of the manual images have a distinctive transmitter bright-up at the top of the image and some of the adaptive images have a bright dot marking the deepest point of every scan line.)

For each pair, the judges were asked to say which image they preferred, or whether they thought there was no significant overall difference. The physicist judged the images from a physical and technical viewpoint rather than a clinical viewpoint: he felt able to

make a finer judgement and so included a category of "much preferred".

The following notation is used to refer to the different categories:

AA - adaptive image much preferred,

A - adaptive image preferred,

C - no overall difference between the images,

M - manual image preferred,

MM - manual image much preferred.

The results of the clinical trials of each algorithm are presented in the section of this chapter dealing with that algorithm. The characteristics of the images produced are described and illustrated . The results of all the evaluations are discussed in Chapter 6.

The images of a test object obtained using manual TGC and algorithms 1 to 6 are shown in figure 5.2 . The images are of the Cardiff Grey Scale Test Object (McCarty and Stewart, 1984). They are presented here so that they can easily be compared and so as to give the reader an indication of the different effects the algorithms produce before the algorithms are described in detail. Figure 5.1 is a sketch of the test object.

All the ultrasound images contained in this chapter extend to a depth of 18 cm .

Figure 5.1 Sketch of test object image.

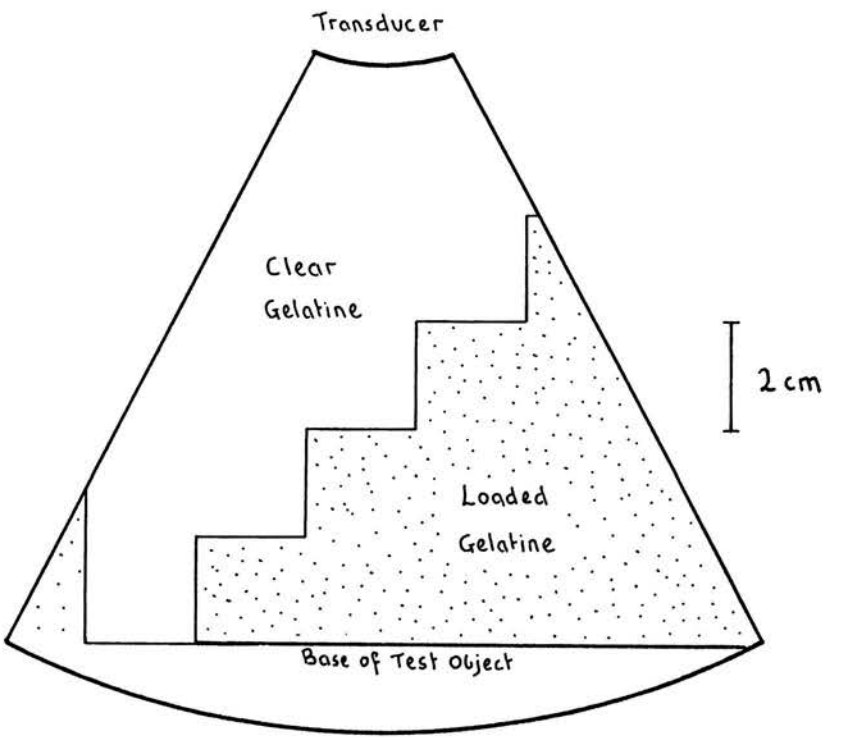

Clear gel (low attenuation) -
two-way attenuation coefficient ≈ 1 dB cm^{-1} at 3.5MHz

Loaded gel -
two-way attenuation coefficient ≈ 6 dB cm^{-1} at 3.5MHz

FIGURE 5.2 : The Cardiff Grey Scale Test Object.

(a) Manual TGC

(b) Adaptive TGC: Algorithm 1

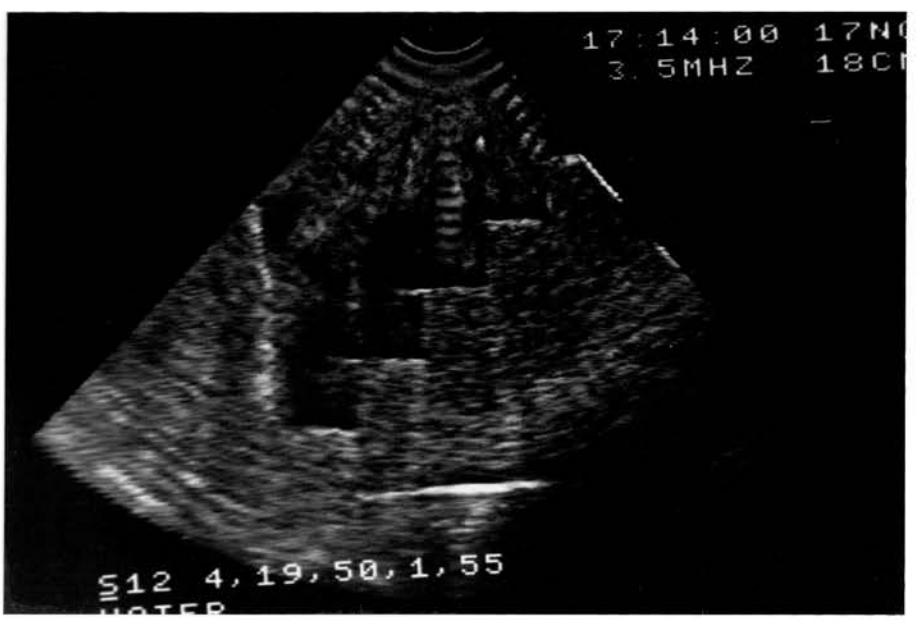

FIGURE 5.2 : The Cardiff Grey Scale Test Object.

(c) Adaptive TGC: Algorithm 2

(d) Adaptive TGC: Algorithm 3

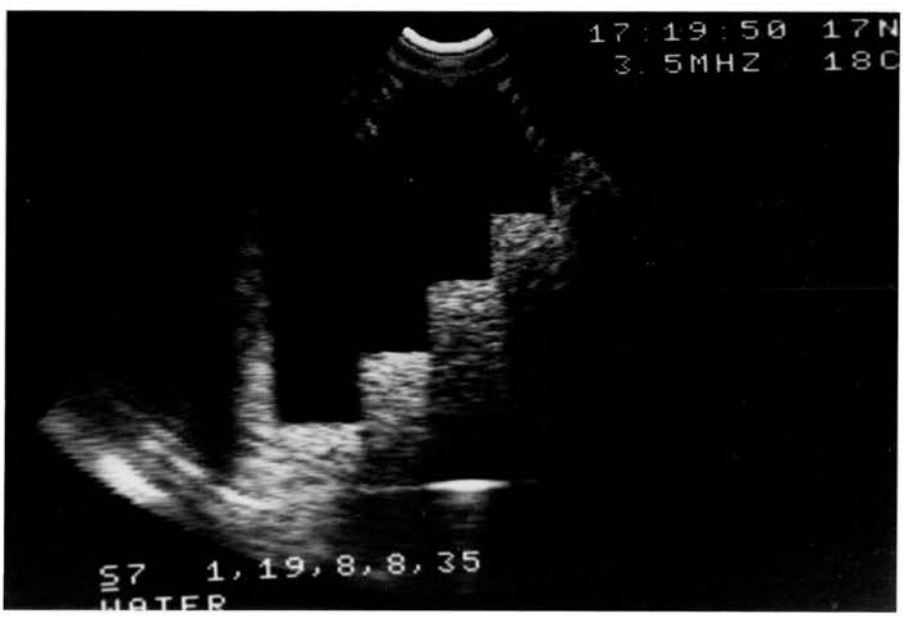

FIGURE 5.2 : The Cardiff Grey Scale Test Object.

(e) Adaptive TGC: Algorithm 3.1

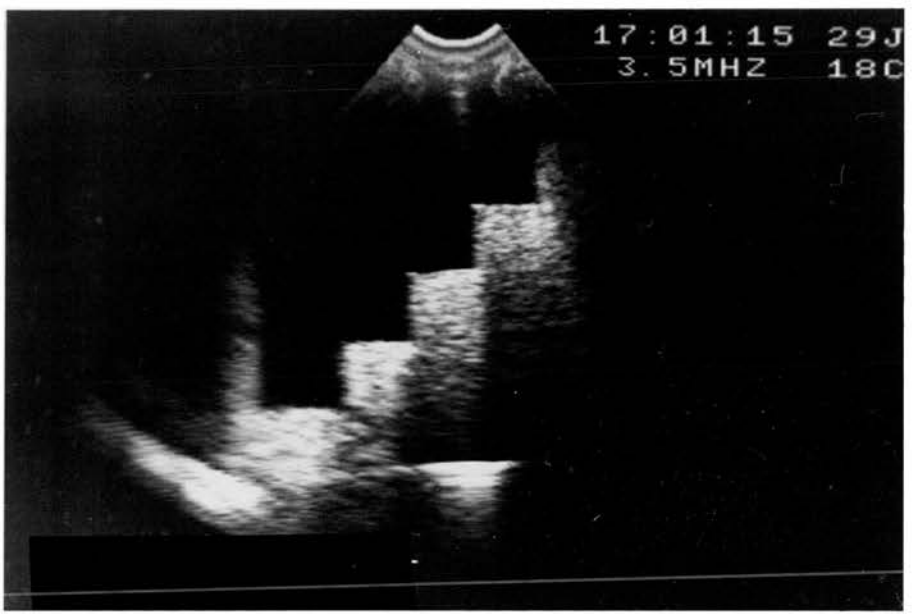

(f) Adaptive TGC: Algorithm 4

FIGURE 5.2 : The Cardiff Grey Scale Test Object.

(g) Adaptive TGC: Algorithm 5

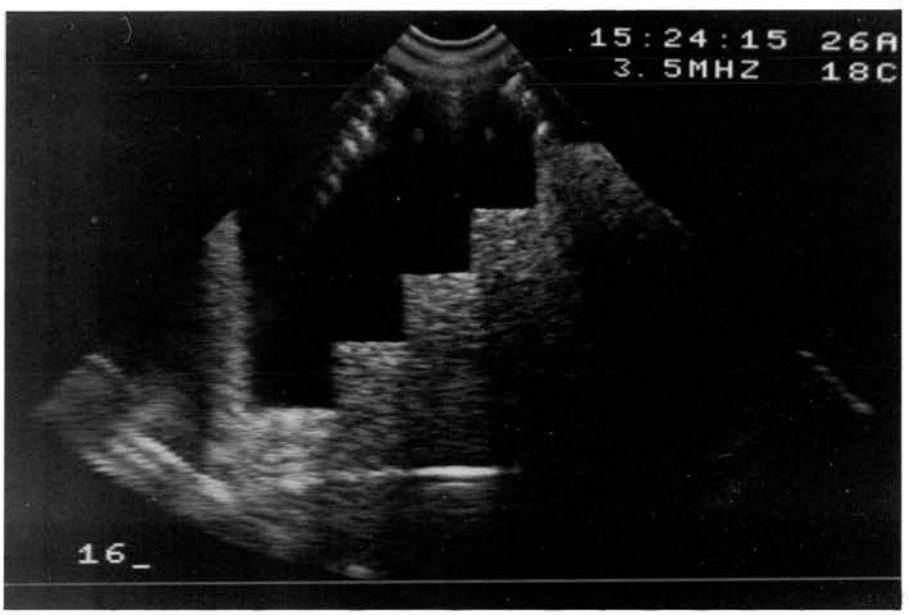

(h) Adaptive TGC: Algorithm 6

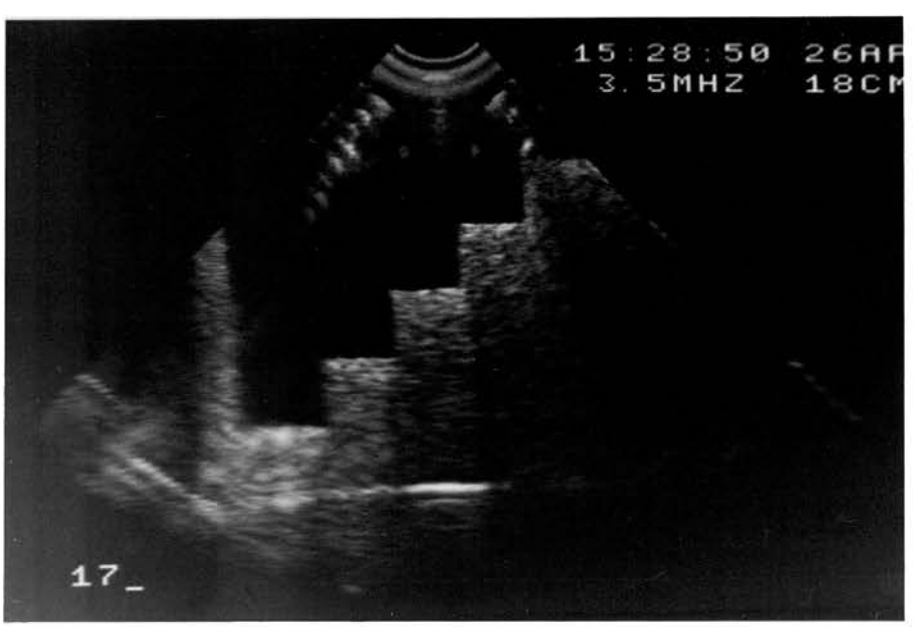

5.4 ALGORITHM 1

5.4.1 Outline

Algorithm 1 is designed to test the technical performance of the versatile TGC system and is not for clinical use. It aims to bring all echo signals to a uniform level defined by the operator. Algorithm 1 takes between 1.5 and 2 seconds to collect and process data from one image.

5.4.2 Detail

A flow diagram of algorithm 1 is shown in figure 5.3 . Algorithm 1 consists of two parts:

(1) Data collection cycle during which echo data is obtained via the external receiver.

(2) Image processing cycle in which the echo data is used to generate TGC functions which control the internal receiver.

5.4.2.1 Data Collection

The probe used for all the evaluations of algorithms 1 to 6 was a mechanical sector scan probe with four 3.5MHz transducers mounted on a rotating wheel. The transducers are focussed at about 7cm. The sensitivities of the transducers differed by up to 2dB. So as to prevent any variation in signal level across the image due to collecting data from different transducers, it is necessary to collect the echo data for each image from one scan frame. Echo data is collected from 32 scan lines evenly spaced across the image. With the probe operating in 80° sector mode the scan lines are spaced 2.5° apart. In the focal region of the transducer, echo samples at the same depth are thus

Figure 5.3 Flow diagram of Algorithm 1

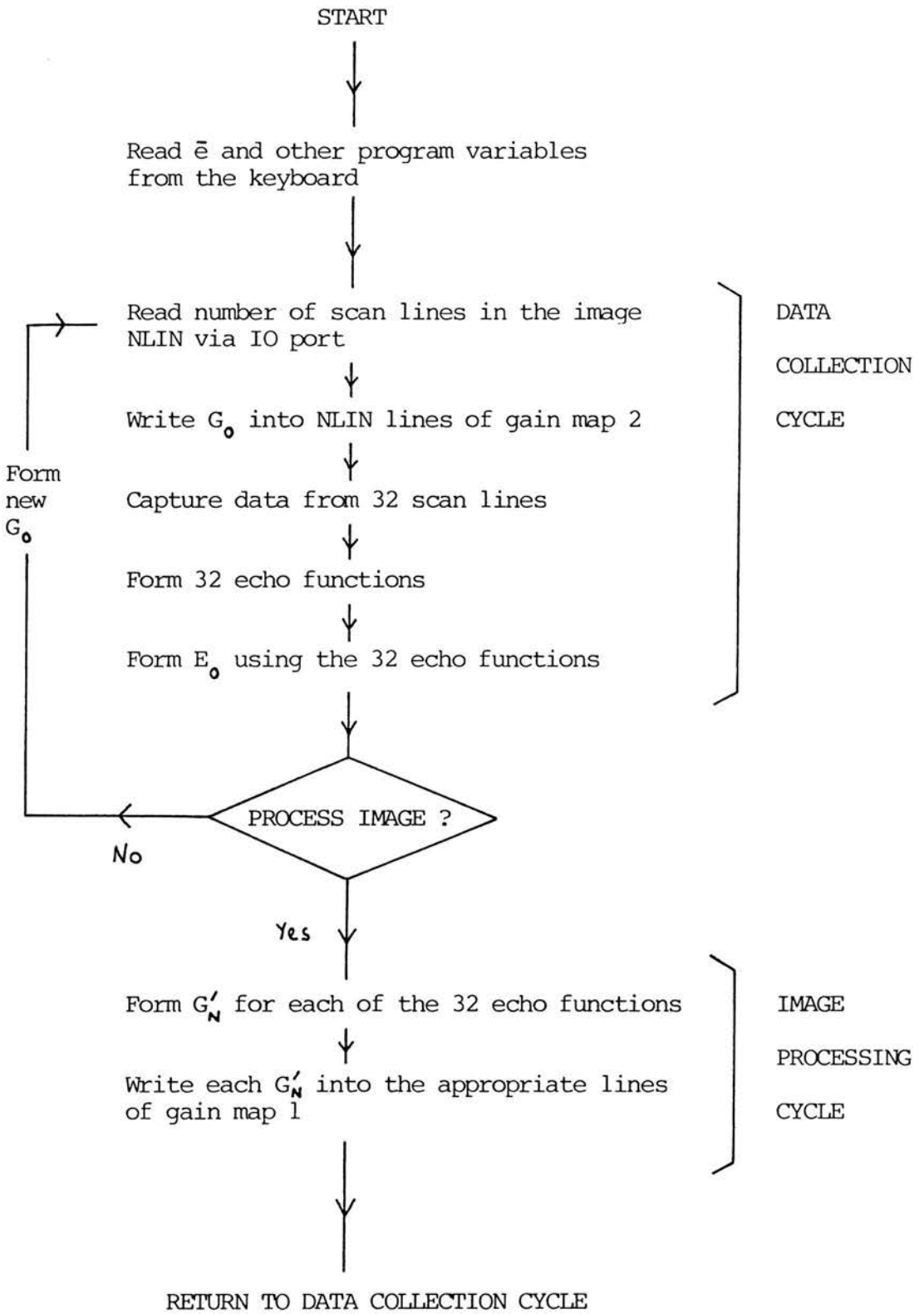

separated by 3 to 4mm laterally. This results in a slight undersampling of the echo signal across the image. The 20dB beamwidth in the focal region is about 5mm and in order to be able to reconstruct all the information in the signal it is necessary to have a sampling interval of less than half the beamwidth (Whittingham, 1981). For the Z machine, this would mean capturing every scan line.

For each scan line stored, the microcomputer calculates an echo function E in which each element is the mean modulus of a 4 μs interval of echo data.

Data collection is performed using a single gain function G_o written into all the lines of gain map 2, controlling the external receiver. It was found that a single gain function could usually be adapted to bring all echo signals within the dynamic range of the 8 bit A to D converter. If necessary , an individual gain function could be set up for each line in gain map 2.

At the end of each data collection cycle a new gain function G_o is calculated. This is done in the following way:

(1) An echo function E_o is formed using the 32 stored echo functions. E_o is given by

$$E_o(k) = \frac{1}{32} \sum_{N=1}^{32} E_N(k) \qquad \text{- Equation 5.2 for } k = 1,64$$

(2) New values of G_o are then calculated so as to bring the mean echo level at each depth to the level $\bar{e}$ defined by the operator:

$$G_o(k)_{NEW} = G_o(k)_{OLD} + 20.\log_{10}\left(\frac{\bar{e}}{E_o(k)}\right) \qquad \text{- Equation 5.3 for } k = 1,64$$

(3) The new G_o is written into all the lines of gain map 2, in readiness for the next data collection cycle.

5.4.2.2 Image Processing

32 gain functions are formed using the 32 stored echo functions. The function for the Nth scan line is given by:

$$G'_N(k) = G_o(k) + 20.\log_{10}\left(\frac{\bar{e}}{E_N(k)}\right) \qquad \text{- Equation 5.4}$$

for k = 1,64

Each gain function G'_N is then written into the appropriate lines of gain map 1, controlling the internal receiver. For the Z machine operating with 100 scan lines per frame, each gain function is written into 3 or 4 consecutive lines of gain map 1.

Describing algorithm 1 in terms of equation 5.1, β always equals 1 and G'_N replaces H'_N.

5.4.3 Simulation Results

No computer simulation was carried out for algorithm 1; the results are trivial.

5.4.4 Imaging Results

The effect of algorithm 1 on the grey-scale test object is shown in figure 5.2b . In this image, $\bar{e}$ = 60. Most of the image is brought to a mid-grey level with the exceptions of

(1) Edges: because the TGC can only change on a scale of 3mm axially, the boundary of the low attenuation

gel and the loaded gel is clearly defined. For the same reason, the appearance of speckle is not affected.

(2) In the deepest parts of the low attenuation gel and the loaded gel the signal levels falls off because the receiver has reached maximum gain and cannot compensate for further attenuation.

5.5 ALGORITHM 2

5.5.1 Outline

Algorithm 2 implements the simple adaptive TGC described by McDicken (see section 1.6) with the modifications that the smoothing of the gain control signal is symmetrical with respect to time, and positive gain slopes are restricted by an upper limit. The algorithm takes between 1.5 and 2 seconds to collect and process data from one image.

5.5.2 Detail

A flow diagram of algorithm 2 is shown in figure 5.4 . The data collection cycle is identical to that of algorithm 1.

At the start of the image processing cycle, 32 gain functions are formed using each of the 32 echo functions so as to bring all the echo signals to a level $\bar{e}$:

$$G_N(k) = G_0(k) + 20.\log_{10}\left(\frac{\bar{e}}{E_N(k)}\right) \qquad \text{- Equation 5.5}$$

So as to try and prevent the gain rising in anechoic regions and bringing up the noise level, an upper limit M_1 is imposed on positive gain slopes as follows:

If $G_N(k) - G_N(k-1) > M_1 \Delta x$ - Equation 5.6

Then $G_N(k) = G_N(k-1) + M_1 \Delta x$ - Equation 5.7

for k = 1,64

(Δ x is the range interval of the TGC function.)

The value of M_1 was determined empirically by scanning the grey-scale test object and two normal abdomens. The value chosen is a

Figure 5.4 Flow diagram of Algorithm 2

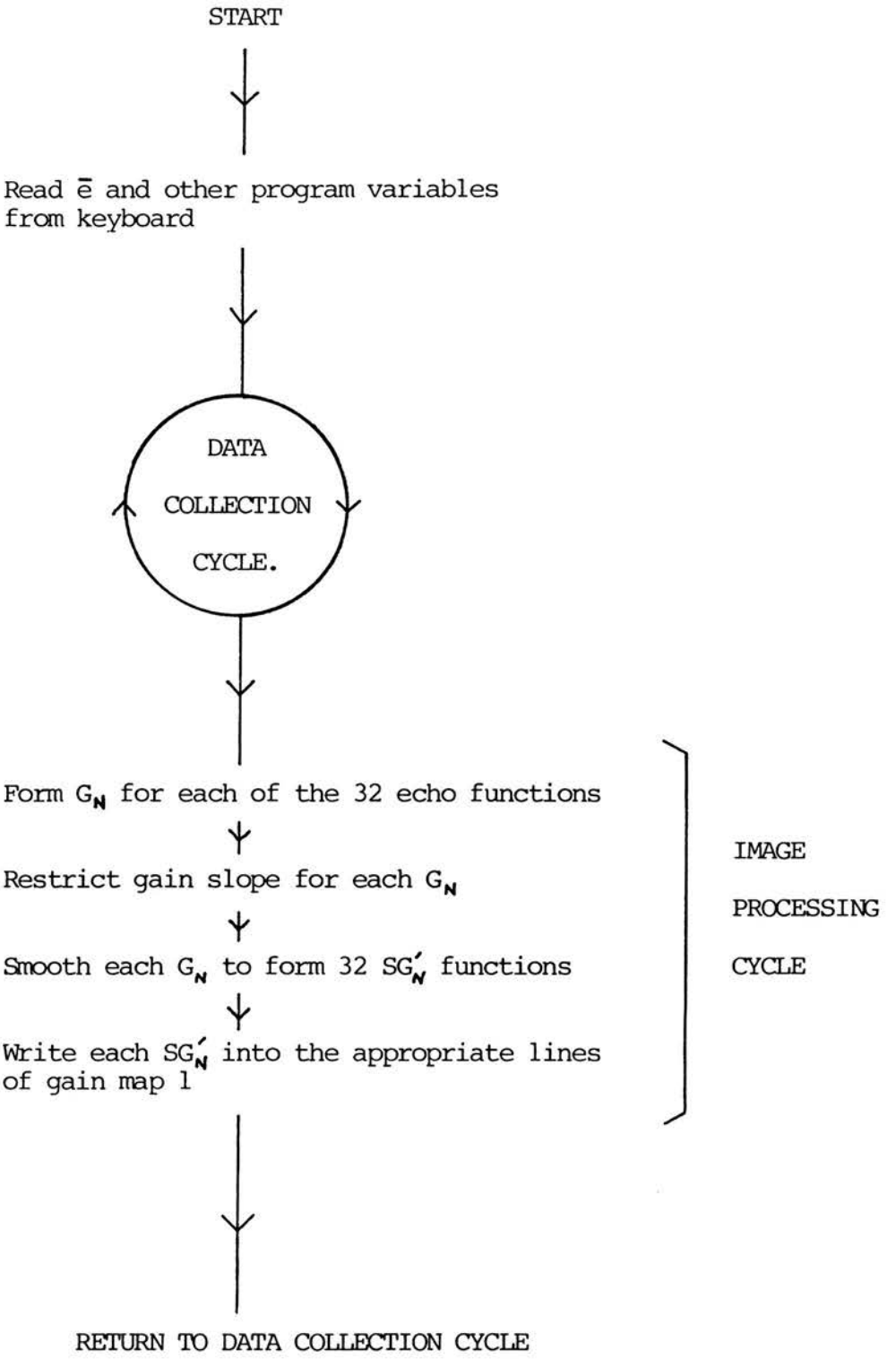

compromise between

(1) the slope required to present soft tissue regions, such as liver, at a uniform level, and

(2) the maximum slope which can be allowed without bringing up the noise level in large blood vessels or large anechoic regions such as the bladder or the low attenuation gel of the test object.

M_1 = 10 dB cm^{-1} was used for scanning at 3.5MHz.

Each gain function is then smoothed. The user selects which one of a number of local smoothing operators is to be applied to the gain functions. The smoothing operators have window sizes of 3, 5, 9 and 17 elements. The smoothing operator works by replacing the central element of the window with the mean value of the elements within the window. For example, suppose that a smoothing operator with a window size of 5 elements is applied to function G_N to produce gain function SG_N. SG_N is obtained from G_N in the following way:

$$SG_N(k) = \frac{1}{4}\left(\frac{1}{2} G_N(k-2) + G_N(k-1) + G_N(k) + G_N(k+1) + \frac{1}{2} G_N(k+2) \right)$$

- Equation 5.8 for k = 1,64

In general, for a window of width W elements (where W is odd):

$$SG_N(k) = \frac{1}{W-1} \sum_{i=k-\frac{W-3}{2}}^{i=k+\frac{W-3}{2}} G_N(i) + \frac{1}{2(W-1)} G_N\left(k-\frac{W-1}{2}\right) + \frac{1}{2(W-1)} G_N\left(k+\frac{W-1}{2}\right)$$

- Equation 5.9 for k = 1,64

The two end elements of the window only carry half the weighting of the others. This means that when the sum of the elements has been formed, the division $\frac{1}{W-1}$ is a division by 2,4,8 or 16. This can be

done rapidly in the microcomputer by shifting bits in a register.

The smoothing is symmetrical with respect to time since equal contributions are made to $SG_N(k)$ by $G_N(k-i)$ and $G_N(k+i)$. It is reasonable to use a symmetrical smoothing operator so that a gain function with constant slope, such as might compensate for attenuation in a uniform tissue region, is not altered by the smoothing operator. An RC filter applied to the analogue gain control signal does not behave symmetrically and shifts the gain signal by an amount dependent on the time constant of the filter. A straight line is shifted by an amount RC.

The purpose of applying smoothing is so that the gain functions only compensate for the general decrease in echo amplitude with depth and do not completely remove the contrast between different tissue types. Consider the situation shown in figure 5.5 where a transducer insonates two regions with the same attenuation but slightly different scattering power. The effects of manual TGC and algorithm 2 are illustrated in figure 5.5 b to e . The manual TGC maintains a constant difference between the signals from the two regions. Algorithm 2 emphasises the boundary of the regions, but the signal levels equalise a distance equal to the width of the smoothing operator on either side of the boundary.

Describing algorithm 2 in terms of equation 5.1, β always equals 1 and SG_N replaces H_N .

5.5.3 Simulation Results - Contrast

The results of the contrast simulation for algorithm 2 are shown in figure 5.6. The smoothing operator used in the simulation has a window size of 13 elements. This matches the time constant of 50 μs which was found by McDicken to give satisfactory results with bi-stable images.

Figure 5.5 Manual TGC and Algorithm 2 :
TGC waveforms and receiver output signals (assuming no speckle). Regions 1 and 2 have two-way attenuation coefficient $\propto$ dB cm^{-1}

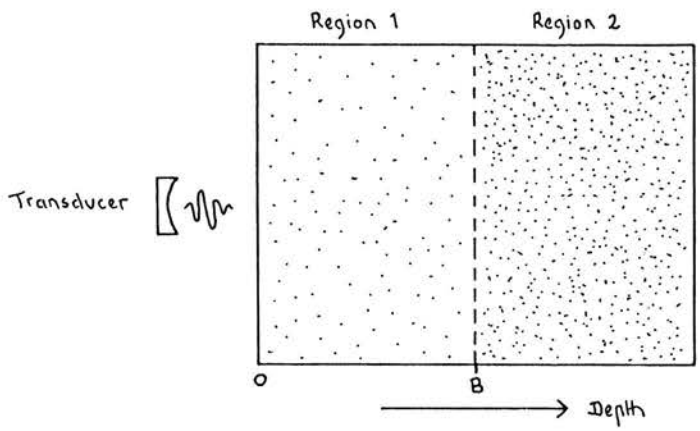

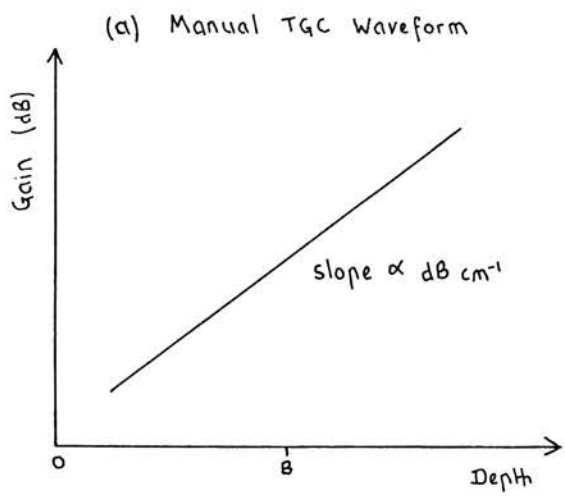

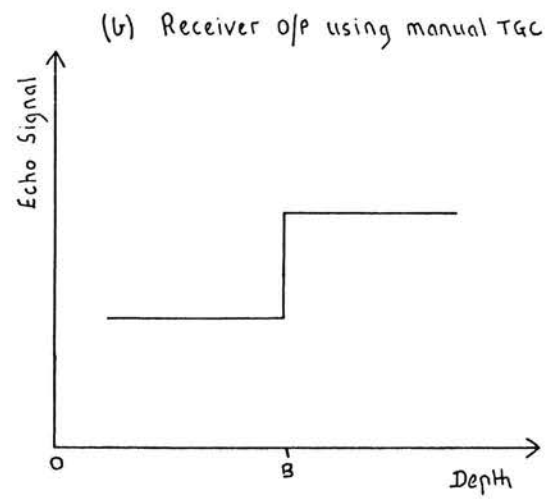

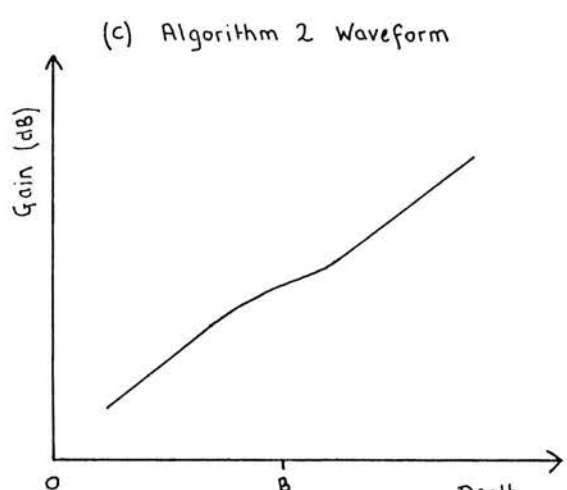

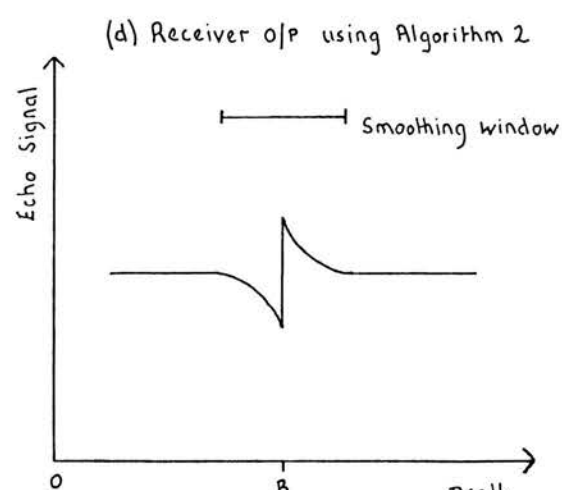

Figure 5.6 Contrast Simulation of Algorithm 2

(Broken lines show simulated manual TGC results.)

(a) +20 dB Objects

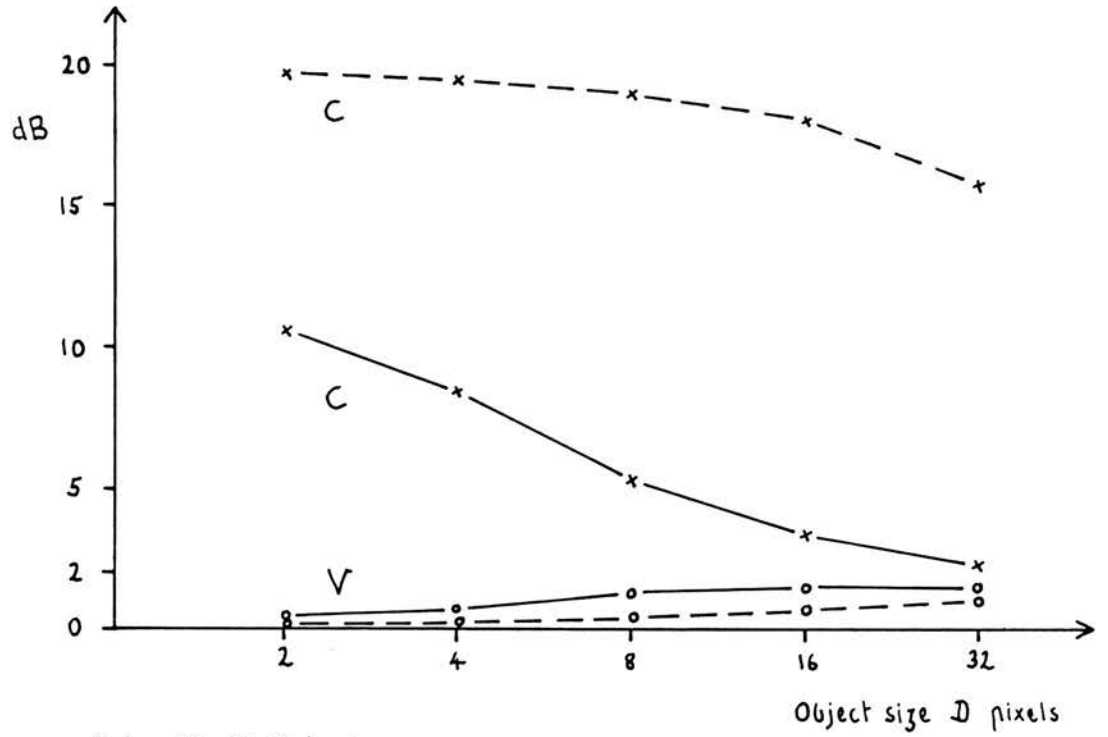

(b) +5 dB Objects

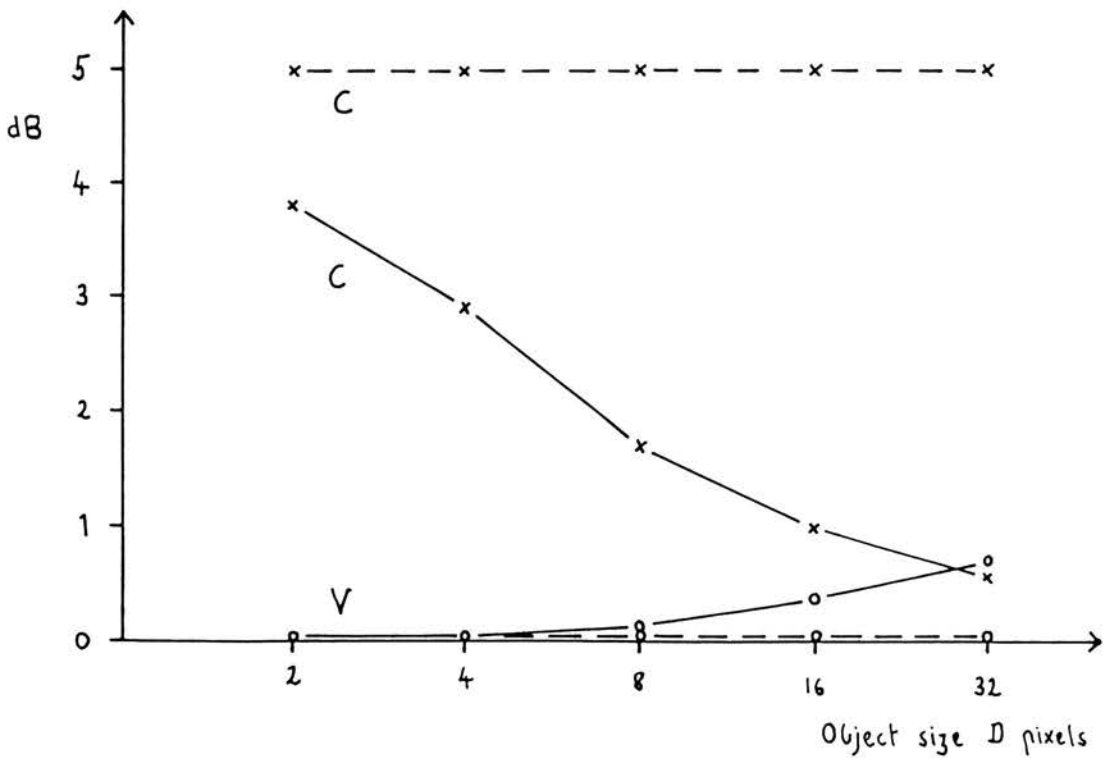

Figure 5.6 Contrast Simulation of Algorithm 2

(Broken lines show simulated manual TGC results.)

(c) -5 dB Objects

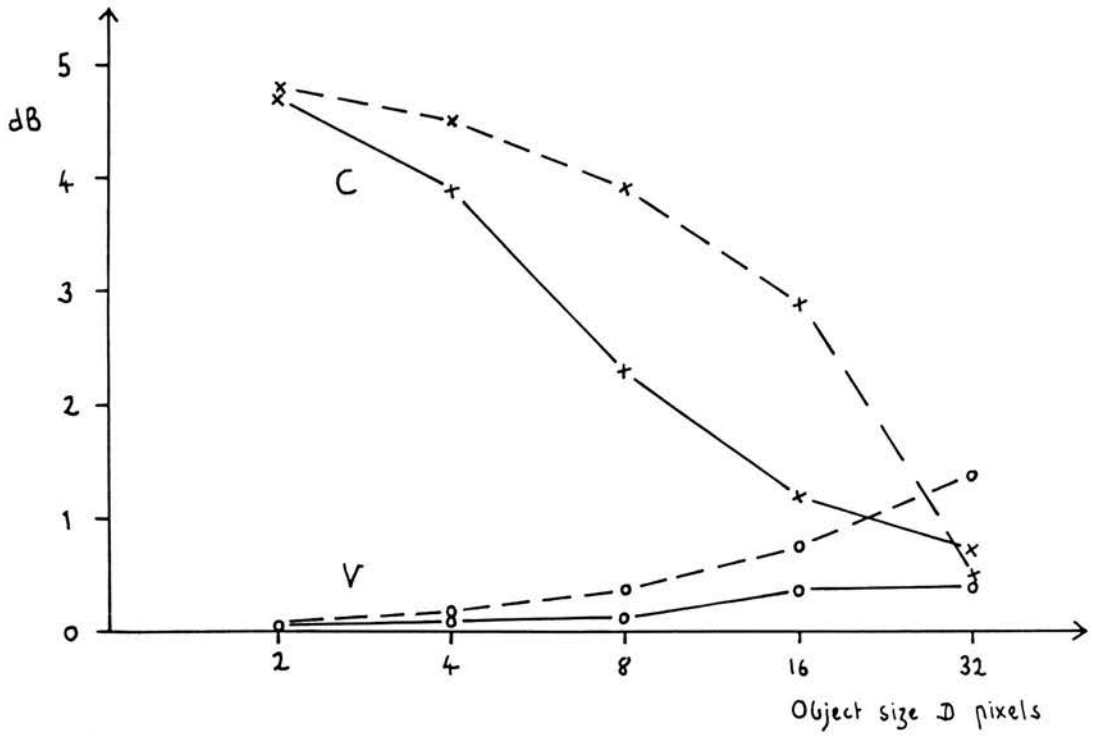

(d) -20 dB Objects

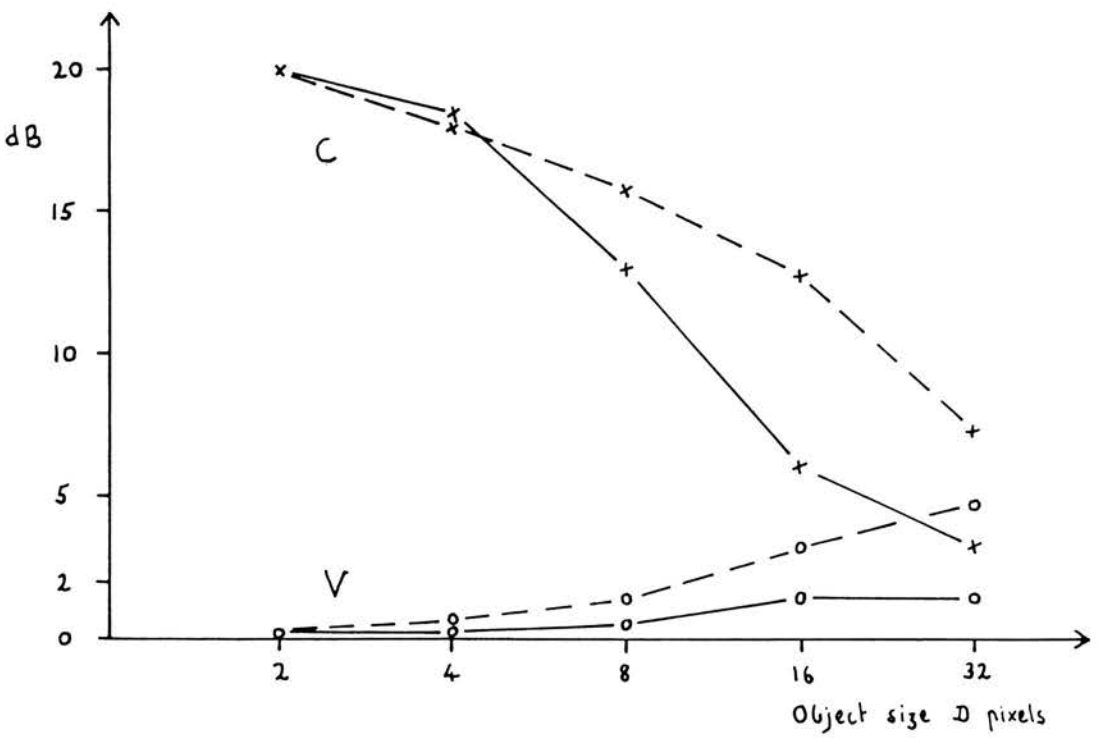

The quantities C and V are defined in section 4.3.1. The unbroken lines in figure 5.6 plot C and V for algorithm 2 and the broken lines are plots of C and V for the simulated manual TGC described in section 4.3.2.

Figure 5.6 shows that for algorithm 2, with all four combinations of attenuation and backscattered amplitude, the object/background contrast C falls off more rapidly with increasing object size than is the case for the simulated manual TGC. For the +20dB and +5dB objects, C falls off much more rapidly for algorithm 2 than for simulated manual TGC, although the object and the background are presented more uniformly by algorithm 2* (That is, they have smaller values of V).

From these results, we might expect the clinical images produced by algorithm 2 to have much less contrast in them than images set up using manual TGC. It is difficult to predict from the simulation results whether this will improve the overall image quality by bringing more regions within the dynamic range of the display, or degrade the image quality by making low contrast regions indistinguishable.

5.5.4 Imaging Results

Figure 5.2c shows an image of the test object obtained using algorithm 2 with a smoothing window of 13 elements. The loaded gel is well presented - the only artifact being the bright up at the edge of each step. The low attenuation gel is poorly presented, with a high signal level in the deepest part. Compared with the manual TGC image (figure 5.2a), figure 5.2c shows the loaded gel more clearly, but the low attenuation gel is not as well presented.

Algorithm 2 was tested on two normal subject and images were obtained of the liver, right kidney, aorta, IVC, pancreas and bladder. The tissue boundaries in the adaptive images were generally well

* for -5dB and -20 dB objects.

defined: for example, the walls of the major vessels, the kidney capsule, the bladder wall and the diaphragm. However, I judged all the images to be inferior to manual TGC images of the same section due to loss of contrast between the different tissue types: for example, liver/kidney and pancreas/liver. This gave the adaptive images a washed-out appearance. The major vessels and the bladder were also noisy.

Attempts were made to improve the performance of algorithm 2 by varying the window size of the smoothing operator from 5 elements to 17 elements and by progressively reducing the maximum gain slope to 4dB cm^{-1}. The results obtained were no more satisfactory. Reducing the size of the smoothing window decreased the contrast in the image even further. Increasing the size of the window resulted in some improvement in contrast but strong reflectors were then pushed into saturation. Reducing the maximum gain slope is not a suitable method for preventing excessive noise in anechoic regions because a slope small enough to prevent noise in the major vessels and in pools of fluid is too small to compensate for attenuation in soft tissue such as liver parenchyma.

Because of these poor preliminary results, algorithm 2 was not tested clinically.

5.6 ALGORITHM 3

5.6.1 Outline

Algorithm 3 was used to investigate several ways of setting up a single TGC function to be applied to all the scan lines in an image. (Also referred to as a global TGC function.) Other workers have derived global TGC functions using either the maximum or the mean echo amplitude within various depth ranges (see sections 1.6 and 2.1).

Algorithm 3 takes 0.5 to 0.7 seconds to collect and process data from one image.

5.6.2 Detail

A flow diagram of algorithm 3 is shown in figure 5.7. The data collection cycle is the same as that for algorithm 1.

At the start of the image processing cycle, E_o is formed by combining the 32 stored echo functions. The user can select one of three ways of combining the echo functions:

(1) By calculating the maximum value at each depth:

$E_o(k)$ = maximum value of

$$\{ E_1(k), E_2(k) \ldots E_N(k) \ldots E_{32}(k) \} \qquad \text{- Equation 5.10}$$

(2) By calculating the median value at each depth:

$E_o(k)$ = median value of

$$\{ E_1(k), E_2(k) \ldots E_N(k) \ldots E_{32}(k) \} \qquad \text{- Equation 5.11}$$

(3) By calculating the mean value at each depth:

$E_o(k)$ = mean value of

$$\{ E_1(k), E_2(k) \ldots E_N(k) \ldots E_{32}(k) \} \qquad \text{- Equation 5.12}$$

The advantage of selecting the maximum value at each depth is that it can be done faster in hardware than calculating the mean value. Selecting the median value would probably take longer than calculating

Figure 5.7 Flow diagram of Algorithm 3

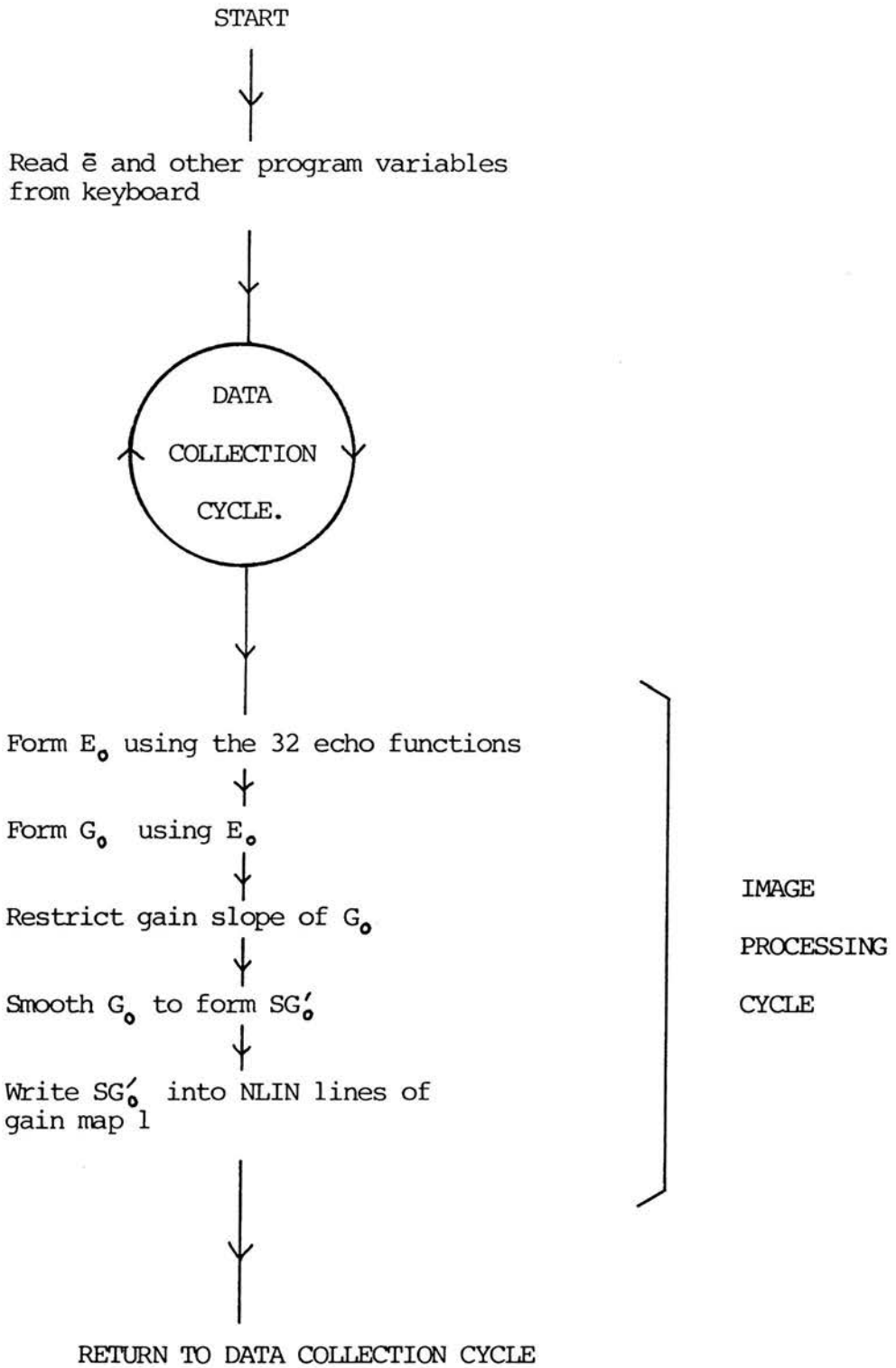

the mean, and the median did not have any potential advantages that were known. However, median filters are widely used in other areas of image processing. They have properties quite distinct from those of mean filters, such as rejecting spike noise and preserving edges (Pratt, 1978). It was decided to use median values in forming E_o so as to observe the effects in this situation.

Once E_o has been calculated, new values for G_o are calculated so as to bring each element of E_o to a mid-grey level $\bar{e}$ (see equation 5.3). The gain slope is then tested for each pair of adjacent elements to see if it exceeds M_1 ,the maximum positive slope allowed . If it does, the slope is restricted to M_1 (see equations 5.6 and 5.7).

A gain function SG_o is then formed from G_o by applying one of the smoothing operators described in section 5.5.2. SG_o is then written into NLIN lines of gain map 1.

5.6.2.1 Smoothing with depth.

Why is it necessary to smooth G_o? This question has been partly answered in section 5.5.2 describing algorithm 2 : smoothing with depth increases the contrast between different tissue regions. However, the results of smoothing the gain function with depth are rather different for algorithm 3 than for algorithm 2. This is because in algorithm 3, the echo data is combined across the image before G_o is formed. So, what is the optimum window size for the smoothing operator in algorithm 3 ? A number of factors have to be considered:

(1) If the smoothing window is too small, light and dark bands will appear across the image. This is because strong signals tend to reduce the gain at their depth, and anechoic regions tend to raise the gain at their depth. Smoothing G_o serves to distribute the effect of strong and weak signals more evenly between the axial and lateral directions. This

is illustrated in figure 5.9 which shows a section through the liver, diaphragm, IVC and other vessels. The image in figure 5.9a was processed using algorithm 3 with a smoothing window of 3 elements. Local regions of high and low signal level on the left side of the image produce dark and light bands across the liver. The strong diaphragm echo heavily suppresses the liver echoes directly in front of it. The image is thus poorly presented.

Figure 5.9b shows the same tissue section processed by algorithm 3 with a smoothing window of 9 elements. The banding has been evened out and the liver appears more uniform. Overall, the image is better balanced than figure 5.9a.

(2) If the smoothing window is large, organ parenchyma is well presented without noticeable banding, but the gain cannot be reduced very much for strong signals and so they often remain in saturation. This is illustrated in figure 5.2e which shows an image of the test object processed using algorithm 3 with a smoothing window of 17 elements. The bright up on the steps of the loaded gel is more pronounced than in figure 5.2d, which was produced using algorithm 3 with a smoothing window of 9 elements.

(3) Large smoothing windows can produce banding artifacts across an image even if the medium being scanned is homogeneous. Consider the gain function required to produce a uniform, mid-grey level image of an homogeneous medium with a two-way attenuation coefficient close to that of soft tissue. The medium is insonated by a fixed focus transducer. The gain function would be similar to that shown in figure 5.10a. The slope of the gain function is greater in the near field than in the focal zone because the transducer is less sensitive in the near field. The gain slope decreases to zero when the maximum gain of the receiver is reached. The effects of smoothing this function with a 9 element

FIGURE 5.9 : Right lobe of liver, IVC and diaphragm.

(a) Adaptive TGC: Algorithm 3.0

(b) Adaptive TGC: Algorithm 3

Figure 5.10 Smoothing the TGC waveform with depth. The waveform in (a) is shown by broken lines in (b) and (c). $\S$ is gain in dB below maximum receiver gain. (See text for details.)

(a) Unsmoothed waveform

P ≈ 3 cm

Q ≈ 10cm

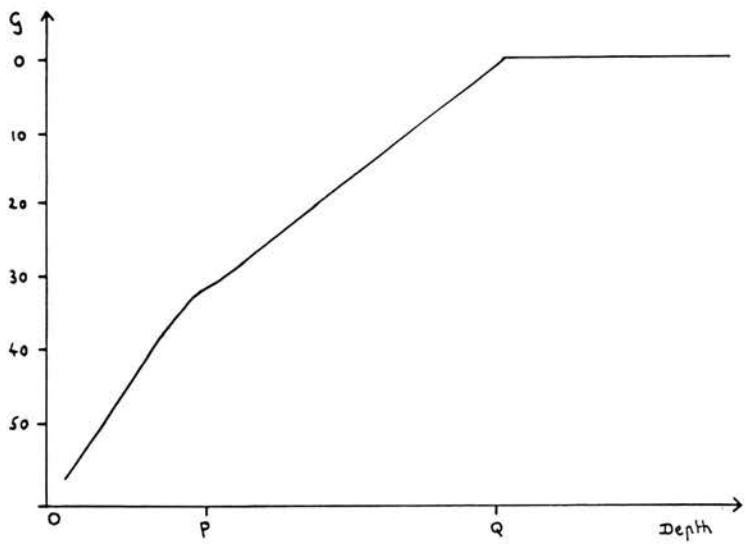

(b) Waveform in (a) smoothed by 9 element window

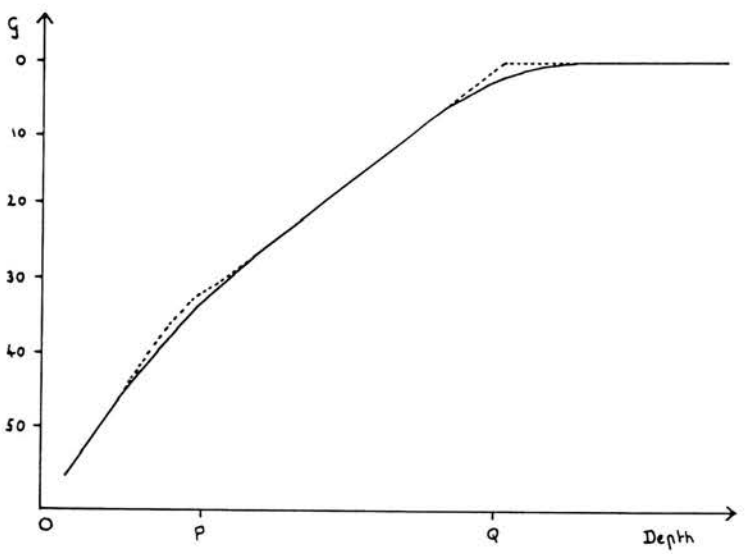

(c) Waveform in (a) smoothed by 17 element window

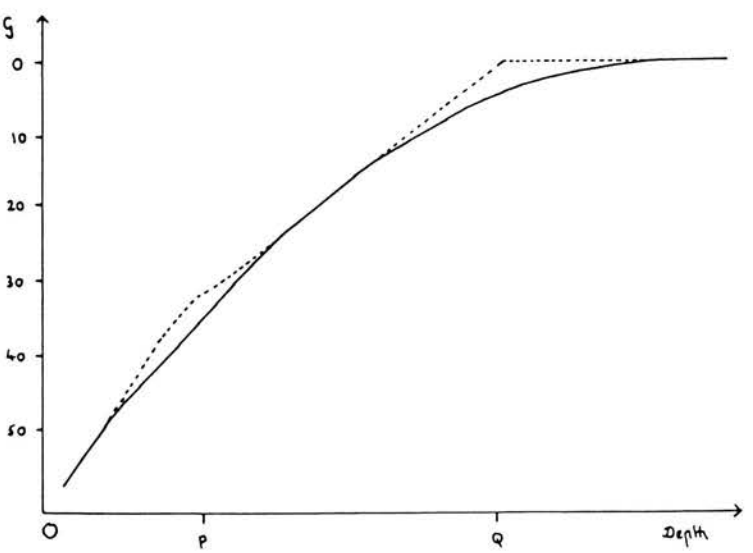

window and a 17 element window are illustrated in figure 5.10 b and c. The larger the window, the greater is the separation of the smoothed and unsmoothed curves at the depths labelled P and Q. Since the unsmoothed function produces a uniform image, a heavily smoothed function produces an image with dark bands across it at depths P and Q. The smaller the window, the less the banding.

There are several possible solutions to this problem:

(i) The sensitivity of the transducer and the limited gain of the receiver can be taken into account when the gain settings are being calculated, and so the curve of figure 5.10a is adjusted to become a straight line before it is smoothed. The gain changes necessary to allow for the transducer sensitivity and limited receiver gain are then re-applied after smoothing has taken place. This procedure is time consuming because it involves several floating point multiplications per element.

(ii) A median smoothing operator can be used instead of a mean smoothing operator. Median operators have the property of leaving monotonically increasing functions unchanged. Although no floating point arithmetic need be involved, median values require considerably more time to calculate than mean values.

(iii) A mean smoothing operator with variable window size can be used. This technique is described further in section 5.8.2 .

(iv) A mean smoothing operator with a constant window size can be used. The window size is a compromise between the size necessary to prevent dark bands at

depths P and Q and the size necessary to eliminate the banding produced by very large and small signals in the image. This is the approach adopted by algorithm 3. Window sizes from 3 elements to 17 elements were tested in abdominal and obstetric imaging and with the test object. A window size of 9 elements was found to be acceptable in many situations.

5.6.2.2 Noise in anechoic regions

A number of features of algorithm 3 tend to prevent the gain rising so far that excessive noise appears in anechoic regions. These are as follows:

(1) A consequence of using the mean signal at each depth to form G_o is that echo signals from tissue at the same depth as an anechoic region tend to reduce the gain at that depth.

(2) A consequence of smoothing G_o is that echo signals from tissue above and below an anechoic region tend to reduce the gain in the anechoic region.

(3) An upper limit is placed on the slope of G_o. As with algorithm 2, the maximum positive slope allowed is a compromise between the slope necessary to prevent noise in pools of fluid and the slope necessary to compensate for attenuation in soft tissue. A range of maximum gain slopes were tested using with the grey-scale test object and in abdominal and obstetric scanning. Values of 10dB cm^{-1} in abdominal work and 8dB cm^{-1} in obstetric work were found to be adequate in

many situations, scanning at 3.5MHz . The lower value in obstetric work reflects the fact that more fluid is usually encountered in obstetric scanning than in abdominal scanning.

Describing algorithm 3 in terms of equation 5.1, β always equals 0 and SG_o replaces H_o .

5.6.3 Simulation Results - Contrast

The simulation of algorithm 3 uses the mean values of E_1 to E_{32} at each depth and a 9 element smoothing operator. This implementation of algorithm 3 was found to give the most satisfactory imaging results (see section 5.6.4).

The simulation results for algorithm 3 and simulated manual TGC are shown in figure 5.8. For +20dB objects, C falls off more rapidly with increasing object size using algorithm 3 than it does for simulated manual TGC. However, algorithm 3 still maintains over 12dB of contrast for an object of 32 x 32 pixels, compared to only 2dB for algorithm 2.

For +5 and -5dB objects the results using algorithm 3 and simulated manual TGC are quite similar. For -20dB objects, the manual TGC retains more contrast with increasing object size but the non-uniformity V is greater as well.

On the basis of these results, we might expect algorithm 3 and manual TGC to behave in a similar way where only small changes in backscattered amplitude and attenuation coefficient are involved. For example, in the liver or spleen. The different effects of algorithm 3 and manual TGC should be visible where there are large changes in signal strength and attenuation coefficient over the image. For example, in obstetric imaging.

Figure 5.8 Contrast Simulation of Algorithm 3

(Broken lines show simulated manual TGC results.)

(a) +20 dB Objects

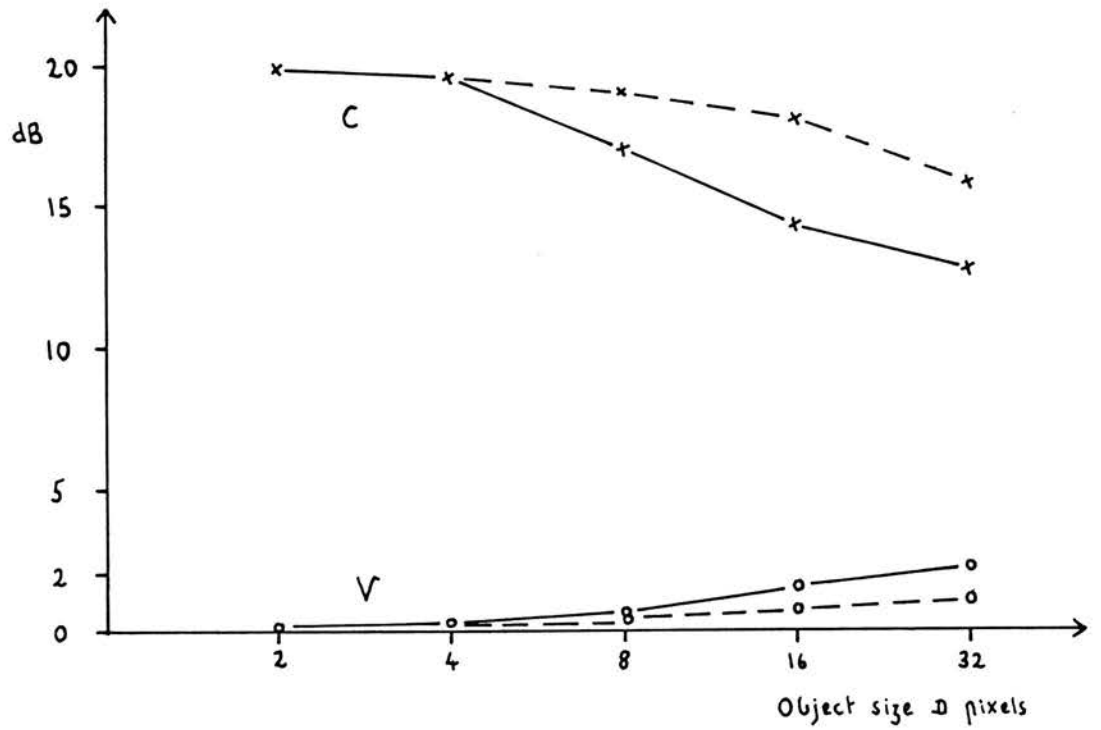

(b) +5 dB Objects

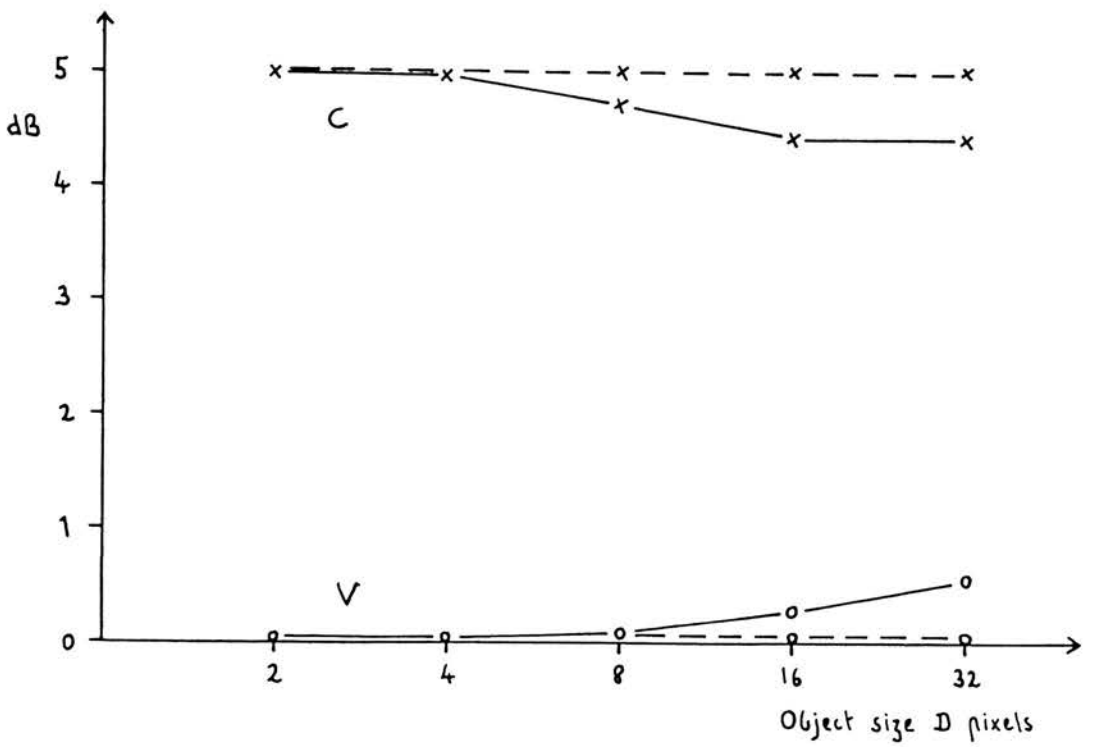

Figure 5.8 Contrast Simulation of Algorithm 3

(Broken lines show simulated manual TGC results.)

(c) -5 dB Objects

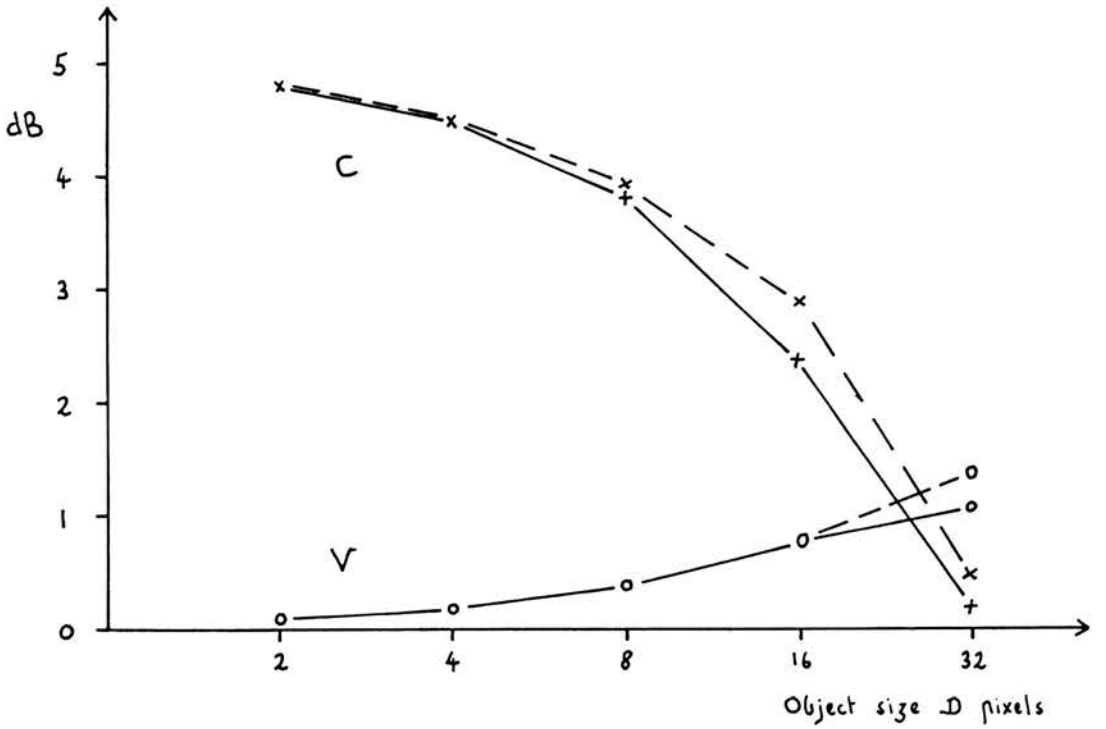

(d) -20 dB Objects

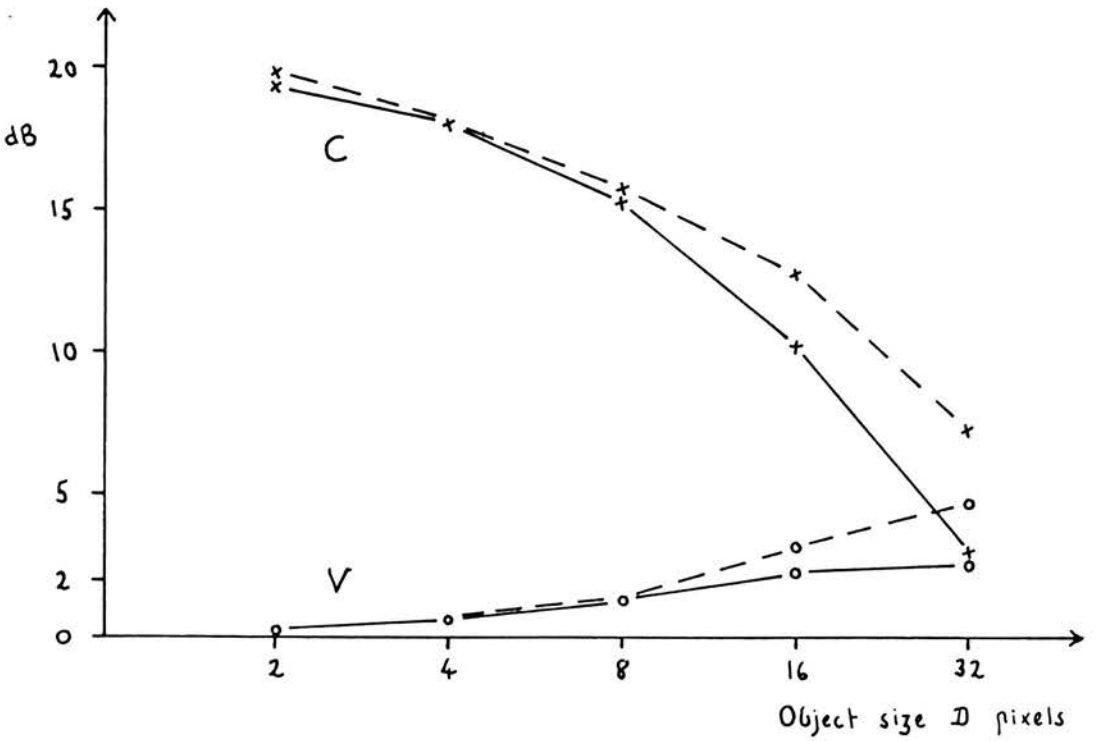

5.6.4 Imaging Results

5.6.4.1 Forming E_o

The effects of the three different methods of forming E_o were assessed using the grey-scale test object. The probe was positioned to give the image shown in figure 5.2 and then moved around slowly over the surface of the test object while algorithm 3 was running.

Forming E_o using the maximum echo amplitude at each depth tended to produce images that were unstable. This was largely due to the fact that any bright reverberation artifacts caused by poor probe contact at the edges of the sector were taken as the maximum signal level at that depth. This problem could be overcome by considering just the echoes from the central portion of the sector. However, reverberation artifacts can often occur over large areas of the sector, such as when scanning between the ribs, and so this solution is probably not acceptable.

Forming E_o using the median echo amplitude at each depth produced results that were more satisfactory than using the maximum amplitude; the gain settings were affected less by reverberation artifacts. However, the gain settings were often sensitive to slight changes in the scan plane. This is a poor feature.

Forming E_o using the mean echo amplitude at each depth gave the most satisfactory results of the three methods. The images were affected less by reverberation artifacts than the images obtained using maximum amplitudes and the gain settings changed smoothly as the scan plane was altered slowly. This result can be explained when we consider that the maximum and median methods both choose a single value from many at each depth, whereas the mean combines all the values at each depth.

A single value chosen from many is more likely to be subject to fluctuations than the mean value. All further discussion of algorithm 3 assumes that the mean echo value is used to form E_o.

5.6.4.2 Test Object

The image of the grey-scale test object shown in figure 5.2d was produced using algorithm 3 with a 9 element smoothing operator. The result is like the manual TGC image - very little noise in the low attenuation gel and a region of saturation on each step of the loaded gel. The penetration into the loaded gel on the right side of the image is not as good as for algorithm 2.

5.6.4.3 Clinical Trial

Algorithm 3 was tested in abdominal and obstetric work using a 9 element smoothing operator. The results obtained were consistent with the contrast simulation results. The simulation indicated that uniform tissue regions would be dealt with in a similar way by algorithm 3 and manual TGC. This was found to be so: figure 5.11 is an example, showing the liver and pancreas.

Where a group of strong reflectors lie at one depth across the image, algorithm 3 can make an improvement over manual TGC by reducing the gain at that depth. This is illustrated in figure 5.12 where the posterior uterine wall and the basal layer of the placenta are more clearly presented in the adaptive image. However, where strong signals occur at a range of depths, the manual TGC and adaptive TGC often had similar effects. This is shown in figure 5.13 where bright-up behind a large pool of liquor extends over 10 cm of depth.

Where an anechoic region more than 1 or 2 cm deep extends right across the field of view, the restricted rate of gain rise is not

FIGURE 5.11 : Section showing the left lobe of the liver, the pancreas, splenic vein, superior mesenteric artery, aorta and superior vena cava.

(a) Adaptive TGC: Algorithm 3

(b) Manual TGC

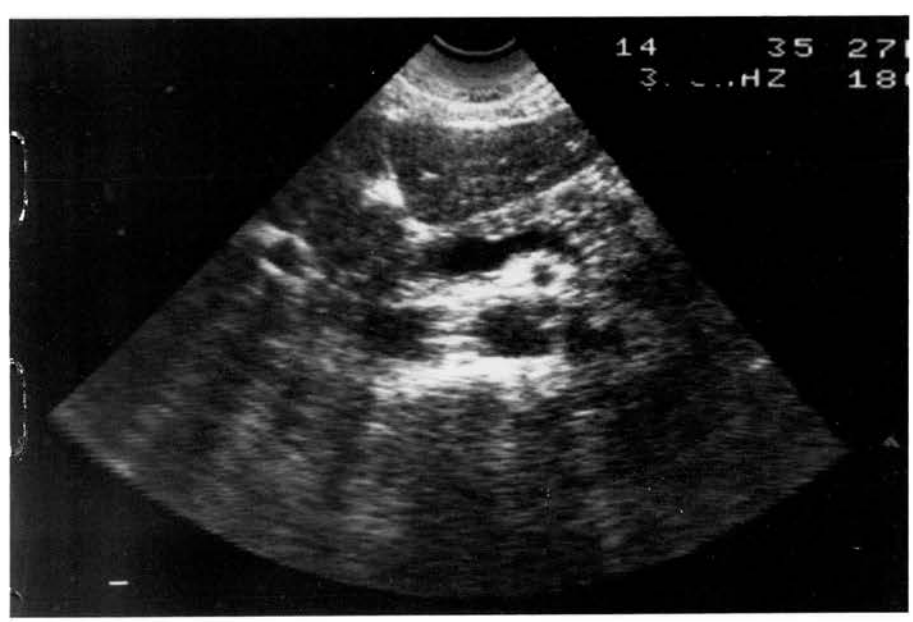

FIGURE 5.12 : 33 week pregnancy showing the chorionic plate, the body and the basal layer of the placenta.

(a) Adaptive TGC: Algorithm 3

(b) Manual TGC

FIGURE 5.13 : 35 week pregnancy showing liquor, fetal limbs and fetal abdomen.

(a) Adaptive TGC: Algorithm 3

(b) Manual TGC

sufficient by itself to prevent the noise level becoming visible in the deepest part of the anechoic region. Figure 5.14a shows the noise level raised in a deep pool of liquor, compared with the manual image of figure 5.14b.

Banding was also observed in a few of the images produced using algorithm 3. Figure 5.15a is an example: the strong liver echoes on the left side of the image suppress the gain at that depth and cause a dark band across the liver on the right side of the image.

The results of the clinical trial are summarised in table 5.1. There are barely a sufficient number of pairs of images for a significant result to be possible using McNemar's χ^2 test. This is not important since the form of algorithm 3 that was used in the trial is similar to the commercial adaptive TGC system whose clinical trials are described in Chapter 2. A number of pairs images of the grey-scale test object were recorded using the commercial adaptive TGC and algorithm 3. Only very slight differences could be observed between the commercial adaptive TGC images and those obtained using algorithm 3.

Figure 5.16a illustrates the variation in the TGC set by algorithm 3 during the scan of a 16 week pregnancy. 10 gain functions were recorded at 30 second intervals during the scan and these are shown in figure 5.16a as "gain functions 1,2..10" . Figure 5.16b shows 10 gain functions recorded in the same way during the scan of a normal liver and right kidney. Algorithm 3 maintained good image quality throughout both scans. Table 5.2 summarises the amount of gain variation with time during the scans.

FIGURE 5.14 : Section showing a deep pool of liquor.

(a) Adaptive TGC: Algorithm 3

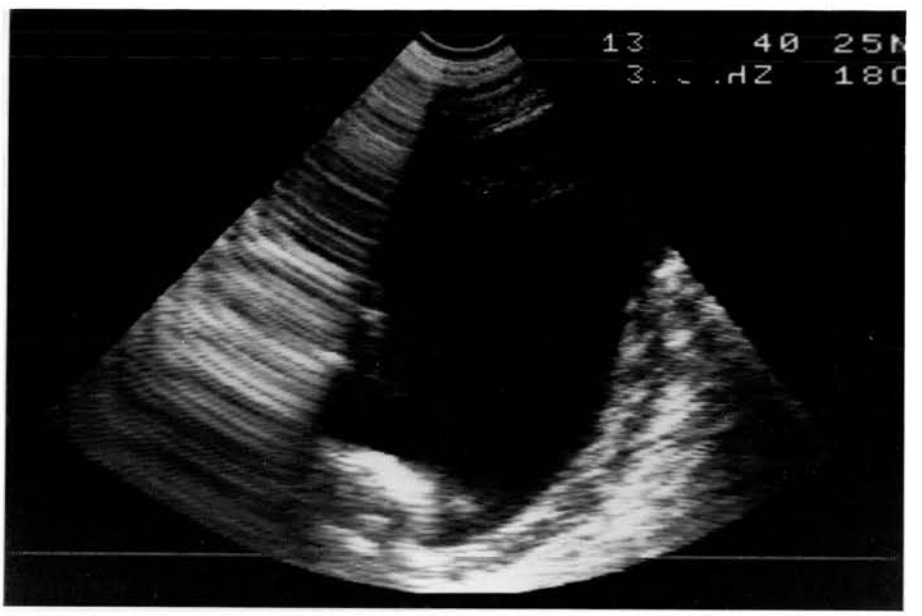

(b) Manual TGC

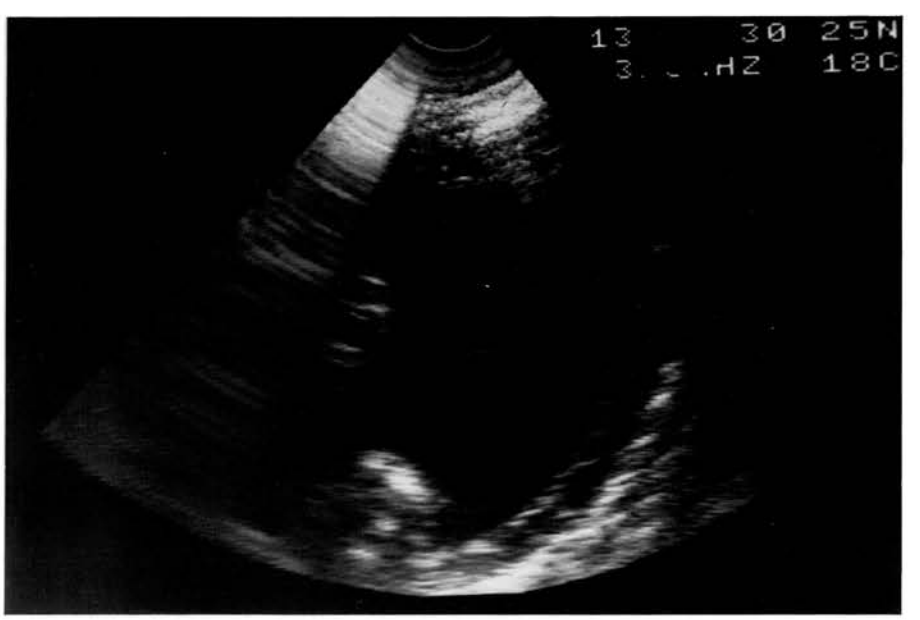

FIGURE 5.15 : Section showing ascites, the right lobe of the liver and right kidney.

(a) Adaptive TGC: Algorithm 3

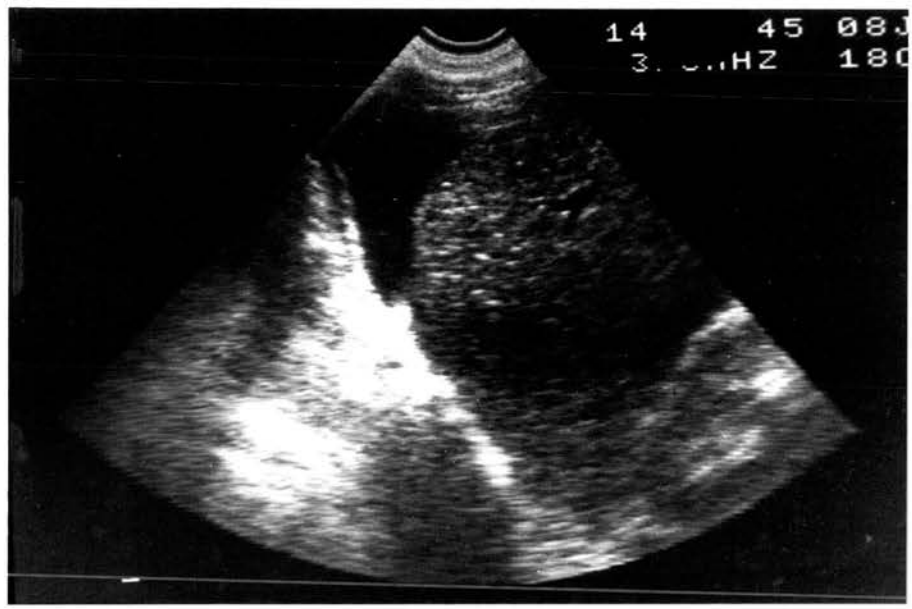

(b) Manual TGC

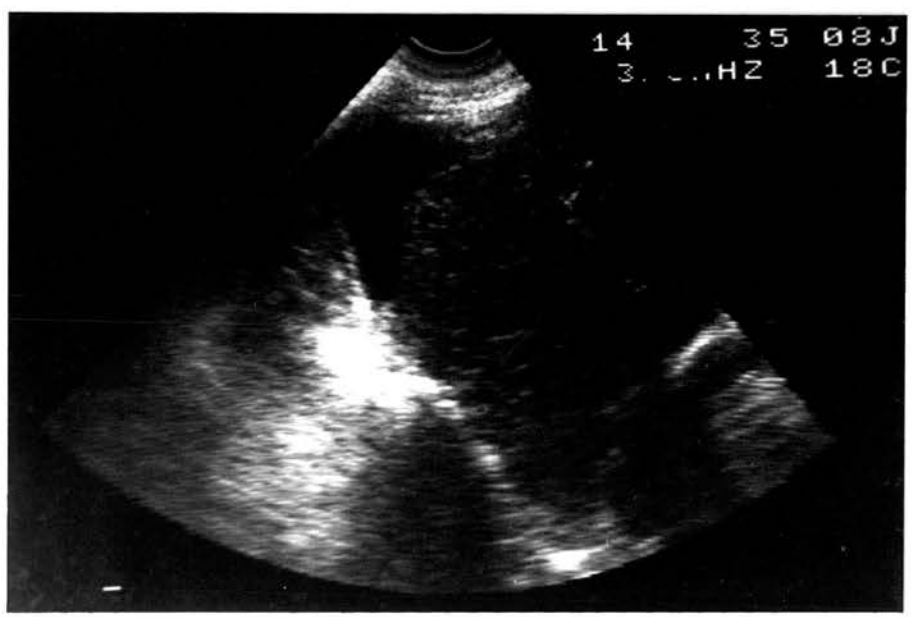

Table 5.1 Clinical Trial of Algorithm 3

(a) Obstetrics :

Number of patients = 9
Total number of pairs of images = 27
Number of comparable pairs of images = 15

CATEGORY	PHYSICIST	RADIOLOGIST
AA	3	8
A	5	
C	6	5
M	0	2
MM	1	
	$\chi^2 = 4.0$	$\chi^2 = 2.5$
	$0.025 < P < 0.05$	$0.1 < P < 0.25$

(b) Abdominal :

Number of patients = 7
Total number of pairs of images = 24
Number of comparable pairs of images = 12

CATEGORY	PHYSICIST	RADIOLOGIST
AA	2	4
A	2	
C	7	6
M	2	2
MM	1	
	$\chi^2 = 0$	$\chi^2 = 0.2$
	$P > 0.9$	$P > 0.5$

Figure 5.16a Gain functions set by Algorithm 3 during an obstetric scan (see text for details).

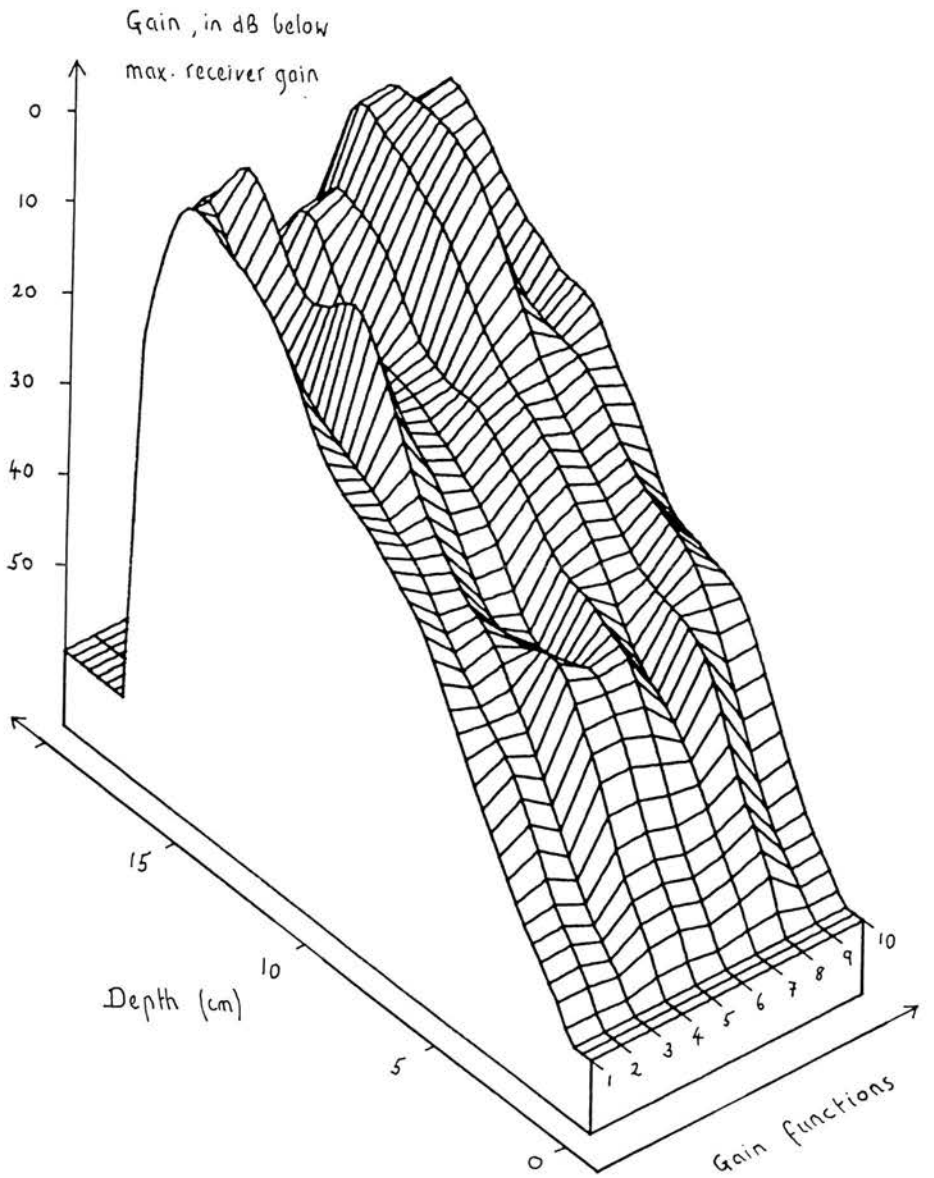

Figure 5.16b Gain functions set by Algorithm 3 during a liver scan (see text for details).

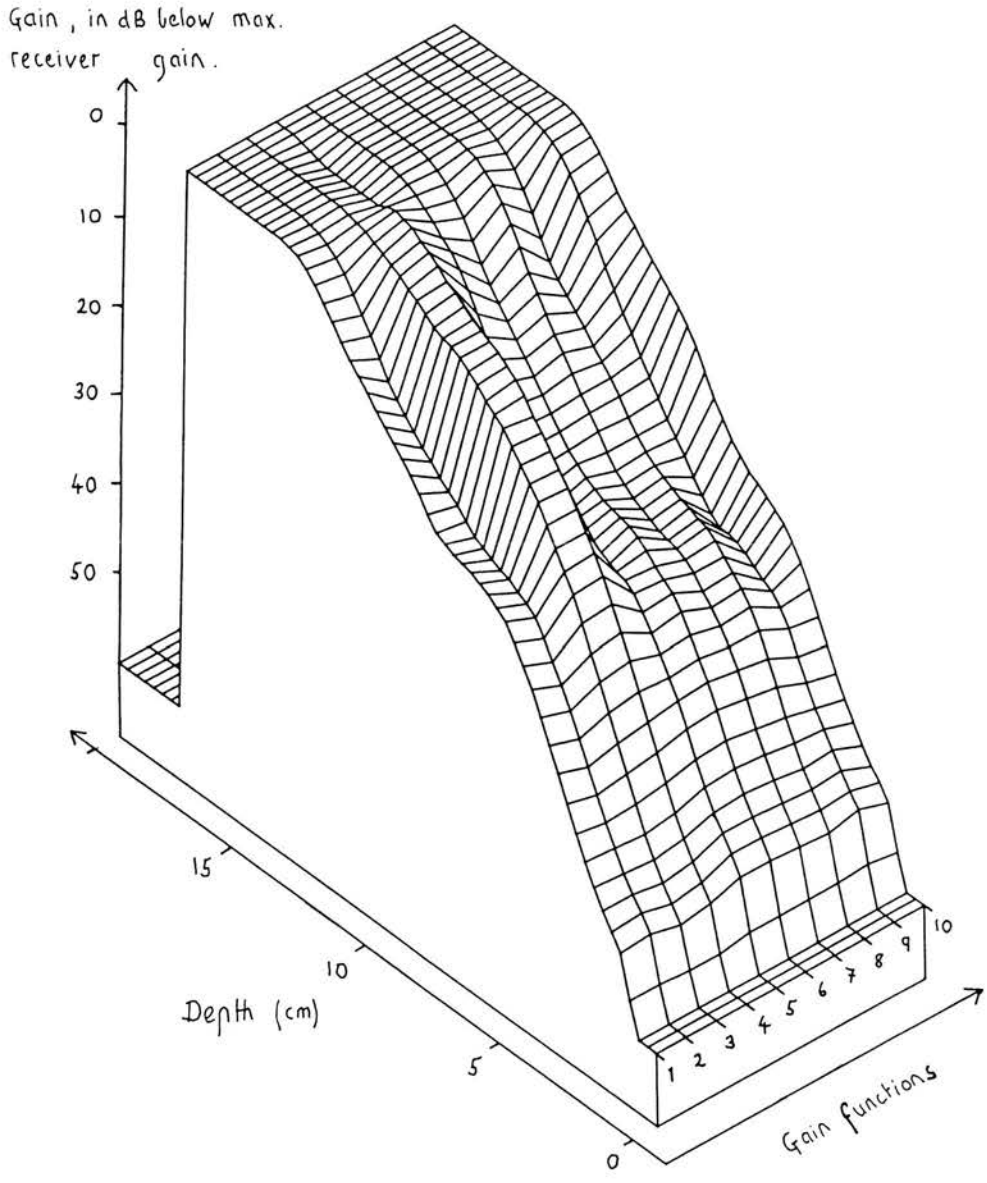

Table 5.2 Variation of gain settings during a scan.

For the 10 gain functions recorded during a scan, define

$\Delta G(y)$ = maximum gain value at depth y - minimum gain value at depth y

Max(ΔG) = maximum value of $\Delta G(y)$ for y in the range 3cm to 15cm.

Med(ΔG) = median value of $\Delta G(y)$ for y in the range 3cm to 15cm.

Min(ΔG) = minimum value of $\Delta G(y)$ for y in the range 3cm to 15cm.

	figure 5.16a	figure 5.16b
Max(ΔG) dB	17·0	15·6
Med(ΔG) dB	9·2	5·3
Min(ΔG) dB	6·1	0·3

5.7 ALGORITHM 4

5.7.1 Outline

Algorithm 4 attempts to produce a balanced image by combining a gain function derived using echo information from the whole image with gain functions formed using echo information from individual scan lines. In this way the algorithm can set a unique gain function for each part of the image. Its main aim is to overcome the problem encountered using both manual TGC and algorithm 3 - that regions of high signal level are often left in saturation. Algorithm 4 does not address the problem of keeping the gain down in large anechoic regions or the lesser problem of large signals creating bands across the image.

Algorithm 4 takes between 1.5 and 2 seconds to collect and process data from one image.

5.7.2 Detail

A flow diagram of algorithm 4 is shown in figure 5.17. Data collection is performed in the same way as in algorithm 1.

During the image processing cycle, gain function SG_0 is formed as for the version of algorithm 3 used in the clinical trial (see section 5.6.4).

32 gain functions are then calculated using the 32 stored echo functions, following equation 5.5.

The gain function G'_N that is applied to the Nth scan line in the image is formed by combining G_N and SG_0 such that

If $G_N(k) > SG_0(k)$ then $G'_N(k) = SG_0(k)$ - Equation 5.13

If $G_N(k) < SG_0(k)$ then $G'_N(k) = [\ G_N(k) + SG_0(k)\ ]/2$ - Equation 5.14

Figure 5.17 Flow diagram of Algorithm 4

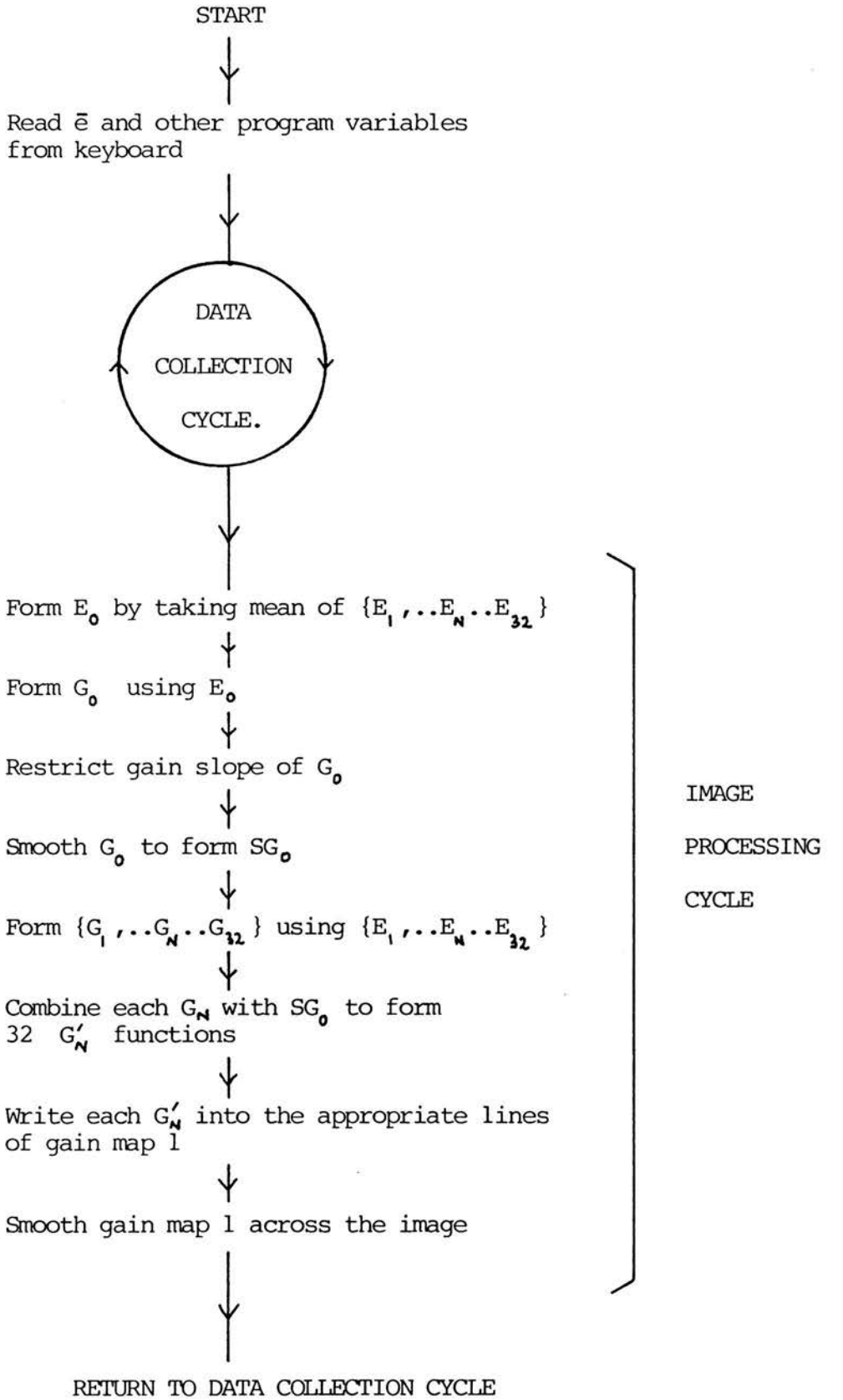

Describing algorithm 4 in terms of equation 5.1,

If $H_N > H_o$ then $\beta = 0$ - Equation 5.15

If $H_N < H_o$ then $\beta = \frac{1}{2}$ - Equation 5.16

Let us consider why this is a better strategy than just setting β always equal to 1 or 0 as in algorithms 2 and 3. The value of each element of SG_o is derived by averaging the signal level across the width of the image and over a depth of 9 elements (27 mm). If $G_N(k) > SG_o(k)$ then we are dealing with a local signal level that is below average. By setting $G'_N(k) = SG_o(k)$, we achieve the same effect as algorithm 3. If $G_N(k) < SG_o(k)$ then we are dealing with a local signal level that is above average. Such signals are the ones that could be in saturation. By setting $G'_N(k) = G_N(k)$ we would bring the signal level right down to mid-grey. However, this would remove the contrast between the signal and the background. By combining a fraction β of G_N with a fraction $(1-\beta)$ of SG_o we can achieve a useful amount of signal compression without removing all the contrast. The value $\beta = \frac{1}{2}$ was determined empirically by imaging the grey-scale test object and two normal abdomens. Using $\beta = \frac{1}{2}$ allows regions of very high signal level (such as the posterior wall of the uterus, the fetal skull, the diaphragm and regions of bright-up) to be presented clearly while still retaining sufficient contrast in regions of lower, but still above average, signal level. (For example, the kidney collecting system and the pancreas.) I would not expect $\beta = \frac{1}{2}$ to give optimum results for all scanners because the fixed signal compression that a scanner uses will affect how much adaptive compression should be applied.

The fact that G_N is unsmoothed means that G'_N can change at 3mm intervals to cope with large signals from specular reflectors.

Because the image is undersampled in the lateral direction (see

section 5.4.2.1) the boundaries between the different gain functions are sometimes visible in the image. This is not a marked effect, and is remedied by lightly smoothing gain map 1 across the image: the 100 or so gain values at each depth are smoothed with a 4 point local mean operator.

This form of adaptive compression should allow better resolution of the structure of large echo signals. The next section describes a one dimensional simulation to illustrate the effectiveness of this technique.

5.7.3 Simulation Results - Spatial Resolution

This simulation is outlined in section 4.4.

The situation simulated consists of a homogeneous background medium insonated by a transducer (see figure 5.18). A sandwich of three reflecting layers is positioned in the medium at about 10cm from, and normal to, the transducer. Each reflector is about 3mm thick. The two outer reflectors return a signal 14dB above the background medium and the central layer returns a signal 10dB above the background medium. The two-way attenuation in the background and the reflectors is 5dB cm^{-1}.

The results of applying several algorithms to this situation are illustrated in figure 5.19. Both the gain functions set by the algorithms and the A-scan lines produced by applying the gain functions are shown.

Figure 5.19 a and b show the A-scan line and gain function produced when algorithm 1 is applied. The gain compensates exactly for the changing signal level and no information about the reflectors is contained in the A-scan.

Figure 5.19 c and d show the A-scan line and gain function produced when algorithm 3 is applied. (Algorithms 2 and 3 are actually

Figure 5.18 Spatial Resolution Simulation :
three reflectors normal to the ultrasound beam.

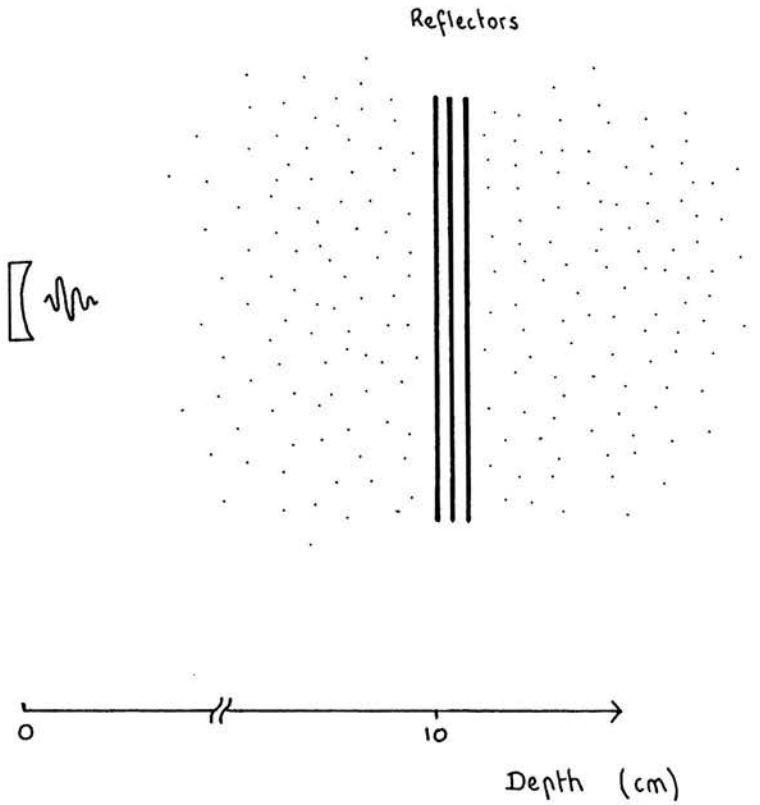

Figure 5.19 Spatial resolution simulation results.
G is gain in dB below maximum receiver gain.
"Signal" is the echo signal at the output of the receiver on a scale of 1 to 255 (255 is the upper limit of the A to D converter).

(a) Echo signal, using gain function in (b)

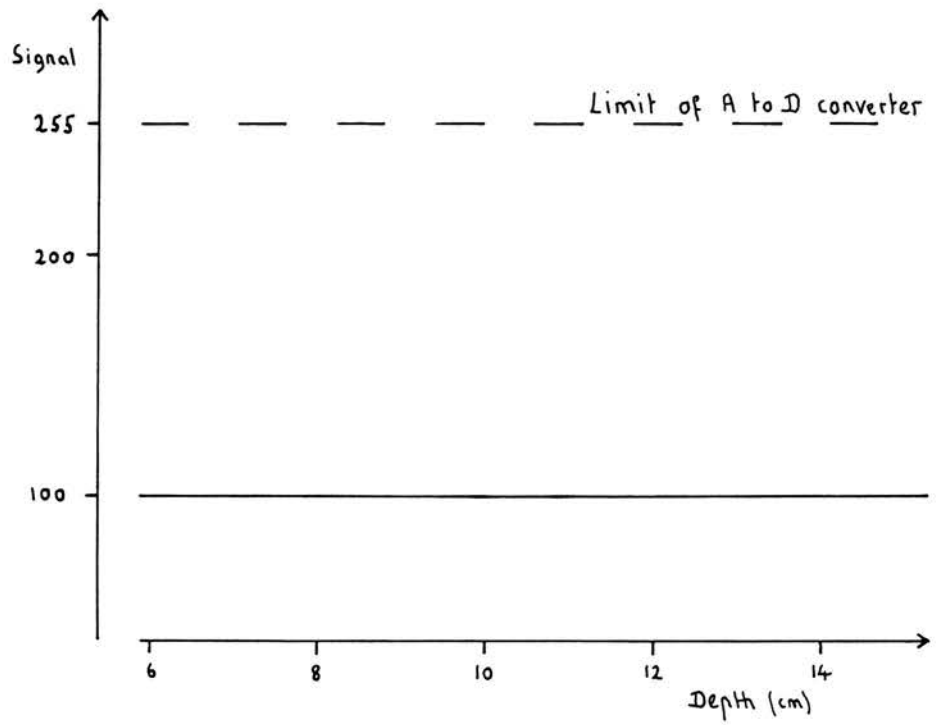

(b) Gain function formed by Algorithm 1

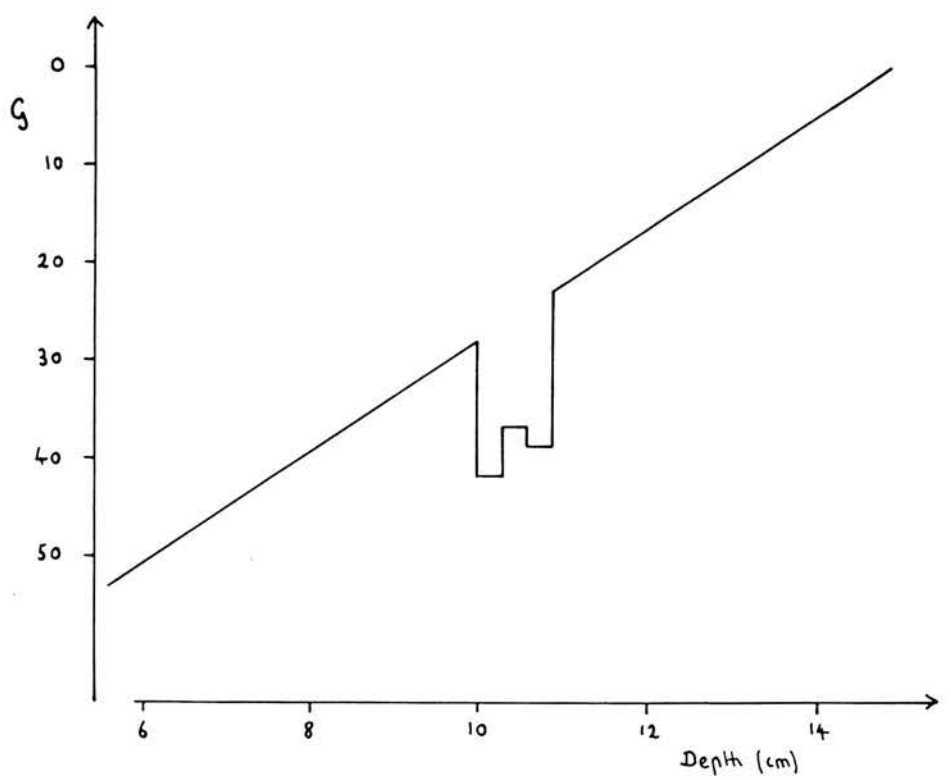

Figure 5.19 Spatial resolution simulation results.
G is gain in dB below maximum receiver gain.
"Signal" is the echo signal at the output of the receiver on a scale of 1 to 255 (255 is the upper limit of the A to D converter).

(c) Echo signal, using gain function in (d)

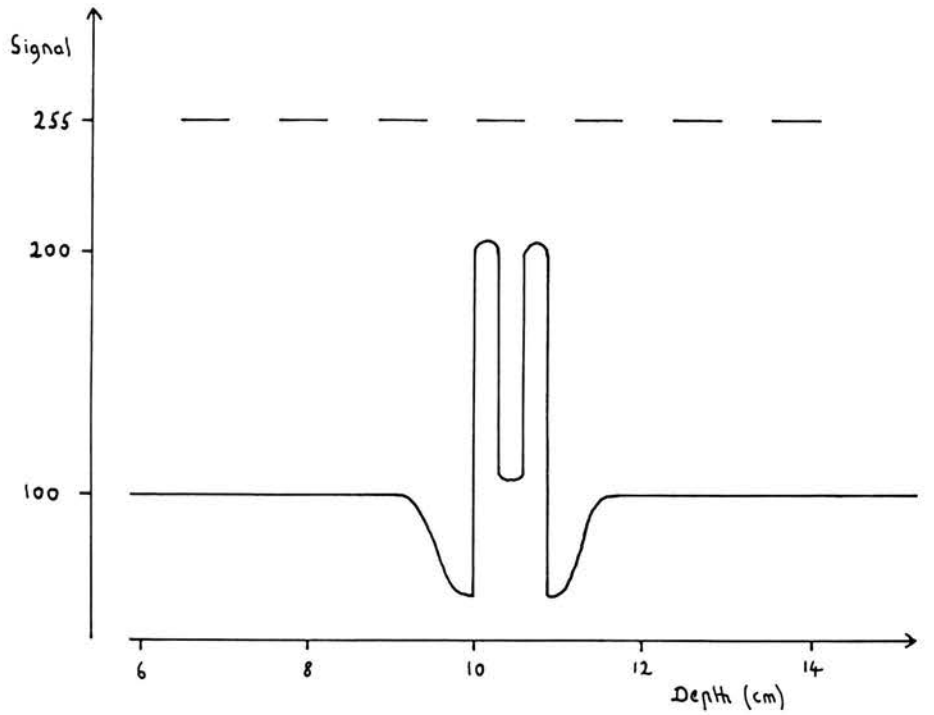

(d) Gain function formed by Algorithm 3
(5 element smooth)

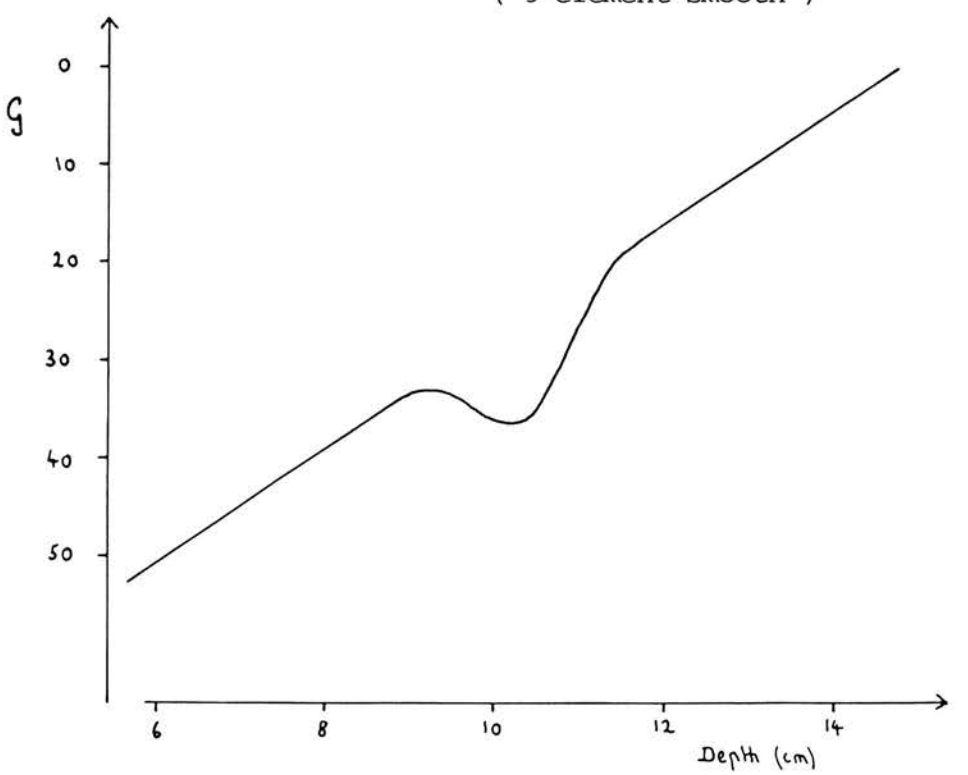

Figure 5.19 Spatial resolution simulation results.
ς is gain in dB below maximum receiver gain.
"Signal" is the echo signal at the output of the receiver on a scale of 1 to 255 (255 is the upper limit of the A to D converter).

(e) Echo signal, using gain function in (f)

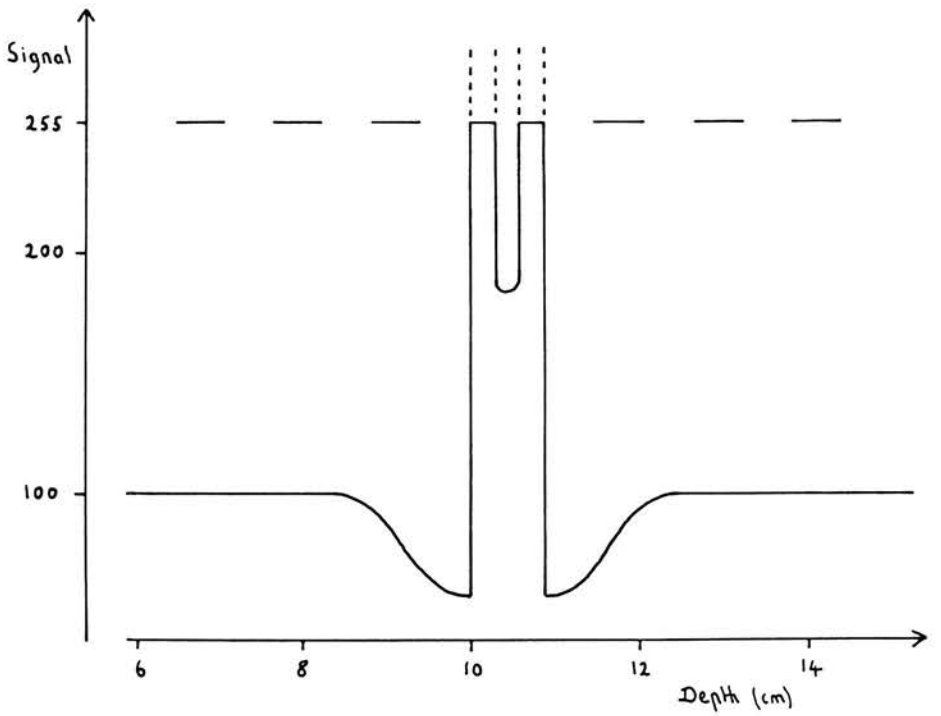

(f) Gain function formed by Algorithm 3
(9 element smooth)

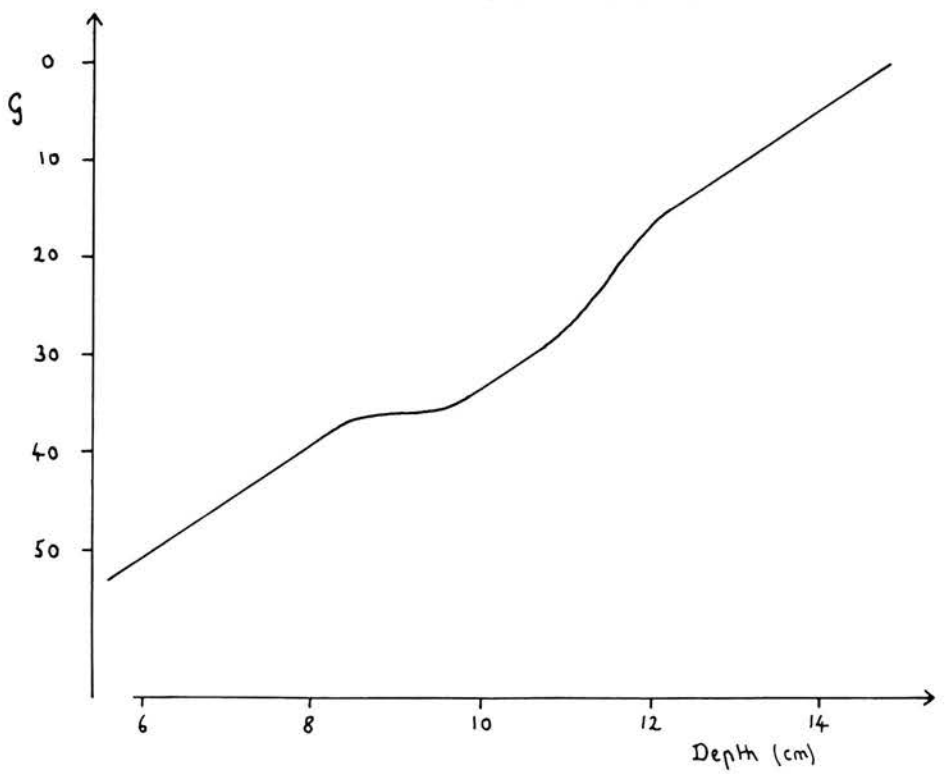

Figure 5.19 Spatial resolution simulation results.
$\mathcal{G}$ is gain in dB below maximum receiver gain.
"Signal" is the echo signal at the output of the receiver on a scale of 1 to 255 (255 is the upper limit of the A to D converter).

(g) Echo signal, using gain function in (h)

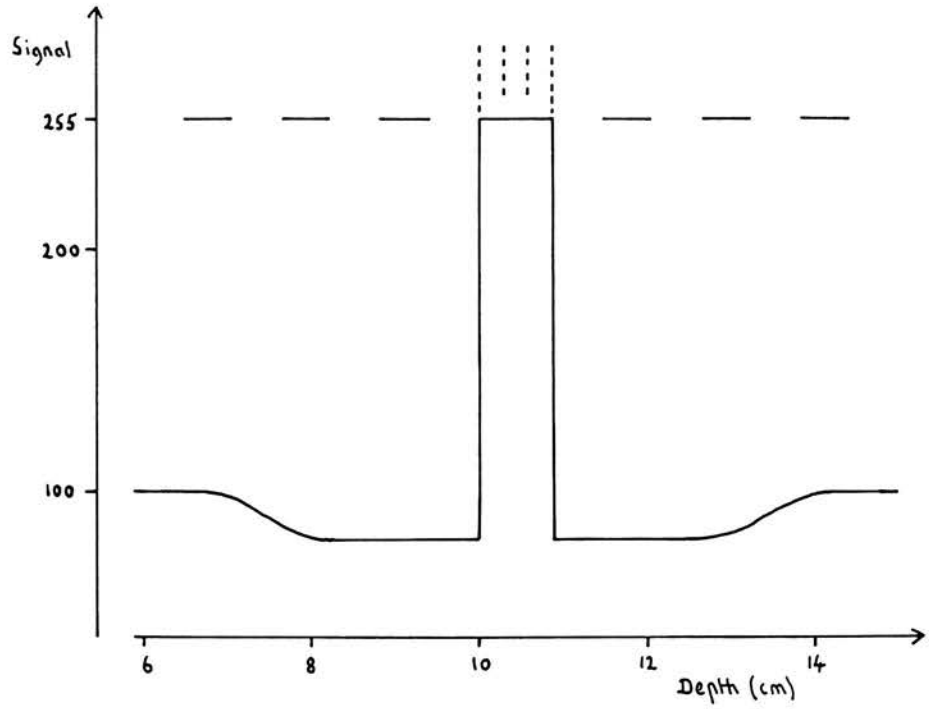

(h) Gain function formed by Algorithm 3
(21 element smooth)

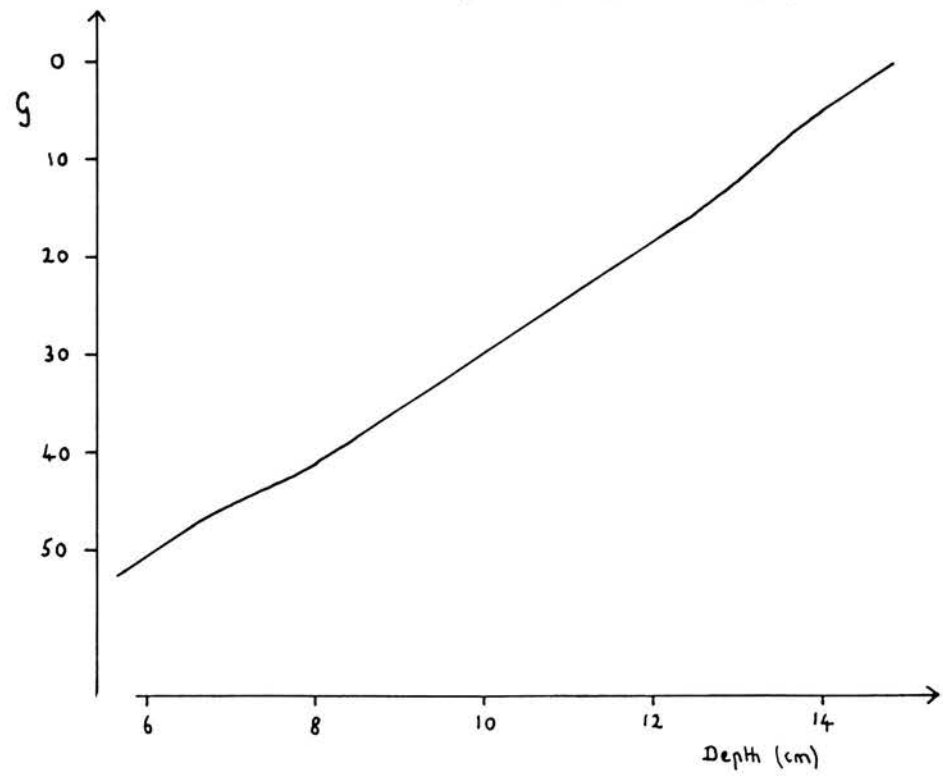

Figure 5.19 Spatial resolution simulation results.
ς is gain in dB below maximum receiver gain.
"Signal" is the echo signal at the output of the receiver on a scale of 1 to 255 (255 is the upper limit of the A to D converter).

(i) Echo signal, using gain function in (j)

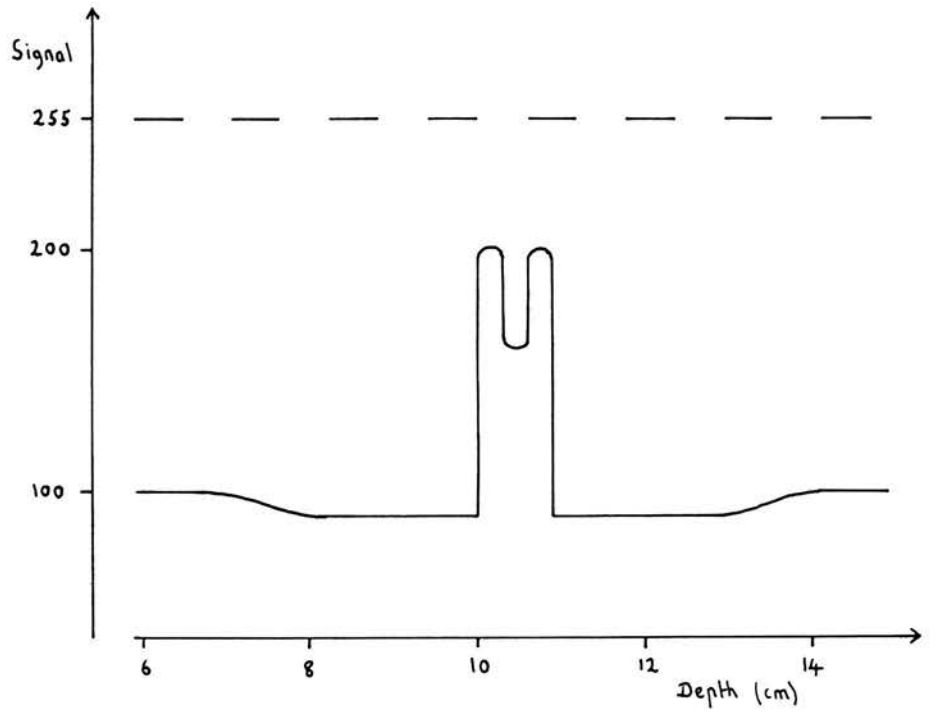

(j) Gain function formed by combining gain functions in (b) and (h) .

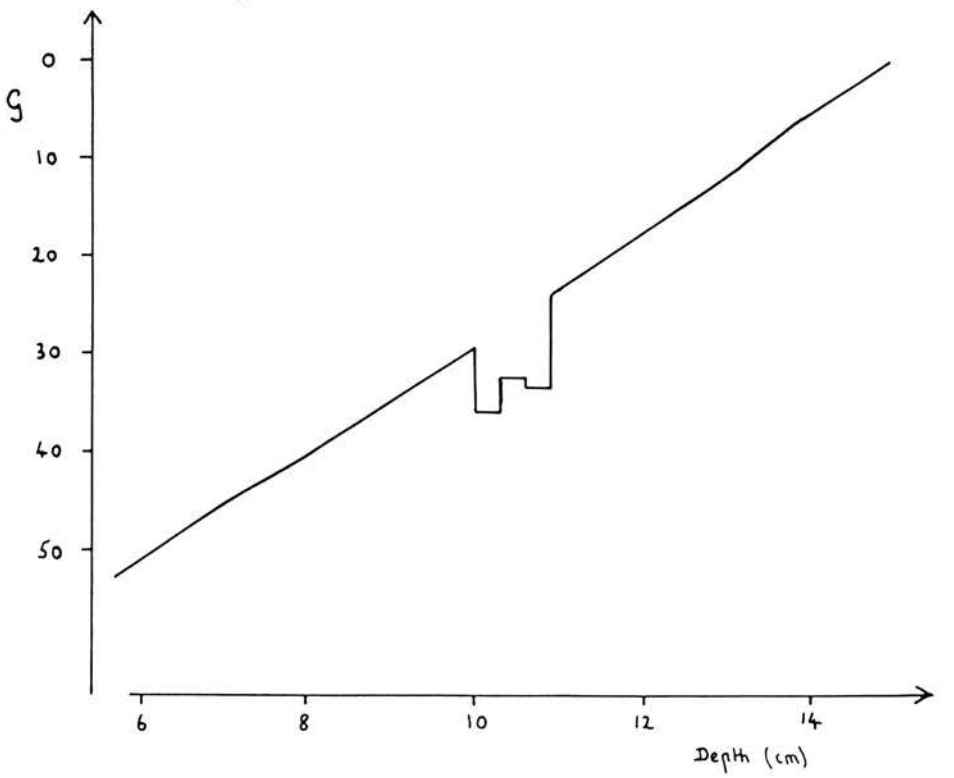

equivalent in this one dimensional situation.) G_o has been smoothed using a 5 element window. The three reflectors are resolved but the signal from the central layer is too low compared with the other two layers. The signal from the background medium is heavily suppressed on either side of the reflectors. This effect would give the appearance of dark bands on a two dimensional image.

Figure 5.19 e and f show algorithm 3 applied with G_o smoothed using a 9 element window, as was the case for the clinical trials of algorithm 3. The three reflectors are resolved and the central layer is at a better level relative to the other two layers than when a 5 element smooth is used. The outer layers are just in saturation. The signal from the background medium is still reduced on either side of the reflectors, but it falls more smoothly than in figure 5.19c and would thus be more acceptable in a two dimensional image.

Figure 5.19 g and h show algorithm 3 applied with G_o smoothed using a 21 element window. The signal from the surrounding medium is better presented than for the 9 element window, but all the reflectors are in saturation. Although the presence of a strong reflecting surface is registered, the internal structure is lost.

Figure 5.19j shows the gain function formed by taking the mean of corresponding elements of the gain functions in figure 5.19b (algorithm 1) and from 5.19h (21 element smooth). Figure 5.19i is the A-scan line produced by applying this new gain function. The result is excellent. The signal from the background is almost uniform, the reflectors are all resolved and the relative strengths of the reflectors are well represented. This technique is similar to that applied by algorithm 4 except that the smoothing window for algorithm 4 is only 9 elements wide and SG_o is combined with G_N only if $G_N < SG_o$. Algorithms 5 and 6 smooth G_o with a window size of 17 elements in the focal zone of

the transducer and so go closer to achieving the result shown in figure 5.19i .

5.7.4 Simulation Results - Contrast

Figure 5.20 shows the contrast simulation results obtained using algorithm 4. As would be expected, the object/background contrast C is approximately halved for the +20 and +5dB objects, and the results for the -5 and -20dB objects are very similar to those obtained using algorithm 3.

An interesting feature of the +20 and + 5dB objects is that C increases for objects larger than 16 x 16 pixels. It is a moot point as to whether it is desirable for the mean contrast to increase or decrease with increasing object size. Where the object and background both have uniform signal level (except for speckle), then the threshold contrast at which the object becomes indistinguishable from the background decreases as the object size increases (Smith et al, 1983). Under these circumstances it would be acceptable for an adaptive TGC algorithm to reduce the contrast between object and background as the object size increased.

However, neither objects nor background are uniform in any of the simulated images except for the case of simulated manual TGC applied to +5dB objects. This makes it difficult to judge from the simulation results how much contrast should be maintained at a given object size so that the object can be clearly distinguished.

5.7.5 Imaging Results

5.7.5.1 Test Object

The image of the grey-scale test object shown in figure 5.2f was

Figure 5.20 Contrast Simulation of Algorithm 4

(Broken lines show simulated manual TGC results.)

(a) +20 dB Objects

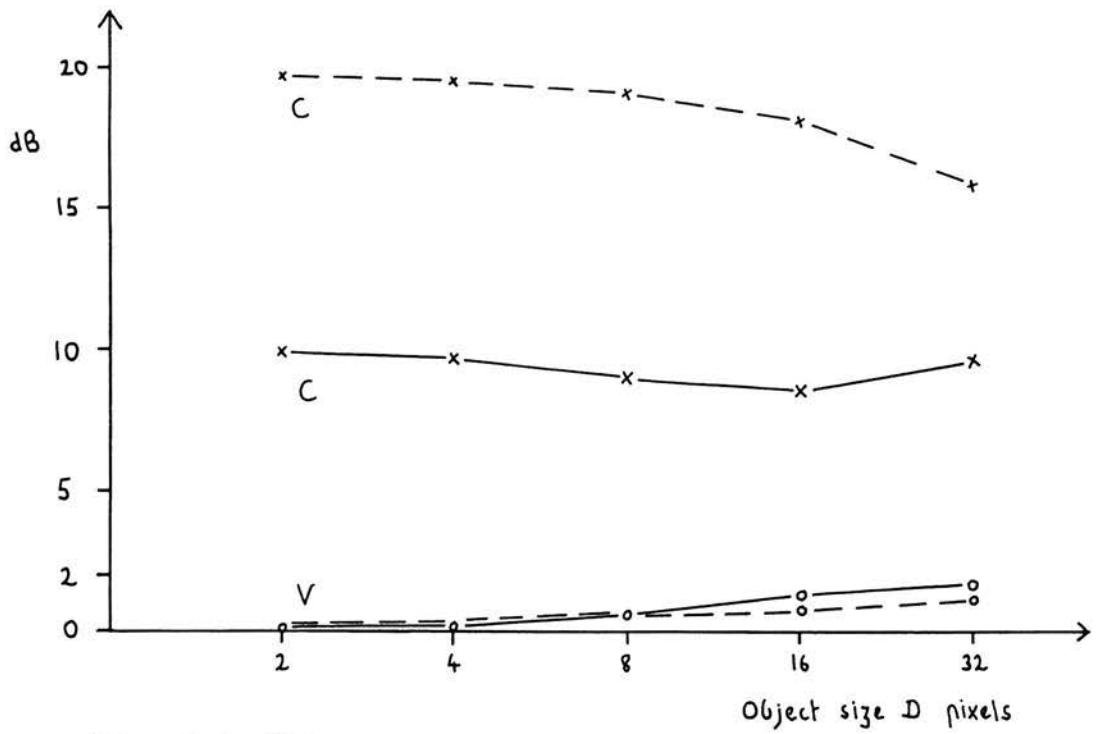

(b) +5 dB Objects

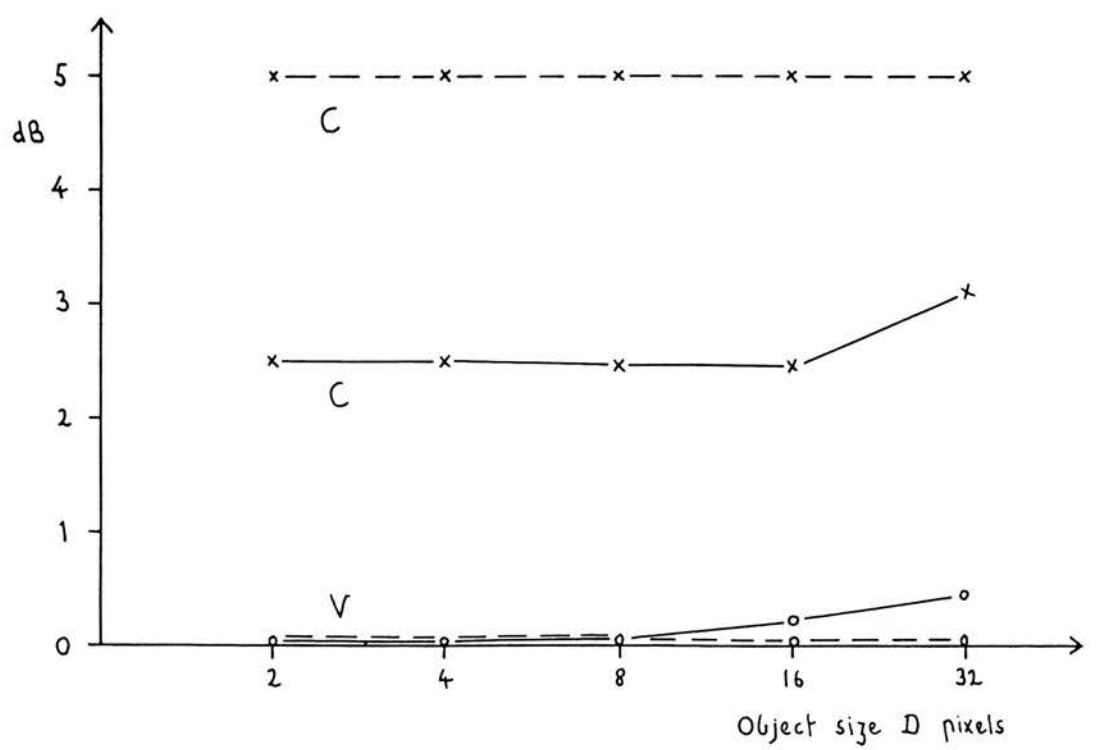

Figure 5.20 Contrast Simulation of Algorithm 4

(Broken lines show simulated manual TGC results.)

(c) -5 dB Objects

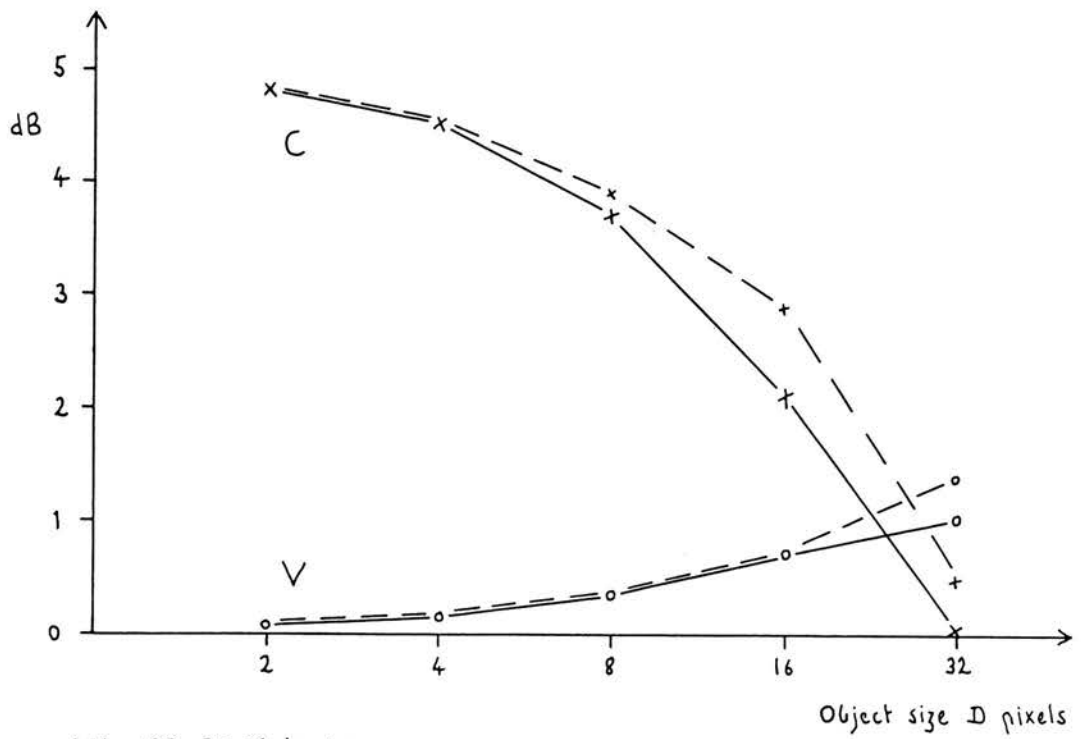

(d) -20 dB Objects

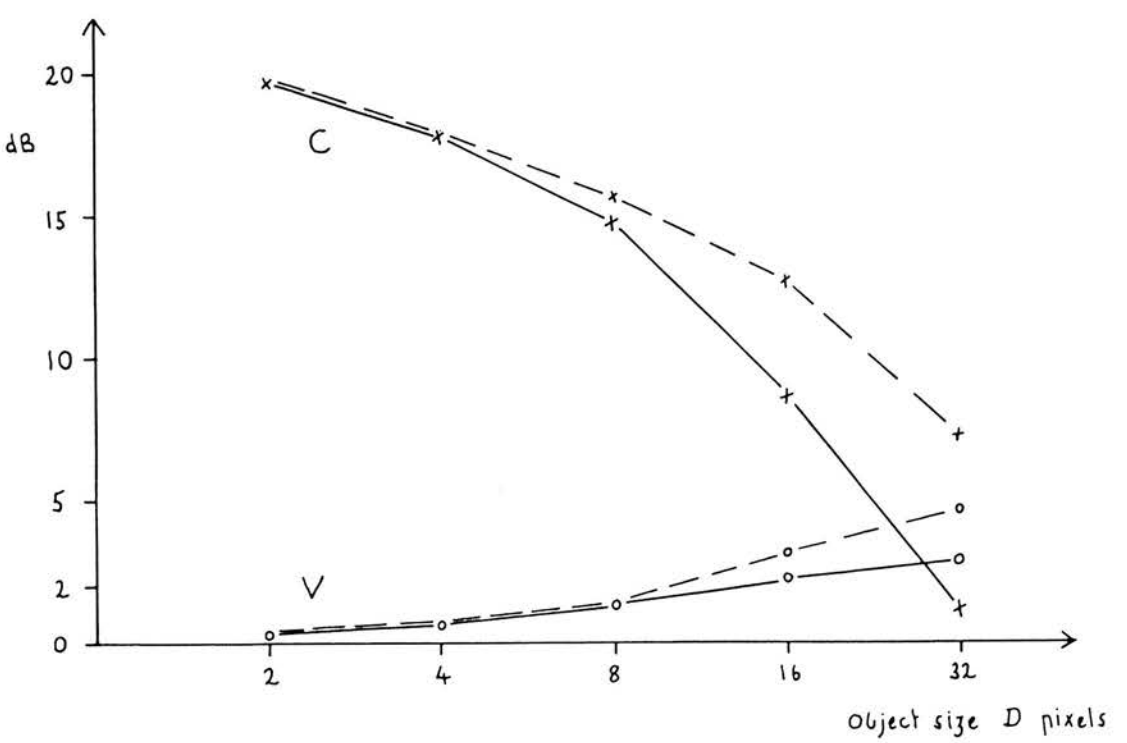

produced using algorithm 4. It shows a marked improvement over algorithms 1 , 2 , 3 and manual TGC . Algorithm 4 keeps the low attenuation gel noise free and removed the regions of saturation on each step of the loaded gel. The penetration into the loaded gel on the right side of the image is not as good as for algorithm 2 but slightly better than manual TGC.

5.7.5.2 Clinical Trial

Algorithm 4 was tested on 11 abdominal and 10 obstetric patients. The results are summarised in table 5.3. Applying McNemar's χ^2 test, we find that the physicist and radiologist preferred significantly more adaptive than manual images in both obstetric and abdominal work.

Algorithm 4 produced good images of the liver and major vessels. Examples are shown in figures 5.21 and 5.22. The presentation of regions of high signal level is noticeably better than that achieved using algorithm 3 or manual TGC. This is illustrated in figures 5.23, 5.24 and 5.25 where algorithm 4 improves the presentation of the fetal skull, the posterior wall and vessels of the uterus, and an image of an early pregnancy.

The same degree of noise in large anechoic regions was encountered using algorithm 4 as with algorithm 3. This was the principal defect in the images produced using algorithm 4. The next section describes an algorithm designed to overcome this problem.

Table 5.3 Clinical Trial of Algorithm 4

(a) Obstetrics :

Number of patients = 10
Total number of pairs of images = 30
Number of comparable pairs of images = 18

CATEGORY	PHYSICIST	RADIOLOGIST
AA	4	13
A	10	
C	4	3
M	0	2
MM	0	
	$\chi^2 = 12.1$	$\chi^2 = 6.7$
	$P < 0.005$	$P < 0.01$

(b) Abdominal :

Number of patients = 11
Total number of pairs of images = 33
Number of comparable pairs of images = 24

CATEGORY	PHYSICIST	RADIOLOGIST
AA	3	13
A	12	
C	6	8
M	3	3
MM	0	
	$\chi^2 = 6.7$	$\chi^2 = 5.1$
	$P < 0.01$	$0.01 < P < 0.025$

FIGURE 5.21 : Transverse section through the right lobe of the liver showing the confluence of two hepatic veins.

(a) Adaptive TGC: Algorithm 4

(b) Manual TGC

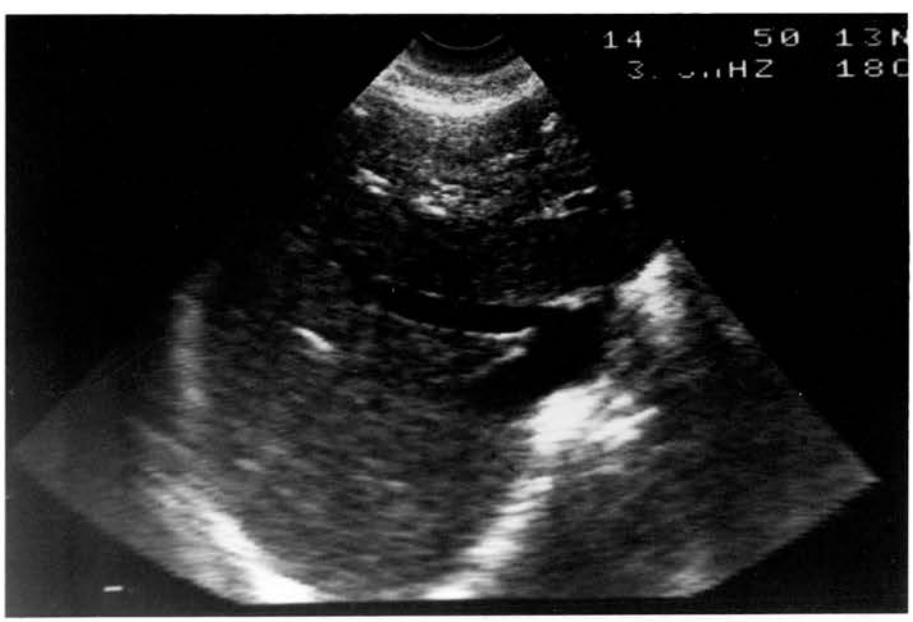

FIGURE 5.22 : Longitudinal section through the IVC showing the portal vein and common bile duct.

(a) Adaptive TGC: Algorithm 4

(b) Manual TGC

FIGURE 5.23 : Oblique section through the head of a 35 week fetus.

(a) Adaptive TGC: Algorithm 4

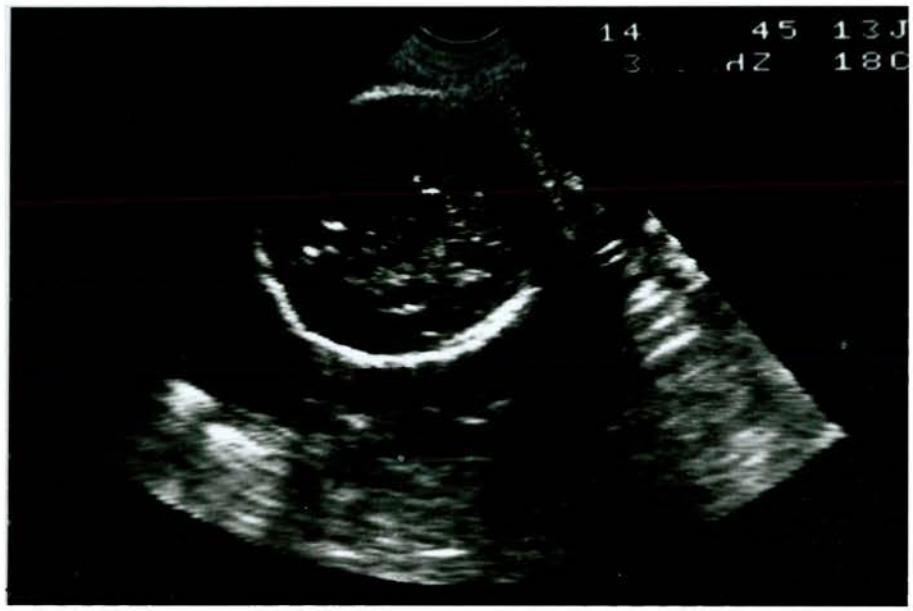

(b) Manual TGC

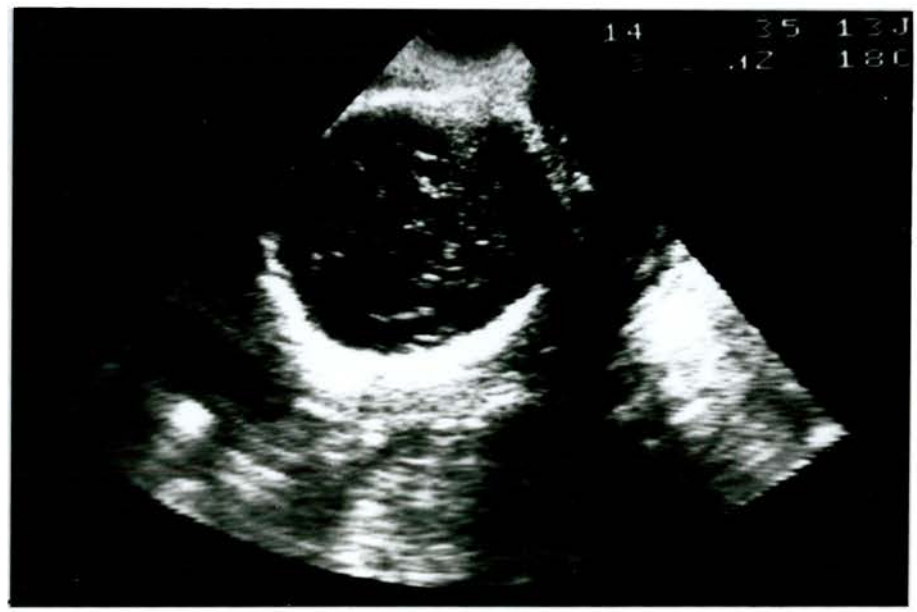

FIGURE 5.24 : Section showing placenta, fetal head, maternal spine and pelvic vessels.

(a) Adaptive TGC: Algorithm 4

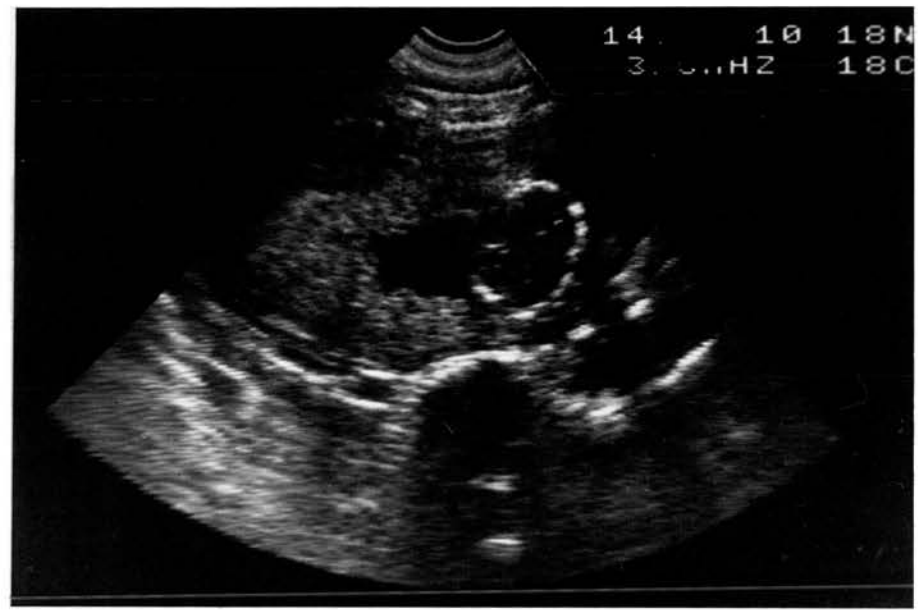

(b) Manual TGC

FIGURE 5.25 : 9 week pregnancy showing a longitudinal section of the uterus, the cervix, fetus and implantation site.

(a) Adaptive TGC: Algorithm 4

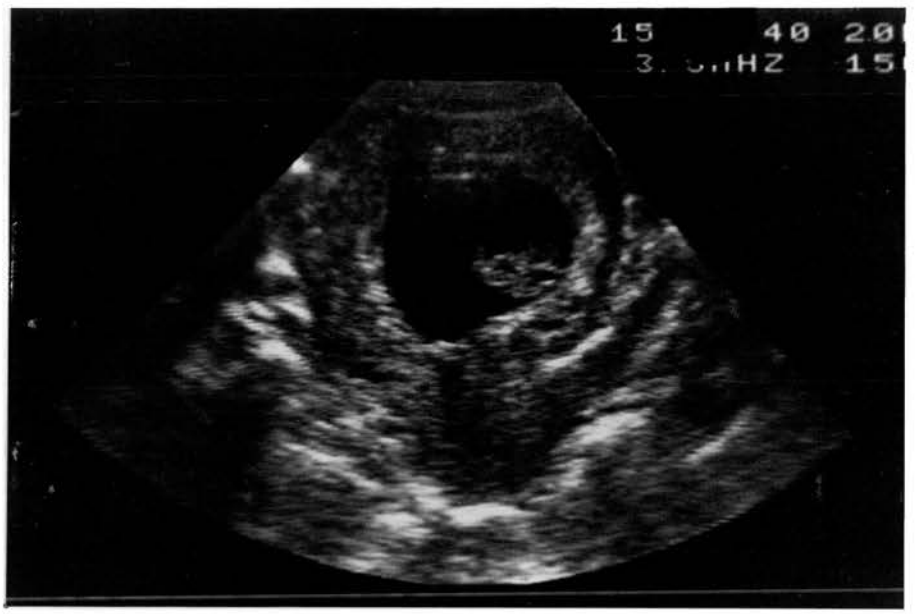

(b) Manual TGC

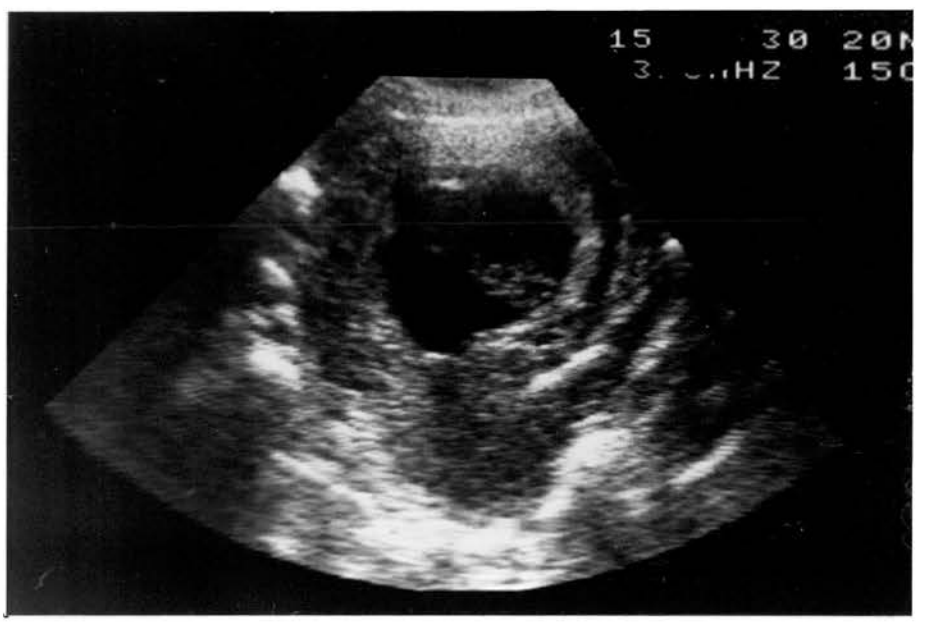

5.8 ALGORITHM 5

5.8.1 Outline

Algorithm 5 attempts to improve on algorithm 4 in two ways:

(1) By using a smoothing operator with variable window size. This allows G_o to be smoothed more heavily in the focal zone of the transducer and so reduces the amount by which large signals can suppress smaller ones close by.

(2) By attempting to detect soft tissue/fluid boundaries, so that the slope of the gain function can be reduced to that appropriate for fluid.

Algorithm 5 takes about 2 seconds to collect and process data from one image.

5.8.2 Detail

Figure 5.26 shows a flow diagram of algorithm 5. The data collection cycle is identical to that of previous algorithms and G_o is formed in the same way as in algorithm 4.

5.8.2.1 Smoothing with depth

SG_o is formed from G_o by using a smoothing operator with variable window size. With reference to figure 5.10, the window size remains sufficiently small in the near field to prevent banding at depth P. It then increases in size so that the focal zone is heavily smoothed. As soon as the leading edge of the window reaches depth Q, the window size progressively decreases so that as the window passes depth Q it is small enough to prevent banding. A plot of the window size versus depth is shown in figure 5.27. Smoothing G_o heavily has two beneficial effects:

(1) It reduces the amount by which large signals suppress smaller

Figure 5.26 Flow diagram of Algorithm 5

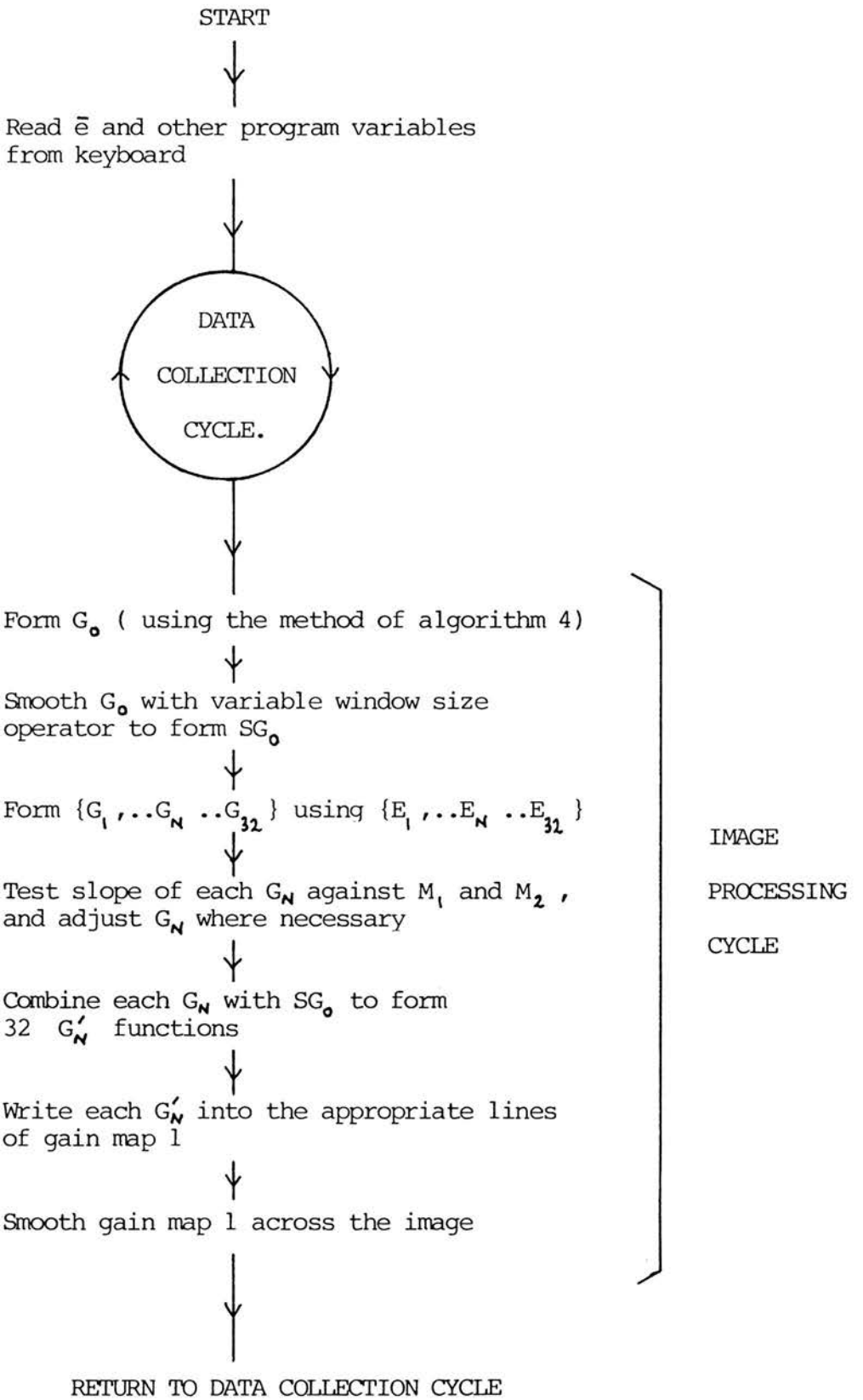

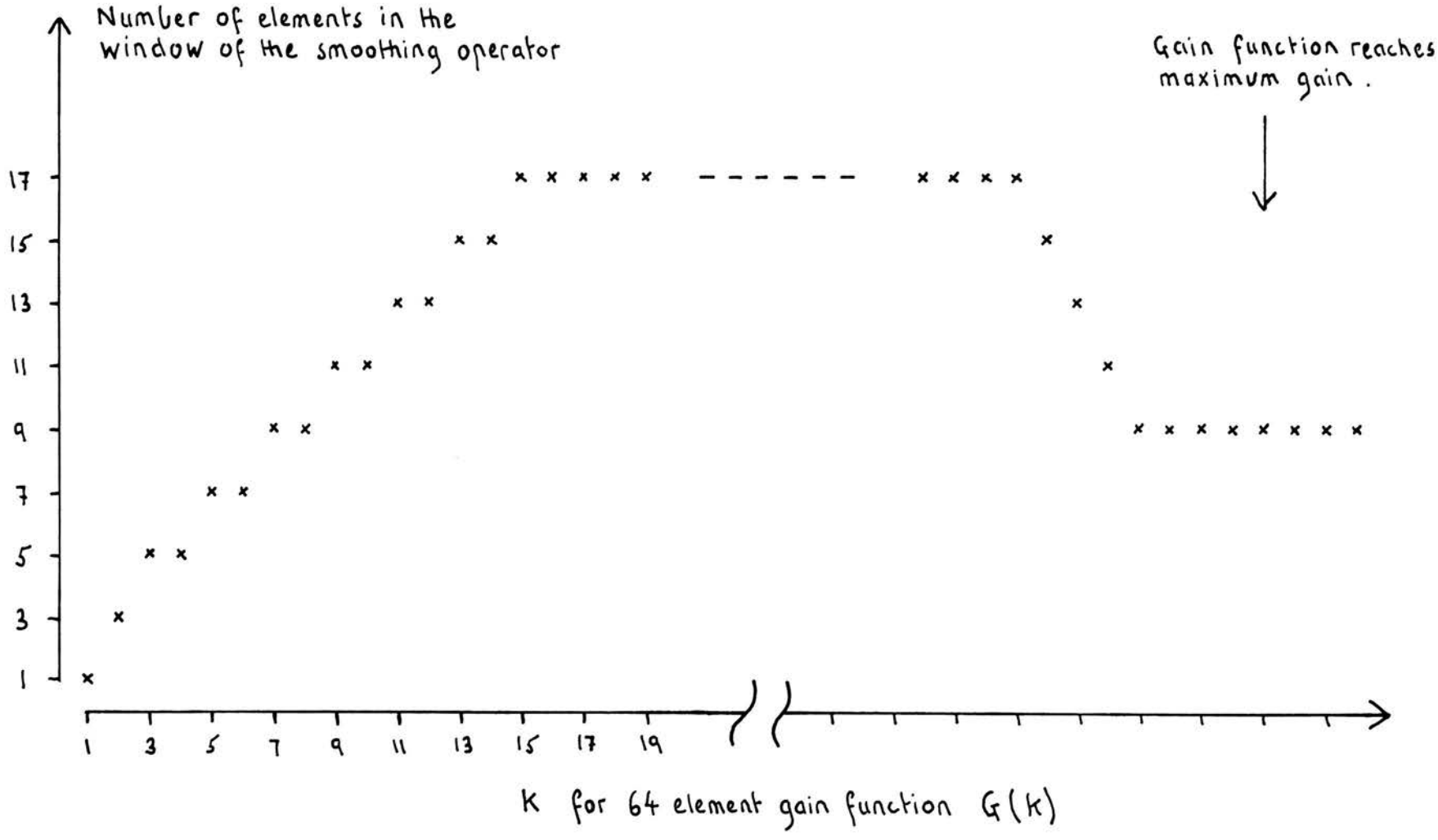

Figure 5.27 Variable Window Smoothing Operator

ones close by.

(2) It reduces the amount that the gain can rise in anechoic regions.

5.8.2.2 Fluid Recognition

Algorithm 5 is designed to recognise regions of fluid by the sudden large drop in signal level that often occurs at soft tissue/fluid boundaries. It was found that this technique is not suitable to be used in the near field because transmitter artifacts and specular reflections from skin, fat and muscle interfaces often result in large signal changes in the near field. Algorithm 5 misinterprets these as soft tissue/fluid boundaries. Fluid detection was thus only applied from the pth element of each gain function (corresponding to depth P in figure 5.10 . For the mechanical sector scan probe, $P \approx 3$ cm).

Algorithm 5 proceeds as follows. For the Nth scan line, G_N is formed as for algorithm 4 . The local slope at each point along G_N is then examined, starting with the pth element and progressing to the 64th element. The local slope is compared with two slopes M_1 and M_2 ($M_2 > M_1$). M_1 corresponds to the maximum allowed slope of algorithms 2,3 and 4 , and M_2 is a threshold such that gain slopes greater than M_2 are interpreted as occurring at soft tissue/fluid boundaries. The following rules are applied:

If $G_N(k) - G_N(k-1) < M_1 \Delta x$ - Equation 5.17

then $G_N(k)$ is left unchanged.

If $M_1 \Delta x < G_N(k) - G_N(k-1) < M_2 \Delta x$ - Equation 5.18

then the slope is restricted to M_1 , the maximum positive slope allowed.

If $G_N(k) - G_N(k-1) > M_2 \Delta x$ - Equation 5.19

then the gain slope is set

such that

$$G_N(k) = G_N(k-1) + M_3 \Delta x \quad \text{- Equation 5.20}$$

where M_3 is a slope suitable to be applied in low attenuation fluids. M_3 was set to 1dB cm^{-1}.

Once G_N has been adjusted in this way, G'_N is formed by combining G_N with SG_0 according to the rules of algorithm 4 (equations 5.13 and 5.14).

As described in section 5.6.4.3, suitable values of M_1 were found to be 10dB cm^{-1} in abdominal work and 8dB cm^{-1} in obstetric work, scanning at 3.5MHz. These values were modified slightly for algorithm 5 to take account of the greater sensitivity of the transducer in the focal zone than in the near field. The values used are given in table 5.4 .

Like M_1 , M_2 was determined empirically. A range of values of M_2 were tested while imaging the low attenuation region of the test object, a full bladder, pools of liquor and large vessels at various distances from the probe. It was found that as well as correctly identifying soft-tissue/fluid boundaries, algorithm 5 misinterpreted other sudden falls in signal level as being fluid boundaries. Such falls in signal level occurred at the boundary of some regions of acoustic shadowing, and also distal to specular reflectors where the signal drops from a peak down to mid-grey. When M_2 was in the range 10 to 40dB cm^{-1} , algorithm 5 correctly identified many soft tissue/liquor and soft tissue/blood boundaries. However, it also misinterpreted many signal changes and produced shadowing distal to specular reflectors and heavy shadowing where there should only have been slight acoustic shadowing. When M_2 was set greater than 100dB cm^{-1} , algorithm 5 detected very few

Table 5.4 Values of M_1 used by Algorithms 5 and 6 for 3.5 MHz scanning

	M_1 in abdominal work (dB cm^{-1})	M_1 in obstetric work (dB cm^{-1})
Near field (< 5cm)	10	8
Focal zone (> 5cm)	8	6

boundaries either correctly or incorrectly. The most useful value of M_2 for the Z machine was found to be around 80dB cm^{-1}. Using M_2 = 80dB cm^{-1}, soft tissue/blood boundaries are rarely identified but soft tissue/liquor and soft tissue/urine boundaries frequently are. A useful amount of noise reduction is then obtained in obstetric imaging. Only the boundaries of heavy acoustic shadowing are incorrectly identified. This is not important, since reducing the gain slope in areas of heavy shadowing does not affect the appearance of the image.

5.8.3 Simulation Results - Contrast

The contrast simulation results for -20dB objects using algorithm 5 with M = 80dB cm^{-1} are shown in figure 5.28. The results for +20, +5 and -5dB objects are all within 0.2dB of those obtained for algorithm 4 and so are not repeated here. The results for -20dB objects show an interesting difference: C is higher and V is lower for all object sizes using algorithm 5 than using either simulated manual TGC or any of the other algorithms. The separation of C and V at an object size of 32 x 32 pixels is 5dB greater using algorithm 5 than it is using simulated manual TGC. This difference is due to the fluid recognition technique of algorithm 5.

These results suggest that algorithm 5 will treat images in a similar fashion to algorithm 4 except for large anechoic regions.

5.8.4 Imaging Results

5.8.4.1 Test Object

Figure 5.2g shows an image of the grey-scale test object obtained using algorithm 5. There is little difference between this image and the image produced using algorithm 4. In particular, both algorithms

Figure 5.28 Contrast Simulation of Algorithm 5

(Broken lines show simulated manual TGC results.)

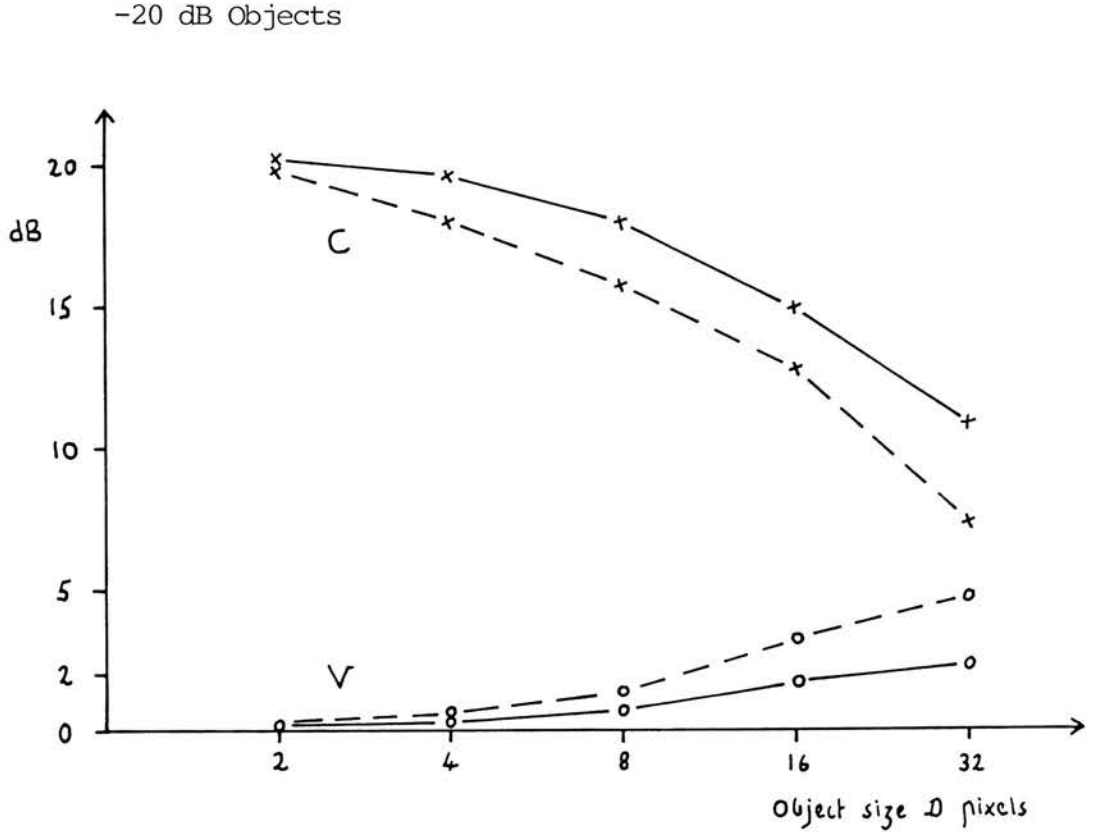

present the low attenuation gel in the same way. This is not surprising because algorithm 4 does not introduce any excessive noise that algorithm 5 could improve upon.

5.8.4.2 Clinical Trials

Algorithm 5 was tested on 23 abdominal and 27 obstetric patients. The results of the trial are summarised in table 5.5. For the physicist's and radiologist's results in both obstetric and abdominal imaging we find that $P < 0.001$. Both judges thus preferred significantly more adaptive than manual images.

A number of the images obtained using algorithm 5 showed a good presentation of large fluid filled regions and the tissues bordering them. Examples are shown in figures 5.29, 5.30 and 5.31. It can be seen that there is less noise in the adaptive images than in the manual ones. However, where small structures are present in fluid filled regions, the adaptive TGC does not set the gain so low that they cannot be seen. Figure 5.32 illustrates this point. The image shows a twin pregnancy and the membrane separating the sacs can be clearly seen in the adaptive image. The membrane cannot be seen so well in the manual image.

There is often a certain amount of debris (particles of skin and mucoleum) present in liquor during the 3rd trimester. Sometimes the signal scattered from the debris is large enough to prevent algorithm 5 identifying the pool of liquor. In these circumstances the signal level in the liquor may be higher than if manual TGC is used. Figure 5.33 shows this situation in a deep pool of liquor.

In abdominal imaging, the soft tissue/blood boundaries of the major vessels were rarely recognised by algorithm 5. However, the vessels are still well presented, as illustrated by figure 5.34.

Algorithm 5 did not degrade the appearance of liver metastases.

Table 5.5 Clinical Trial of Algorithm 5

(a) Obstetrics :

Number of patients = 23
Total number of pairs of images = 66
Number of comparable pairs of images = 49

CATEGORY	PHYSICIST	RADIOLOGIST
AA	29	39
A	16	
C	3	10
M	1	0
MM	0	
	$\chi^2 = 40.2$	$\chi^2 = 37.0$
	$P < 0.001$	$P < 0.001$

(b) Abdominal :

Number of patients = 27
Total number of pairs of images = 82
Number of comparable pairs of images = 49

CATEGORY	PHYSICIST	RADIOLOGIST
AA	18	39
A	26	
C	4	9
M	1	1
MM	0	
	$\chi^2 = 39.2$	$\chi^2 = 34.2$
	$P < 0.001$	$P < 0.001$

FIGURE 5.29 : Longitudinal section through a full bladder showing the cervix, uterus and bowel wall.

(a) Adaptive TGC: Algorithm 5

(b) Manual TGC

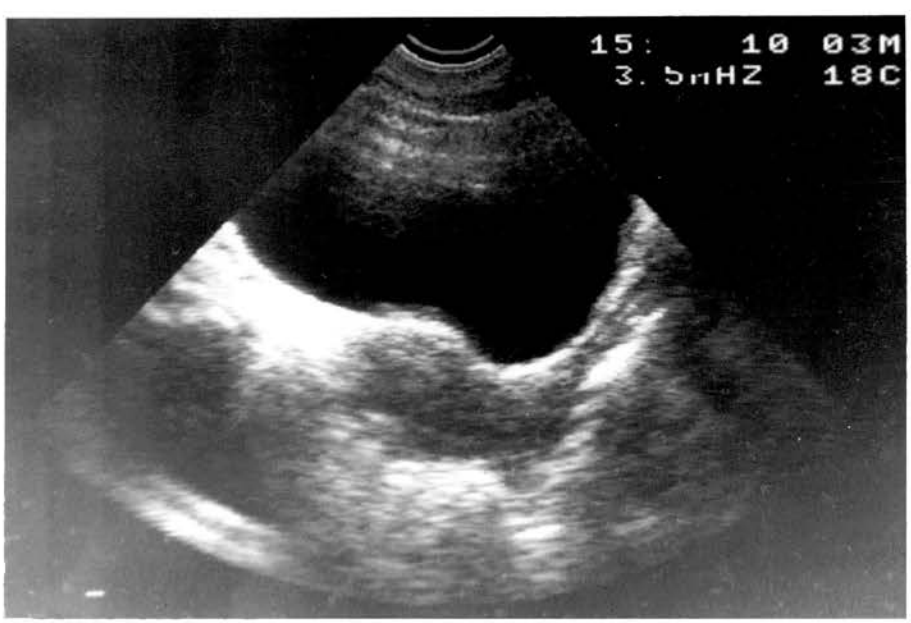

FIGURE 5.30 : 36 week pregnancy showing liquor and fetal limbs.

(a) Adaptive TGC: Algorithm 5

(b) Manual TGC

FIGURE 5.31 : Section through a posterior placenta showing the body of the placenta and the basal layer.

(a) Adaptive TGC: Algorithm 5

(b) Manual TGC

FIGURE 5.32 : Twin pregnancy showing fetal abdomens, anterior and posterior placentas, the membrane separating the sacs, and the maternal aorta.

(a) Adaptive TGC: Algorithm 5

(b) Manual TGC

FIGURE 5.33 : 34 week pregnancy showing anterior placenta, liquor and fetal limbs.

(a) Adaptive TGC: Algorithm 5

(b) Manual TGC

FIGURE 5.34 : Section through the junction of the right and left lobes of the liver showing right atrium, IVC and intra-hepatic vein.

(a) Adaptive TGC: Algorithm 5

(b) Manual TGC

Figure 5.35 shows a 2 cm diameter lesion with a complex echo pattern. The lesion can be seen more clearly in the adaptive image. Algorithm 5 also maintains good contrast between the kidney cortex and the liver (see figure 5.36). Strong reflectors, such as the diaphragm, are crisply presented and do not heavily suppress the signals from adjacent parenchyma (see figures 5.36 and 5.37).

FIGURE 5.35 : Section showing kidney (top left) and a solid well defined lesion with a complex echo pattern (centre).

(a) Adaptive TGC: Algorithm 5

(b) Manual TGC

FIGURE 5.36 : Right kidney, seen through the liver.

(Patient supine.)

(a) Adaptive TGC: Algorithm 5

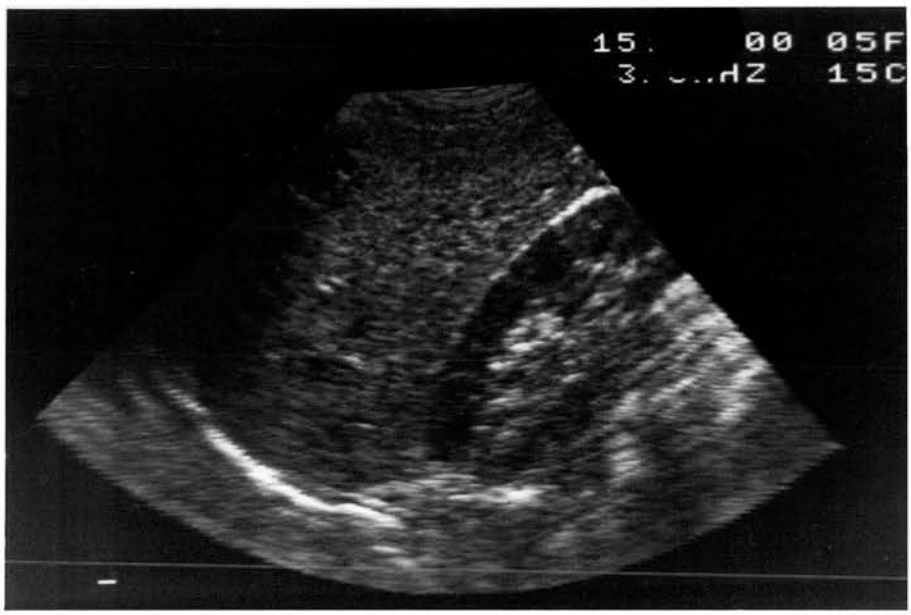

(b) Manual TGC

FIGURE 5.37 : Right lobe of liver, showing the portal vein and diaphragm.

(a) Adaptive TGC: Algorithm 5

(b) Manual TGC

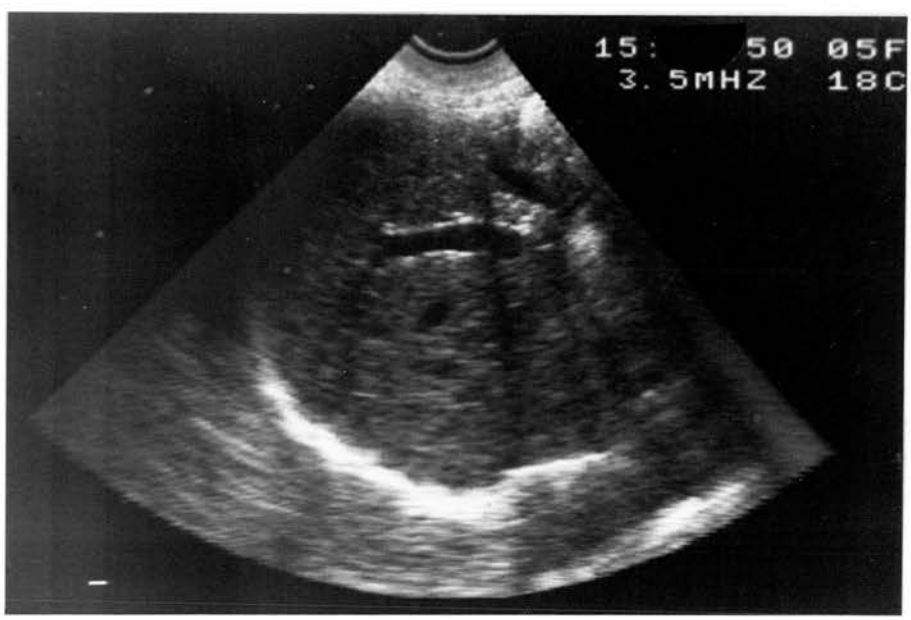

5.9 ALGORITHM 6

5.9.1 Outline

Algorithm 6 is identical to algorithm 5, except that it explores a different method of forming G_o .

The algorithm takes about 2 seconds to collect and process data from one image.

5.9.2 Detail

A flow diagram of algorithm 6 is shown in figure 5.38. The data collection cycle is the same as for previous algorithms.

During the image processing cycle, algorithm 6 forms 32 gain functions using the 32 stored echo functions (following equation 5.5) before calculating G_o . G_o is then calculated using

$$G_o(k) = \frac{1}{32} \sum_{N=1}^{32} G_N(k) \qquad \text{for } k = 1,64 \qquad \text{- Equation 5.21}$$

An upper limit is then placed on the positive slope of G_o : the same values of M_1 are used as for algorithm 5 (see section 5.8.2).

SG_o is formed from G_o using the variable window size smoothing operator described in section 5.8.2.1.

The fluid recognition algorithm described in section 5.8.2.2 is applied to the 32 gain functions, and they are then combined with SG_o following the method of algorithm 4 (equations 5.13 and 5.14).

5.9.3 Simulation Results - Contrast

The contrast simulation results for algorithm 6 are all within 0.3dB of the results obtained using algorithm 5, and so they are not included here.

Figure 5.38 Flow diagram of Algorithm 6

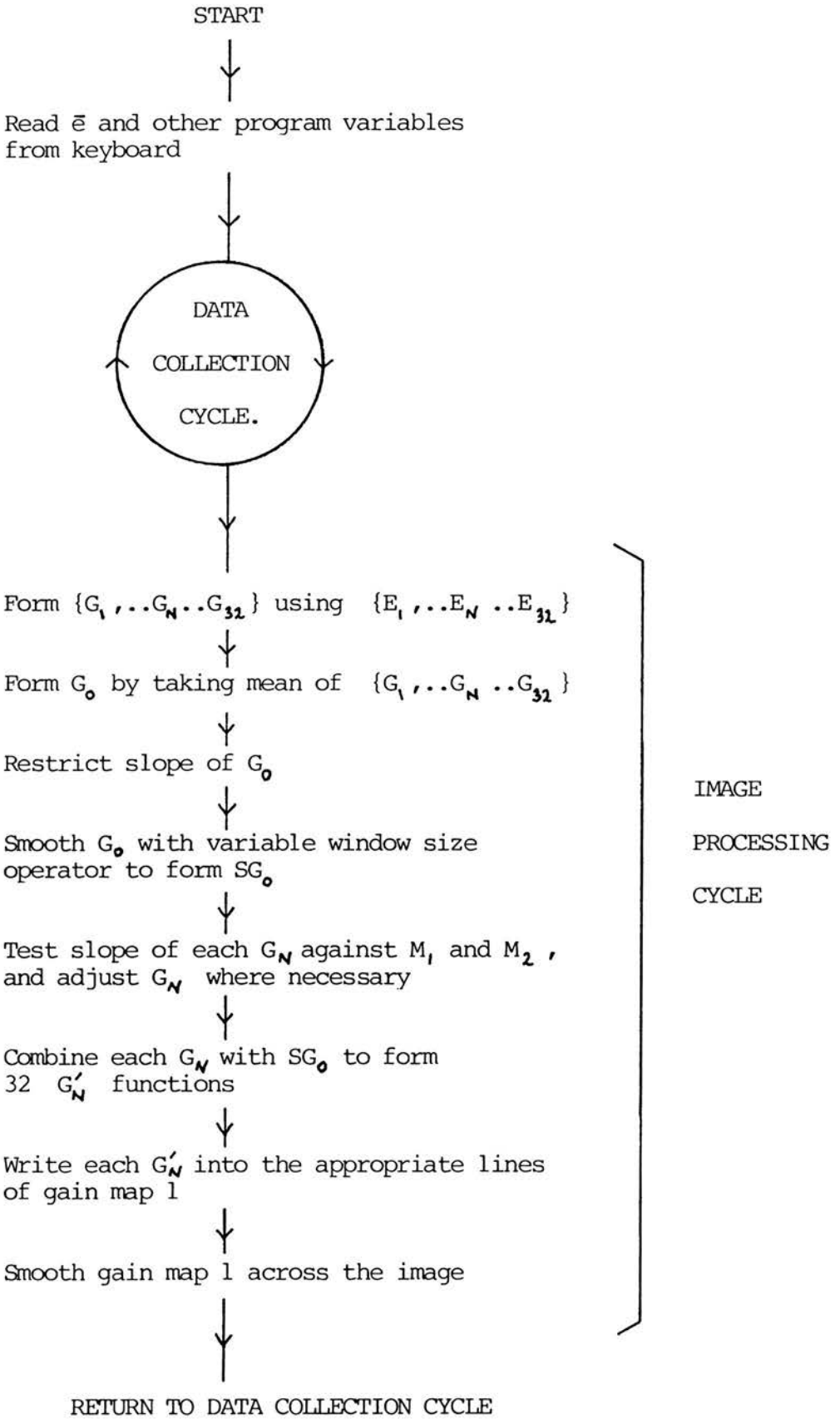

5.9.4 Imaging Results

5.9.4.1 Test Object

Figure 5.1h shows an image of the grey-scale test object produced using algorithm 6. It is similar to the image produced using algorithm 5.

5.9.4.2 Clinical Trial

Algorithm 6 was tested on 11 abdominal and 14 obstetric patients. The results are summarised in table 5.6. For the two judges' results in both obstetric and abdominal imaging we find that $P < 0.01$. Both judges thus preferred significantly more adaptive than manual images.

By combining the 32 gain functions to form G_o , we are effectively applying a logarithmic compression to the echo data before averaging it across the image. This reduces the weight given to large signals so that they have less tendency to suppress small signals close by. However, such a compression also reduces the ability of large and mid-level signals to suppress noise in anechoic regions at the same depth. It is difficult to judge which effect is more pronounced in the clinical images that were obtained: a direct comparison between algorithms 5 and 6 would be necessary to determine this.

Two examples of pairs of images obtained using algorithm 6 in obstetric work are shown in figures 5.39 and 5.40 and two examples obtained in abdominal work are shown in figures 5.41 and 5.42.

Figures 5.43, 5.44 and 5.45 illustrate the variation of the gain settings with depth and across the image. Part (a) of each figure is an image produced using algorithm 6 and part (b) is a three dimensional plot of the gain map of the image. Table 5.7 summarises the amount of gain variation across the image at each depth for the images in figures 5.43, 5.44 and 5.45 .

Table 5.6 Clinical Trial of Algorithm 6

(a) Obstetrics :

Number of patients = 16
Total number of pairs of images = 42
Number of comparable pairs of images = 27

CATEGORY	PHYSICIST	RADIOLOGIST
AA	10	16
A	13	
C	4	8
M	0	3
MM	0	
	$\chi^2 = 21.0$	$\chi^2 = 7.6$
	$P < 0.001$	$0.005 < P < 0.01$

(b) Abdominal :

Number of patients = 11
Total number of pairs of images = 35
Number of comparable pairs of images = 27

CATEGORY	PHYSICIST	RADIOLOGIST
AA	8	13
A	12	
C	7	13
M	0	1
MM	0	
	$\chi^2 = 18.1$	$\chi^2 = 8.6$
	$P < 0.001$	$0.001 < P < 0.005$

FIGURE 5.40 : 38 week pregnancy showing a large pool of liquor, umbilical cord and fetal limbs

(a) Adaptive TGC: Algorithm 6

(b) Manual TGC

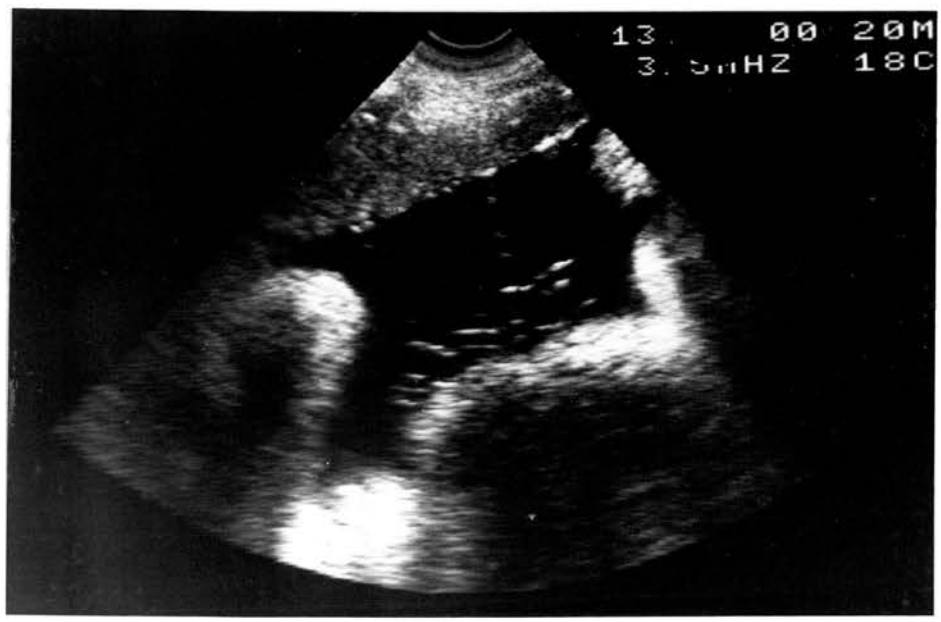

FIGURE 5.4\ : A calcified kidney containing a stone, viewed through the right lobe of the liver.

(a) Adaptive TGC: Algorithm 6

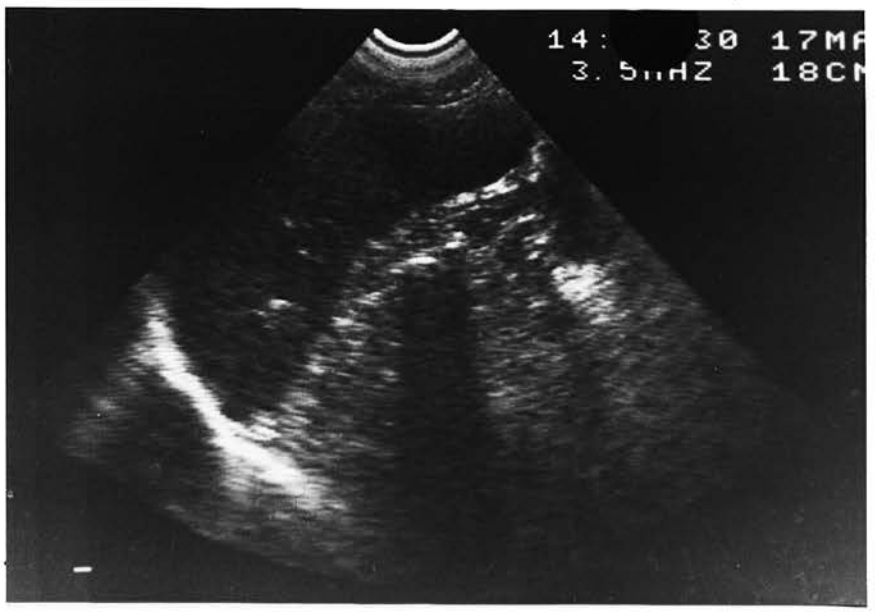

(b) Manual TGC

FIGURE 5.42 : Longitudinal section through a normal kidney.
(Patient prone.)

(a) Adaptive TGC: Algorithm 6

(b) Manual TGC

Figure 5.43 Placenta and posterior uterine wall :
image and gain map formed by Algorithm 6.

(a) Adaptive TGC image

(b) Gain map of (a)

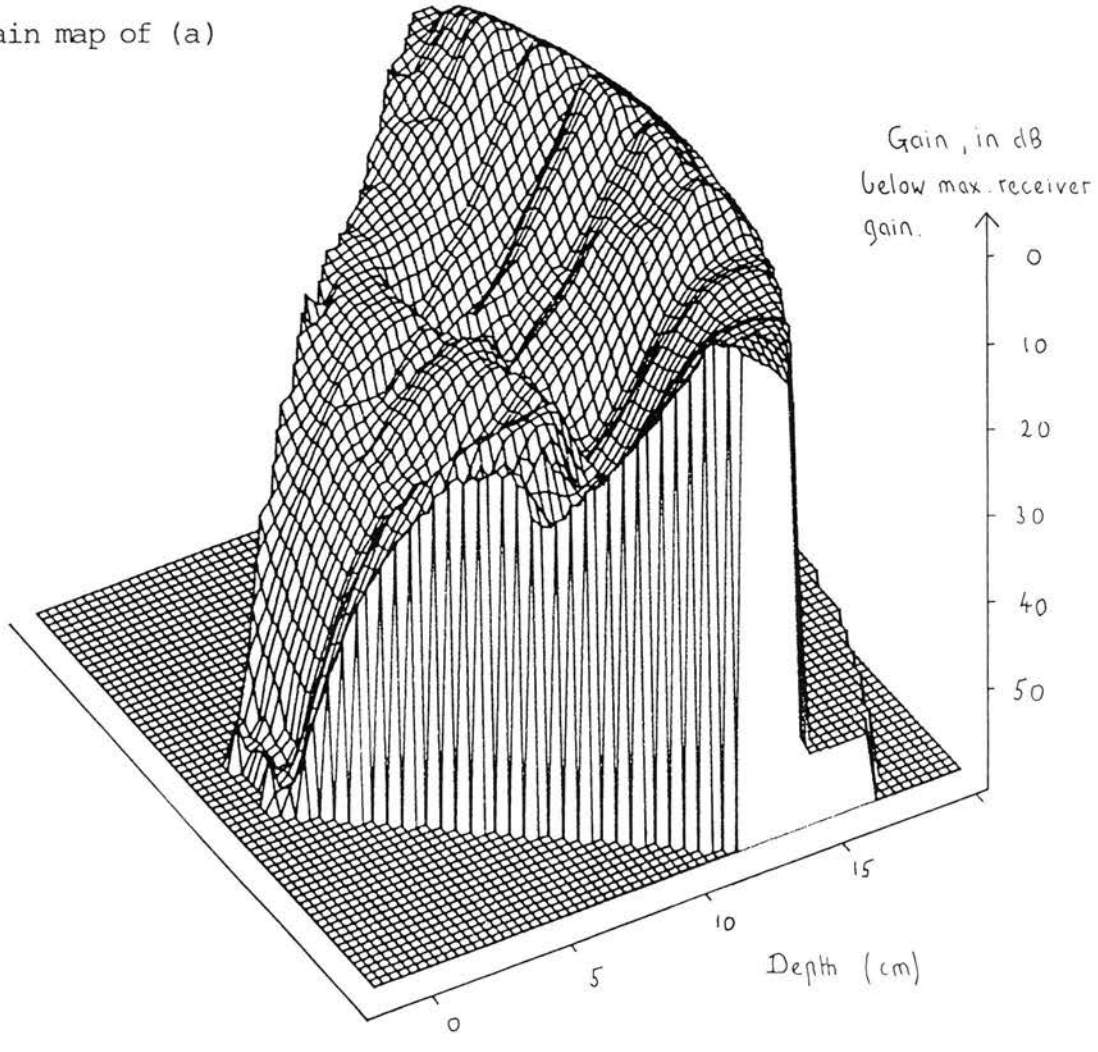

Figure 5.44 Fetal head and placenta :

image and gain map formed by Algorithm 6.

(a) Adaptive TGC image

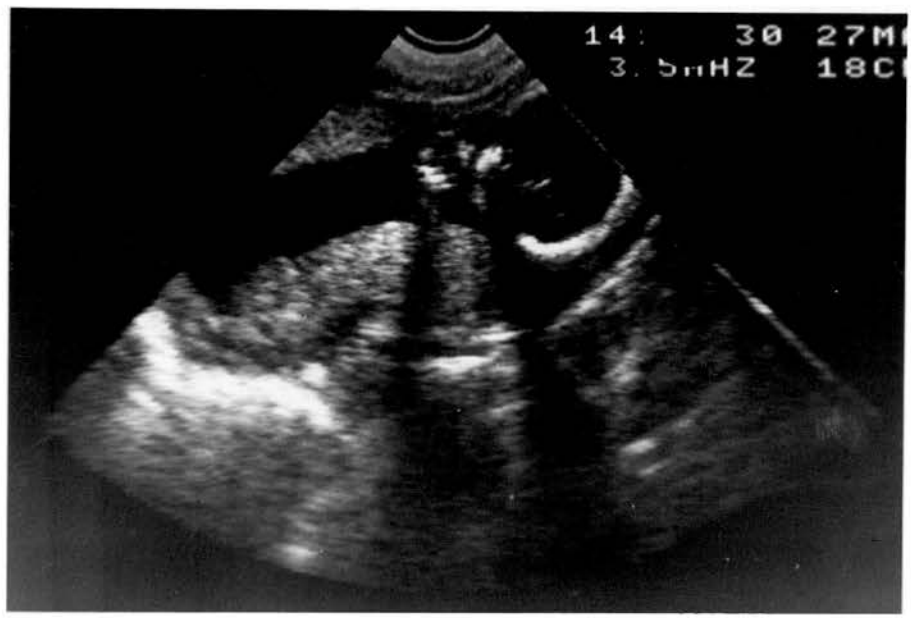

(b) Gain map of (a)

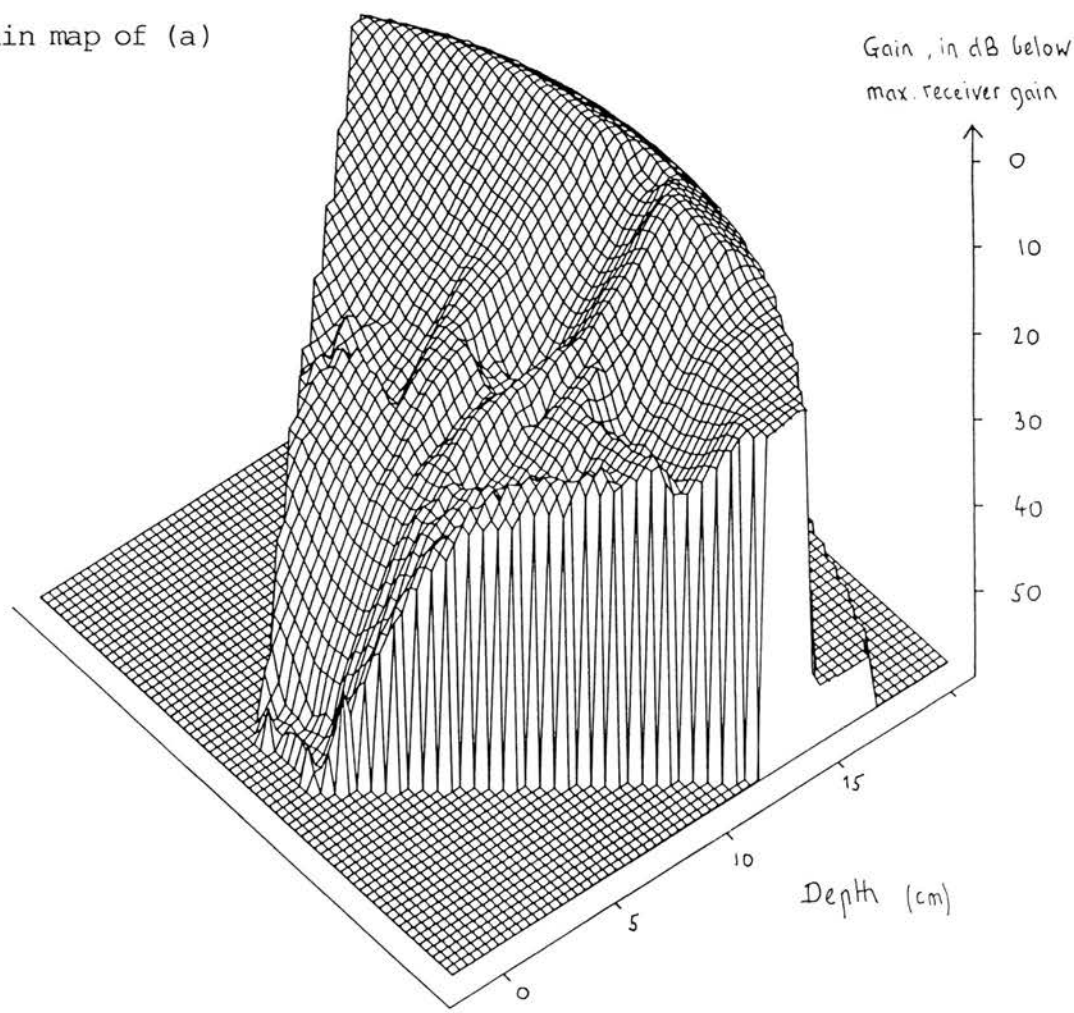

Figure 5.45 Aorta : image and gain map formed by Algorithm 6.

(a) Adaptive TGC image

(b) Gain map of (a)

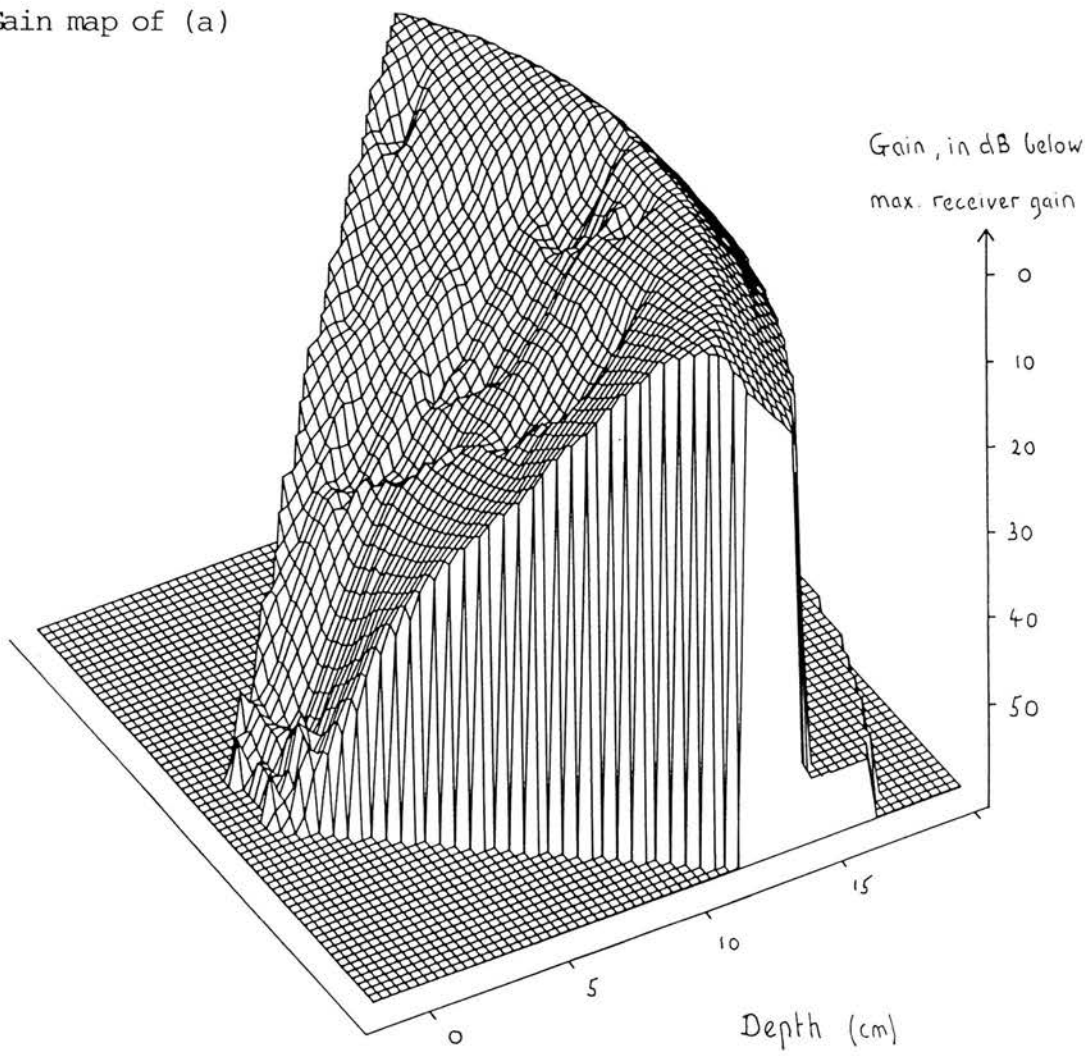

Table 5.7 Variation of gain settings across an image.

Values of Max(ΔG), Med(ΔG) and Min(ΔG) for the 32 gain functions set up for each image :

	Image in figure 5.43a	Image in figure 5.44a	Image in figure 5.45a
Max(ΔG) dB	10.6	16.2	9.6
Med(ΔG) dB	5.7	8.1	4.8
Min(ΔG) dB	2.2	3.8	0.0

Max(ΔG), Med(ΔG) and Min(ΔG) are defined in table 5.2 .

Chapter 6

SUMMARY AND DISCUSSION OF RESULTS

Chapter 5 described six algorithms for adaptive TGC and presented the results of testing them by computer simulation, by imaging a test object and by clinical trial. This chapter draws together the results contained in Chapter 5.

Algorithms 1 to 4 have been described as developing the relationship

$$H'_N = \beta H_N + (1-\beta)H_o \qquad \text{(Equation 5.1)}$$

Where for algorithm 1, $\beta = 1$

algorithm 2, $\beta = 1$

algorithm 3, $\beta = 0$

algorithm 4, $\beta = 0$ or $\frac{1}{2}$

With β always equal to 1, we usually obtain images in which each soft tissue region, considered separately, is well presented. That is, it has a uniform signal level within the range of the display and its boundaries are well preserved. However, the overall balance of the image is poor because the contrast between different tissue types is lost.

With β always equal to 0, we obtain images in which the overall balance is usually well maintained but there are often particular regions that are poorly presented; information is lost because the signal level is either too low or in saturation.

Algorithm 4 applies $\beta = 0$ to below average signals and $\beta = \frac{1}{2}$ to

above average signals. (The averaging in this case takes place over a depth of several centimetres and across the width of the image.) Algorithm 4 can thus apply a different gain function to each part of the image and in this way it combines the best features of algorithms 1, 2 and 3 .

Algorithm 5 is based on algorithm 4, but also addresses the problem of the gain rising steadily with depth in pools of fluid and displaying noise. Fluid regions are identified by the fall in signal level that occurs at a soft tissue/fluid boundary. Algorithm 5 also reduces the tendency of strong reflectors to suppress adjacent smaller signals. This is done by heavily smoothing G_o in the focal zone of the transducer.

Algorithm 6 follows algorithm 5, except that G_o is formed by combining the set of gain functions $\{ G_1 , G_2 \ldots G_N , \ldots G_{32} \}$ rather than the set of echo functions $\{ E_1 , E_2 \ldots E_N , \ldots E_{32} \}$.

Figure 6.1 illustrates the different effects of algorithms 2 to 6 and manual TGC. The six images of figure 6.1 are, as closely as could be obtained, the same transverse section through a full bladder. Figure 6.1a shows the image obtained using manual TGC. The urine is almost free from noise but the rear wall of the bladder is in saturation preventing the structure of the ureters from being resolved.

Algorithm 2 introduces excessive noise into the urine. Although there are no saturated areas, there is little contrast at all in the image.

Algorithm 3 introduces some noise into the urine, less than algorithm 2 but more than manual TGC. The ureters are brought partly out of saturation. The strong signals from the rear wall of the bladder suppress signals at the same depth on either side of the rear wall.

Algorithm 4 improves the presentation of the ureters but still

FIGURE 6.\ : Transverse section through a normal bladder showing the ureters.

(a) Manual TGC

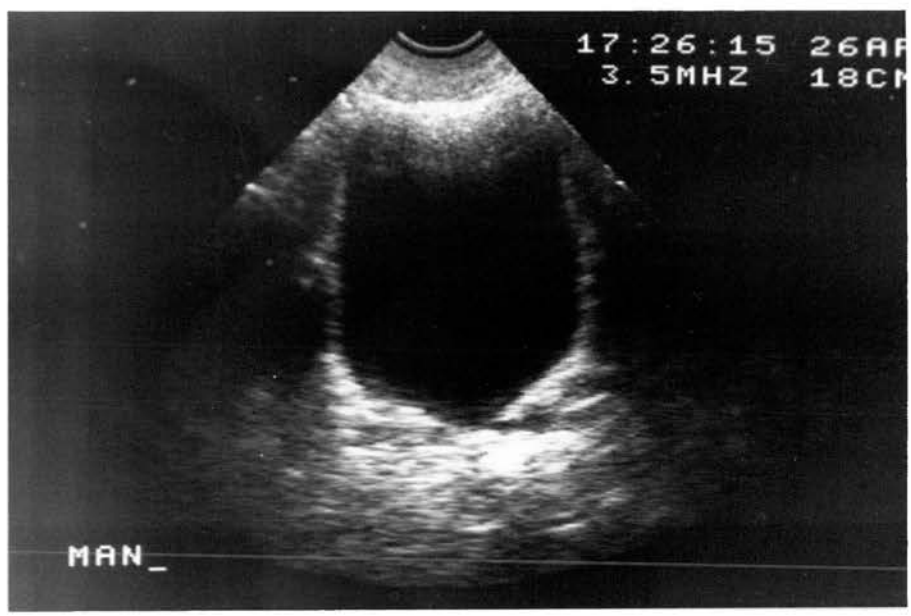

(b) Adaptive TGC: Algorithm 2

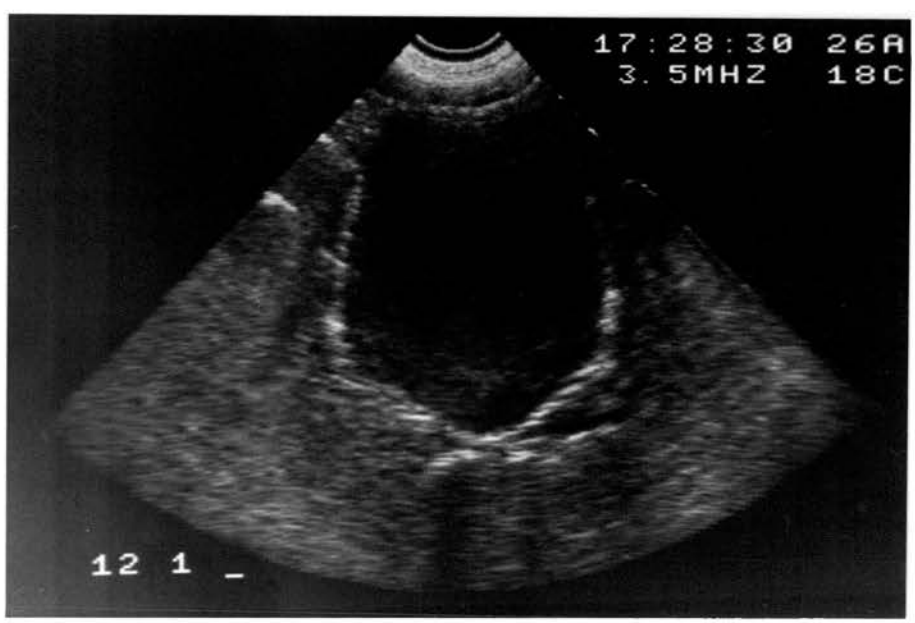

FIGURE 6.\ : Transverse section through a normal bladder showing the ureters.

(c) Adaptive TGC; Algorithm 3

(d) Adaptive TGC: Algorithm 4

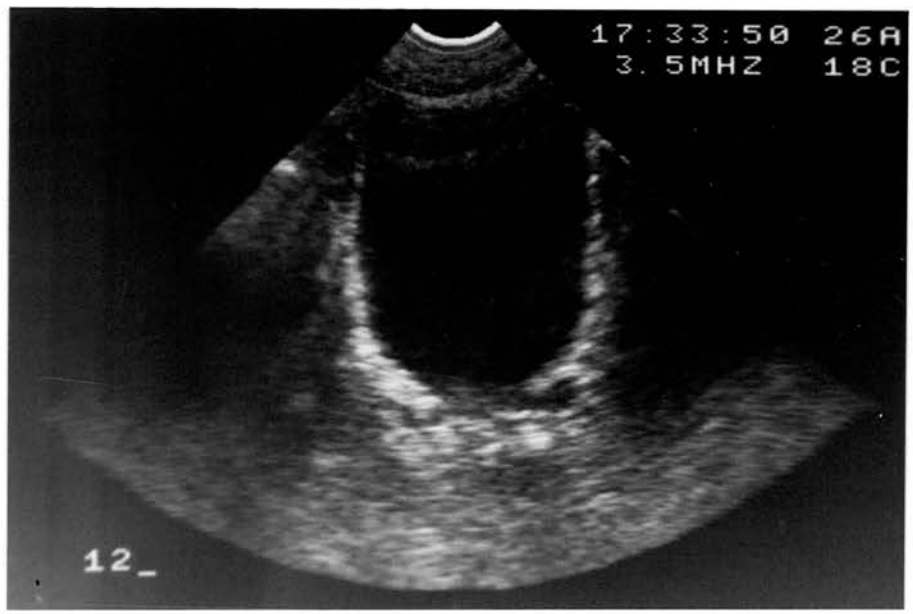

FIGURE 6.1 : Transverse section through a normal bladder showing the ureters.

(e) Adaptive TGC: Algorithm 5

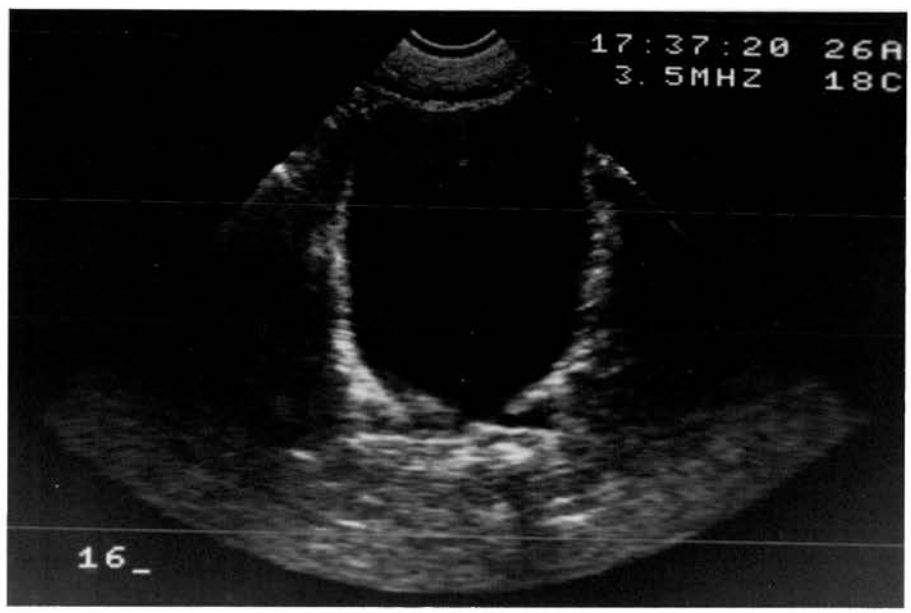

(f) Adaptive TGC: Algorithm 6

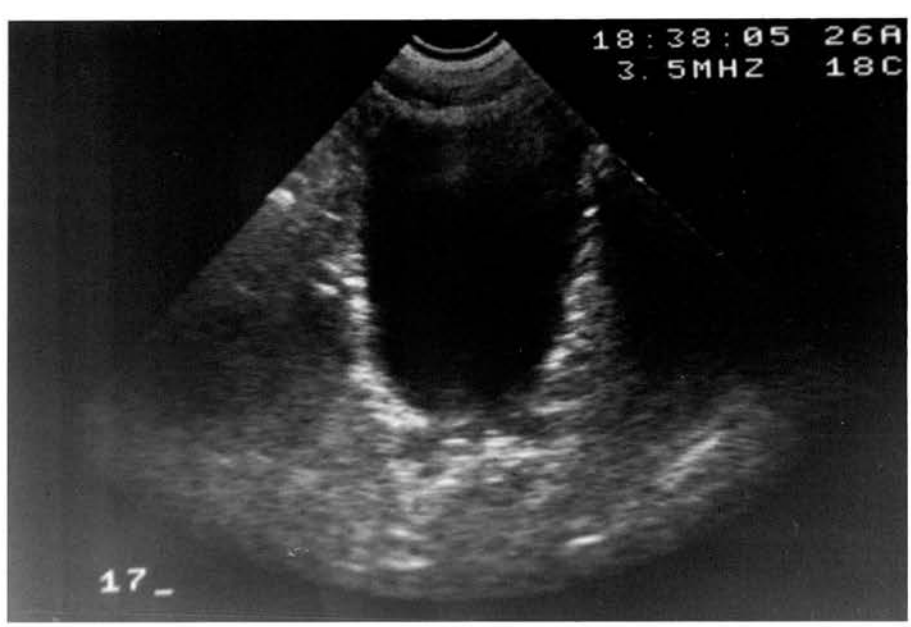

leaves as much noise in the urine as algorithm 3.

Algorithm 5 maintains the same good presentation of the ureters as algorithm 4 while reducing the signal suppression on either side. The noise level in the urine is reduced to about that of manual TGC. This is the best image of the six.

It is more difficult to include the image for algorithm 6 in the comparison because the section has changed somewhat. The ureters are clearly resolved. There appears to be slightly more noise in the urine than for algorithm 5, and less signal suppression on either side of the rear wall of the bladder.

The clinical trials of algorithms 4, 5 and 6 showed that they produce significantly better images than manual TGC in both obstetric and abdominal imaging. Algorithms 4, 5 and 6 adapt the TGC across the image as well as with depth. The clinical trial of a commercial adaptive TGC (effectively algorithm 3) showed that a global adaptive TGC function can produce significantly better images than manual TGC in obstetrics and similar images to manual TGC in abdominal work.

Can we use the results of the clinical trials to compare the various adaptive TGC algorithms? Statistical tests can be applied, but their power is limited here for two reasons:

(1) The number of pairs of images in many of the groups is small.

(2) For many of the groups, the split between the adaptive preferred/manual preferred categories is very uneven: there are few images in the manual preferred category.

The largest groups are those produced using algorithm 5 and the commercial system. Applying the test for trends in contingency tables (Maxwell, 1961) to the results of algorithm 5 and the commercial

adaptive TGC, we find that $P < 0.001$ in both obstetric and abdominal imaging (see table 6.1). The judges thus preferred significantly more images produced using algorithm 5 than using the commercial system.

Although different scanners were used for the two trials, it is reasonable to compare these groups of results because the electronics and display systems of the MARTI and Z series scanners are almost identical, and the images were all judged using the same criteria.

Using the versatile TGC system, there is a trade-off between image quality and processing time: algorithm 3 only requires 0.5 seconds to process one image whereas algorithms 5 and 6 require about 2 seconds.

It is concluded that adaptive TGC, capable of adapting both across the image and with depth, can consistently produce better images than a global TGC function set up either manually or by an adaptive system.

When implemented in real-time, adaptive TGC can reduce the number of control adjustments required in obstetric scanning by a factor of four. This is a considerable advantage over manual TGC because it allows a more efficient use of staff and easier staff training.

The next chapter briefly discusses further developments of adaptive TGC: the implementation of algorithm 5 in a hard-wired system and the development of more sophisticated methods of gain control.

Table 6.1 Comparison of the clinical trial results of Algorithm 5 and the commercial adaptive TGC. (Applying the test for trends in contingency tables.)

(a) Obstetrics (the tables show the number of pairs of images in each category).

Physicists results :

CATEGORY	ALGORITHM 5	COMMERCIAL ADAPTIVE TGC
AA	29	48
A	16	
C	3	53
M	1	5
MM	0	

$\chi^2_{trend} = 23.4$ $P < 0.001$

Radiologists results :

CATEGORY	ALGORITHM 5	COMMERCIAL ADAPTIVE TGC
A	39	48
C	10	48
M	0	10

$\chi^2_{trend} = 15.7$ $P < 0.001$

Table 6.1 Comparison of the clinical trial results of Algorithm 5 and the commercial adaptive TGC. (Applying the test for trends in contingency tables.)

(b) Abdominal (the tables show the number of pairs of images in each category).

Physicists results :

CATEGORY	ALGORITHM 5	COMMERCIAL ADAPTIVE TGC
AA	18	66
A	26	
C	4	30
M	1	12
MM	0	

$\chi^2_{trend} = 11.0$ $P < 0.001$

Radiologists results :

CATEGORY	ALGORITHM 5	COMMERCIAL ADAPTIVE TGC
A	39	17
C	9	79
M	1	12

$\chi^2_{trend} = 46.9$ $P < 0.001$

Chapter 7

FURTHER DEVELOPMENTS OF ADAPTIVE TGC

7.1 ALGORITHMS

7.1.1 Boundary Detection

Algorithms 5 and 6 introduce the idea of recognising particular regions (pools of fluid) by their boundaries, and then setting the TGC accordingly. This is an idea worth developing.

Each bounded region could be assigned its own TGC weighting factor. The boundaries of low contrast regions could be enhanced, making them more easily seen in the image.

The identification of boundaries in ultrasonic images is made difficult by the presence of acoustic noise. Spatial filters have been developed which help to discriminate between acoustic noise and genuine resolved structures (Bamber and Daft, 1986; Loupas et al, 1986; Loupas et al, 1987). However, these techniques are still in their infancy and would not yet be able to provide an adaptive TGC algorithm with accurate information about all the boundaries in an image.

7.1.2 Learning Algorithms

The algorithms described in this text are adaptive in that they use echo data to adjust the TGC for each location in the image so as to suit both the local signal level and the overall signal level. The adjustment is performed according to the rules laid down in the algorithm. After two iterations at most, the algorithm satisfies its own criteria completely and the TGC settings do not change on subsequent iterations. However, the more demanding criteria detailed in section 5.1 will only have been met part way. For example, presenting different

tissue regions at different uniform levels. An operator experienced in ultrasonic imaging can often see parts of the image that would benefit by further TGC adjustments. One way of making use of the operator´s experience would be to incorporate a learning mechanism into the adaptive TGC algorithm. The algorithm would then be able to take advantage of additional information supplied by the operator. Once the algorithm had set up an image, the operator would supply the computer with information about changes in the TGC settings that would improve the image further. The learning algorithm would then assimilate these changes and alter its rule base accordingly. In this way, the algorithm would gradually improve its ability to present ultrasonic images.

An efficient way for the operator to supply the computer with TGC information is to use a touch sensitive screen. The touch sensitive screen overlays the ultrasonic image and supplies the computer with the coordinates of locations touched by the operator. In this way the computer can be supplied with information about which parts of the image are to be adjusted and how much the TGC is to be changed. The computer then alters the gain map accordingly, and the observer can immediately see if any further adjustments are necessary. The hardware to do this is described in the next section.

7.2 HARDWARE

7.2.1 Touch sensitive screen

An infra-red touch screen manufactured by Microvitec Ltd. has been purchased. It comprises an array of infra-red emitters and detectors and control logic mounted in a frame designed to fit around the screen of a 14 inch monitor. The resolution of the array is 120 divisions horizontally by 90 vertically. The touch screen passes to the

microcomputer the co-ordinates of points on the screen that are touched by an object such as a finger or pencil. Data is transmitted via an RS432 serial link.

The touch screen has two modes of operation at present:

(1) Single point - after reading in a single pair of co-ordinates the gain of an area approximately 2 cm around the point can be altered.

(2) Defined area - after reading in 3 pairs of co-ordinates defining a sector shape, the gain within this sector can be altered.

In both (1) and (2) the gain is altered by sliding a finger up or down at the left side of the screen - the microcomputer interprets co-ordinates from this part of the screen as a cue to alter the gain. The gain change in dB is proportional to the distance moved by the finger along the side.

The usefulness of the touch screen has yet to be evaluated. It has the potential to be used both in conjunction with learning algorithms and in its own right, to allow to operator to adjust the gain in small regions of the image.

7.2.2 Real-time adaptive TGC

The versatile TGC system has been used to test a variety of methods of adaptive TGC. However, it cannot implement the most successful algorithms (5 and 6) in real-time. Dedicated hardware is required to do this. The commercial development of a hard-wired system that will implement algorithm 5 in real-time is now at an advanced stage.

REFERENCES

Bamber J C (1986); 'Attenuation and absorbtion' in Physical Principles of Medical Ultrasonics (edited by Hill C R), pp118-199. John Wiley, New York.

Bamber J C and Daft C (1986); 'Adaptive filtering for reduction of speckle in ultrasonic pulse-echo images'. Ultrasonics, Vol 24, 41-44.

Barnes R W, Nomeir A, Pardue G T and Nuss P H (1975); 'An ultrasound receiver with programmable time gain control'. J. Clinical Ultrasound, Vol 3, 121-124.

Blackwell R (1983); 'New developments in equipment' in Clinics in Obstetrics and Gynaecology, Vol 10, pp371-394.

Bowen B A and Brown W R (1981); VLSI Systems Design for Digital Signal Processing, Vol 1, pp182-191. Prentice-Hall, New Jersey.

Brown H T (1981); 'Ultrasonic signal detection' in Physical Aspects of Medical Imaging (edited by Moores B M, Parker R P and Pullan B R), pp127-140. John Wiley, New York.

Clinics In Diagnostic Ultrasound, Volumes 1-19. Churchill Livingstone, New York.

DeClercq A and Maginness M G (1975); 'Adaptive gain control for dynamic ultrasound imaging'. IEEE Ultrasonics Symp. Proc., CHO 994-4SU, 59-63

Dehne J S (1978); 'Image processing techniques for real-time imagery'. Proc. NATO Adv. Study Inst. on Pattern Recognition and Signal Processing (Paris), pp205-224

Duck F A and Hill C R (1979); 'Mapping true ultrasonic backscatter and attenuation distribution in tissue - a digital reconstruction approach' in Ultrasonic tissue characterization II (edited by Linzer M), NBS Special Publication 525, pp247-251, Washington DC US Govt. Printing Office.

Everitt B S (1977); The Analysis of Contingency Tables, pp20-22. Chapman and Hall, London.

Farrell E J (1982); 'Backscatter and attenuation imaging from ultrasonic scanning in medicine'. IBM J. Res. Develop., Vol 26, 746-758.

Greenleaf J F, Gisvold J J and Bahn R C (1982); 'A clinical prototype ultrasonic transmission tomographic scanner' in Acoustical Imaging Vol 12 (edited by Ash E A and Hill C R), pp579-587. Plenum Press, New York.

Hill C R, editor (1986); Physical Principles of Medical Ultrasonics. John Wiley, New York.

Hogan T (1982); Osbourne CP/M User Guide, 2nd Edition. Osbourne/McGraw-Hill, California.

Horowitz P and Hill W (1982); The Art of Electronics. Cambridge University Press, New York.

Hunt J W, Arditi M and Foster F S (1983); 'Ultrasound transducers for pulse-echo medical imaging'. IEEE Trans. Biomed. Eng., Vol BME-30, 453-481.

Itoh K, Shibuya N, Kajiwara T, Kogamei N, Yokoi H and Yoshikawa Y (1979); 'The auto brightness control'. Proc. 35th Meeting. Jpn. Soc. Ultrasound Med., 69-70.

Kobayashi J and Sekeba K (1978); 'Clinical data using variable dynamic range and automatic gain control method'. Jpn. J. Med. Ultrason. (Supp), 157-158.

Korba L W and Cousin A J (1979); 'An automatic over-range correcting circuit'. Med. Biol. Eng. Comput., Vol 17, 133-134.

Kremkau F W and Taylor K J W (1986); 'Artifacts in ultrasound imaging'. J. Ultrasound Med., Vol 5, 227-237.

Leeman S, Ferrari L, Jones J P and Fink M (1984); 'Perspectives on attenuation estimation from pulse-echo signals'. IEEE Trans. on Sonics and Ultrasonics, Vol SU-31, 352-360.

Leventhal L A and Saville W (1983); Z80 Assembly Language subroutines. Osbourne/McGraw-Hill, California.

Libes S and Garetz M (1981); Interfacing to S-100/IEEE 696 microcomputers. McGraw-Hill, California.

Loupas T, McDicken W N and Allen P (1987); 'Noise reduction in ultrasonic images by digital filtering'. Brit. J. Radiology, Vol 60, 389-392.

Loupas T, McDicken W N and Allen P (1986); 'An adaptive weighted median filter for speckle suppression in medical ultrasonic images'. Submitted to IEEE Trans. on Circuits and Systems.

Maginness M G (1979); 'Methods and terminology for diagnostic ultrasound imaging systems'. Proc. of the IEEE, Vol 67, 641-653.

Maxwell A E (1961); Analysing Qualitative Data, pp63-72. Methuen, London.

McCarty K and Stewart W (1984); The Cardiff Test System Instruction Manual. Diagnostic Sonar Ltd., Livingston, Scotland.

McDicken W N (1981); Diagnostic Ultrasonics - Principles and Use of Instruments, 2nd Edition. John Wiley, New York.

McDicken W N, Evans D H and Robertson D A R (1974); 'Automatic sensitivity control in diagnostic ultrasonics'. Ultrasonics, Vol 12, 173-176.

Melton H E Jr., Collins S M and Skorton D J (1983); 'Automatic real-time endocardial edge detection in two-dimensional echocardiography'. Ultrasonic Imaging, Vol 5, 300-307.

Melton H E Jr. and Skorton D J (1983); ´Rational gain compensation for attenuation in cardiac ultrasonography´.
Ultrasonic Imaging, Vol 5, 214-228.

O´Donnell M (1983); ´Quantitative volume backscatter imaging´.
IEEE Trans. on Sonics and Ultrasonics, Vol SU-30, 26-36.

Ophir J and Maklad N F (1979); ´Digital scan converters in diagnostic ultrasound imaging´. Proc. of the IEEE, Vol 67, 654-663.

Ophir J, Shawker T H, Maklad N F, Miller J G, Flax S W, Narayana P A and Jones J P (1984); ´Attenuation estimation in reflection: progress and prospects´. Ultrasonic Imaging, Vol 6, 349-395.

Peli T and Lim J S (1981); ´Adaptive filtering for image enhancement´.
IEEE Proc. Int. Conf. Acoustics Speech and Signal Processing (Atlanta), CH1610-5, 1117-1120.

Pincu M, Schwartz G, Corday S R, Fujibayashi Y and Meerbaum S (1986); ´Attenuation correction in echocardiography´.
Ultrasonic Imaging, Vol 8, 86-106.

Pratt W K (1978); Digital Image Processing, pp331-333.
John Wiley, New York.

Pye S D, McDicken W N, Wild S R and Anderson T (1986); ´Automatic swept gain in ultrasonic imaging´ in Inst. Physical Sciences in Medicine Report no.47: Physics in Medical Ultrasound (edited by Evans J A), ppl73-175. Inst. Physical Sciences in Medicine, London.

Pye S D, Wild S R, McDicken W N, Ashford S, Elliott V, MacNamara A and Millar D (1983); ´A clinical trial of automatic gain control in obstetric ultrasonics´. Brit. J. Radiology, Vol 56, 964-968.

Pye S D, Wild S R, McDicken W N and Montgomery H (1985); ´A clinical trial of automatic gain control in abdominal ultrasound´.
Brit. J. Radiology, Vol 58, 869-872.

Robinson D E and Knight P C (1982); 'Interpolation scan conversion in pulse-echo ultrasound'. Ultrasonic Imaging, Vol 4, 297-310.

Robinson D E, Kossoff G, Radovanovich G and Warren P (1979); 'Signal processing of line mode echogram data by computer'. Proc. 24th Meeting of the AIUM, 35.

Robinson E A (1984); 'Image reconstruction in exploration geophysics'. IEEE Trans. on Sonics and Ultrasonics, Vol SU-31, 259-270.

Schafer M E and Lewin P A (1984); 'The influence of front-end hardware on digital ultrasonic imaging'. IEEE Trans. on Sonics and Ultrasonics, Vol SU-31, 295-306.

Smith S W, Wagner R F, Sandrik J M and Lopez H (1983); 'Low contrast detectability and contrast/detail analysis in medical ultrasound'. IEEE Trans. on Sonics and Ultrasonics, Vol SU-30, 164-173.

Uchida R ,Hagiwara Y, Kasai C and Irie T (1974); 'Resolution improvement of ultrasonic diagnostic equipment by means of echo AGC method'. Proc. 26th Meeting Jpn. Soc. Ultrasound Med. 131.

Uchiumi I, Takamizawa K, Hashiguchi M, Iinuma K, Takehara Y, Matsukawa M and Hisada Y (1979); 'Study of gain control with skin trigger method'. Proc. 35th Meeting Jpn. Soc. Ultrasound Med., 67-68.

Venetsanopoulos A M and Cappellini V (1986); 'Real-time image processing' in Multidimensional Systems: Techniques and Applications (edited by Tzafestas S G), pp345-399. Marcel Dekker, New York.

Wells P N T (1977); Biomedical Ultrasonics. Academic Press, London.

Whittingham T A (1981); 'Real-time ultrasonic scanning' in Physical Aspects of Medical Imaging (edited by Moores B M, Parker R P, and Pullen B R), pp153-165.

APPENDIX 1

Published Papers